



**EUROPEAN  
MECHANICAL  
SCIENCE**

**2022**

**VOLUME: 6**

**ISSUE: 3**

***E-ISSN: 2587-1110***



“

**EDITOR IN CHIEF**

**PROF. DR. MUSTAFA ÖZCANLI**

”

## Editor in Chief

Mustafa Ozcanli (Automotive Engineering, Cukurova University, Turkey)

## Editors

Sandra Spaszkievicz (West Pomeranian University of Technology, Poland)  
Iva Petrikova (Applied Mechanics, Technical University of Liberec, Czech Republic)  
Elżbieta Piesowicz (West Pomeranian University of Technology, Poland)  
Tomeh Elias (Vehicles and Engines, Technical University of Liberec, Czech Republic)  
Aleksandra Borsukiewicz (West Pomeranian University of Technology, Poland)  
Alptekin Ergenç (Automotive Engineering, Yildiz Technical University, Turkey)  
Hasan Serin (Automotive Engineering, Cukurova University, Turkey)  
M. Atakan Akar (Automotive Engineering, Cukurova University, Turkey)  
Ahmet Çalık (Mechanical and Metal Technologies, Mersin University, Turkey)  
Tayfun Ozgur (Automotive Engineering, Cukurova University, Turkey)

## Layout Editor

Ahmet Calik (Mersin University, Turkey)

## Secretary

Erdi Tosun (Cukurova University, Turkey)  
Şafak Yıldızhan (Cukurova University, Turkey)

## Indexed / Abstracted in:

TR-Dizin, CrossRef, Index Copernicus, Journal Factor, Rootindexing, ResearchBip, JournalFactor, JIFACTOR, Google Scholar, I2OR, Cosmos Impact Factor, International Innovative Journal Impact Factor (IIJIF), Scientific Indexing Services, InfoBase Index, Scientific Journal Impact Factor

## Aims and Scopes

European Mechanical Science (EMS) is an international, peer reviewed journal which publishes full length original research papers, reviews related to all areas of Mechanical Engineering such as: Solid Mechanics, Materials Engineering, Automotive Engineering, Fluid Mechanics, Thermal Engineering, Engine and Power Engineering, Dynamics & Control, Robotics & Mechatronics, Transportation Engineering, Computational Mechanics, Design, Systems, Manufacturing, Bio-Medical Engineering; Process Engineering, Aerospace Engineering. No charges are required from the Authors to publish the articles.EMS is a quarterly published journal operating an online submission and peer review system. It allows authors to submit articles online and track their progress via its web interface.

## Contents

### – Review Article

- Analysis of different methods of suppressing generator noise reaching indoor noise 161  
Hatice Mehtap Buluklu, Filiz Bal Koçyiğit, Ercan Köse

### – Research Article

- Comparison of pure-hydrogen production performances of blast furnace slag, and metal powders in sodium borohydride hydrolysis reaction 179  
Feride Cansu Iskenderoğlu, Mustafa Kaan Baltacıoğlu

### – Research Article

- Thermo-hydraulic performance investigation of a heat exchanger tube inserted with twisted tapes modified with various twist ratio and alternate axis 189  
Mahmut Uyanik, Toygun Dagdevir, Veysel Ozceyhan

### – Research Article

- Estimation of three-point bending behavior using finite element method for 3D-printed polymeric sandwich structures with honeycomb and reentrant core 196  
Meltem Eryildiz

### – Research Article

- Computer aided numerical damage analysis of the axle shaft 201  
Hamit Adin, Raşit Koray Ergün, Mehmet Şükrü Adin

### – Research Article

- Validation of A356T6 automobile wheel fatigue strength using the finite elements method 207  
Okan Ceylan, Ferhat Aydoğan

# Analysis of different methods of suppressing generator noise reaching indoor noise

Hatice Mehtap Buluklu<sup>1\*</sup>, Filiz Bal Koçyiğit<sup>2</sup>, Ercan Köse<sup>3</sup>

<sup>1</sup>Tarsus University, Graduate Education Institute, Production Engineering ABD, Tarsus/Mersin, <sup>2</sup>Atılım University, Fac. Of Fine Art Design and Architecture, Dept. Of Arch., Ankara, Turkey, <sup>3</sup>Tarsus University, Faculty of Electrical-Electronics Engineering, Tarsus/Mersin, Turkey

**Orcid:** H. M. Buluklu (0000-0002-1912-9598), F. Bal-Koçyiğit (0000-0003-4191-0724), E. Köse (0000-0001-9814-6339)

**Abstract:** The noise which occurs during the operation of the auxiliary power units is a disturbing factor, although its level varies depending on the environment. This high level of noise in occupational areas can cause not only health but also accidents risks. While silencers are mostly preferred for active noise control, acoustic foam or textile products are preferred according to passive control methods. In this review, the noises produced by the generators were examined and the studies in the literature on suppressing these noises were evaluated by making comparative analyzes. New recommendations have been developed according to the results of the comparative analysis. In case the sampled natural gas generator is closed with 2 mm thick plywood and a steel framed box covered with an acoustic sponge, the sound pressure level is approximately 30 dB in low frequency diesel + electric generators using a silencer according to active control methods. In measurements; It was observed that it decreased from 93.2 to 88.4 dB. While materials such as an acoustic sponge, which are preferred in passive control methods, are open-celled and porous structures, it is advantageous to have sound absorption capacity, but it can be a disadvantage due to its synthetic content.

**Keywords:** Sound, Noise, Acoustic, Generator Noise, Active Control Methods.

## 1. Introduction

While technological developments offer important opportunities, they can also bring many negativities. One of the undesirable conditions is the disturbance effect caused by vibration and noise. The noise continues to be one of the important problems of today, as it is disturbing and can threaten human health if exposed for a long time. To protect cities and residential areas from noise, measures to be taken against noise in industrial areas and sensitive areas of the city are increasing and new studies are being carried out in this regard. To protect cities and residential areas against noise, which is included in the “Regulation on the protection of buildings against noise” of the Official Gazette published in 2018, measures to be taken against noise in industrial areas and sensitive areas of the city are increasing and standards are being brought in this regard [1].

“Regulation on the Protection of Buildings Against Noise” was published in the Official Gazette No. 30082 on May 31, 2017, and entered into force on May 31, 2018 [2]. In order to better understand these studies and noise, its relationship with sound should be examined.

Sound, which occurs as a result of the compression and relaxation of molecules through a medium such as solid,

liquid and gas, as a result of the effect of vibrations emitted from an energy source and is perceived by a receiving mechanism such as the human ear or microphone, can be expressed as noise even though these vibrations are disturbing [3,4,5]. Accordingly, noise is also accepted as an acoustic phenomenon perceived by a person or group, defined as unpleasant or disturbing. When exposed to noise, physiological or psychological responses occur [6]. If the unwanted sound is louder, an increase in these responses can be observed. Although sound is known as an objective concept that can be measured and whose existence does not change from person to person, factors such as the intensity of the noise, its frequency, the amount of background noise, hearing loss and psychological effects vary from person to person [4,7], occurring in the industrial area for production purposes, which remains constant in a certain time interval, and instantaneous noises with a high level occurring in less than one second [7]. Additionally; in different environments, noise from construction, music from entertainment, noise from traffic and airplane noise, etc. noise has been reported [8].

The sound pressure level and exposure times of these noises are important. These standards are determined by the ILO (International Labor Organization) in terms of work, and it is preferred that the sound pressure levels cre-

\* Corresponding author.  
Email: hmehtap@yahoo.com



ated by the sound are not above certain limits according to the determined working times. In ILO standards, the operating time at 90 dB is determined as 8 hours [9].

At the same time, NVH (Noise Vibration and Harshness) is determined by noise legislation and increasing customer demands. In this sense, acoustic behavior should also be known [10]. Gerges et al. According to (2001), noise, which can be a common occupational hazard in many workplaces, is common in the iron and steel industry, foundries, sawmills, textile mills, airports, and aircraft maintenance shops, crushing mills, etc. As noise-induced hearing loss in environments is known as the most common occupational disease [11], exposure to high noise levels can cause permanent damage to hearing [12]. In the study of Valley (2001), it was stated that noise is a factor that negatively affects the quality of life of people, since it has significant environmental effects, although it is temporary [13]. The aforementioned negativities enabled the development of solution proposals. For this reason, studies on occupational sound levels have been made in some sources, and reference values are listed for each source [14].

For example, noises originating from mechanical parts such as wind turbines, which can be described as mechanical noises, can be listed as auxiliary equipment such as gearbox, generators, drift drivers, cooling fans, hydraulics [15].

Some devices, tools, or machines, which are described as auxiliary equipment, are disturbing factors that can be encountered as noise sources. It is inevitable to take necessary measures to minimize such noises [16]. To determine the harmful effects of sound pressure on people and to be more controlled, evaluations can be made by arranging noise maps [17]. Caliskan et al. (2011) stated in their study that these maps, in addition to being regional or local, are preferred to be prepared at certain times of the day [18]. It is stated that a noise map should be made for the stage, tent, generators and other structures that are planned to be used temporarily on the facility or an area [19]. In this study, noise map for generators can be drawn since the issue of noise in generators is examined. Thus, areas that are significantly affected by environmental noise can be distinguished and appropriate measures can be taken in these areas [20]. Today, the necessity of using commercial and industrial generators, commercial workplaces and industrial production areas leads to the need to evaluate the noise generated by these generators [21]. The source of the sound, the path of the sound and the receiver, which are known as the parameters for feeling the presence of the sound, should be evaluated separately. In this sense, one of the most important factors in taking the noise under control is to reduce the noise at its source. Therefore, the environment can be protected from the noise generated at the source. Another important point is that the noise can be reduced in the area where it spreads. However, it is known

that reduction at the source is more effective [22]. E.g; in the evening i.e. in quieter situations, loud radios, generators etc. It is important to minimize the disturbance problem [23]. In our study, reducing the noise in generator types with different materials with acoustic properties will provide an innovation in this regard. Generator types; Examples of portable (portable or emergency) models that work with natural gas and/or propane, which cause constant noise, are permanently installed, are fixed, work with diesel or gas, which cause intermittent noise, and are preferred in residential or commercial areas [24]. Noise levels will be within the specified range. The weatherproof and sound attenuated enclosure construction will limit the noise level to 70 dBA at 7 meters or 80 dBA at 1 m at full continuous load [25]. These measurements can be logarithmic or arithmetic. In a study in which the difference is expressed depending on the measurement of these two concepts, when a measurement is taken at a distance of 7 meters from all four sides of a generator, right, left, front and rear; 93 dB measured logarithmically and 90.5 dB measured arithmetically. It has been determined that the logarithmic measurement of the sound pressure level gives healthier results. In addition, it was stated that the sound pressure level of a generator should be measured from four different directions as mentioned [26].

In measuring the common generator noise level, the dB(A) value, which is the A-weighted sound pressure level, is measured at a distance of 7 meters in free space. The free area should not be on surfaces that reflect the sounds of the generator, such as walls and buildings, close to the measurement area [27]. In another study on the importance of distance and noise; It is stated that a generator at a distance of 15.24 meters produces 107 dB (A) of noise. It is also important to regularly test and maintain backup generators [28]. The measurement of air emitted noise is included in the International Standard ISO 8528-10 [29]. This measurement standard is taken into account in the studies that can be done about the measures taken to reduce noise in generators. In line with the standards, sound insulation procedures are carried out to allow the operation of tools and devices that should be used in road and construction works, paying attention to the time period that is sensitive to noise, to eliminate noise disturbance and to prevent health problems, especially in settlements [30].

At the same time, applications such as insulation works to reduce generator noise, placing sound-absorbing barriers on suction louvers and using fan silencers are the methods used to reduce generator noise [31].

The contributions of this study to the literature on the analysis and evaluation of the noise level arising during the operation of generator types according to their nature and environment are summarized as follows:

- i. Studies in the literature for acoustic masking meth-

ods, which have important contributions in minimizing the noise produced by generators, were examined in detail and the results were compared.

- ii. When the active noise level reduction methods in the application were examined, it was seen that the most efficient results were obtained by using a silencer.
- iii. When the passive noise level reduction methods in practice are examined, it has been seen that different quality products obtained from the acoustic sponge with porous, in other words, open-cell structures, or textile materials with sound-absorbing features provide advantages. In this sense, the acoustic contributions of each product are presented.
- iv. The importance of the distance parameter in increasing the efficiency of alternative solutions determined for reducing noise in generators is also mentioned. This situation has brought positivity to the studies carried out.
- v. Although many materials with sound absorption features are advantageous among the materials used, it can also be seen that they cause disadvantages due to the synthetic raw materials in their content. To overcome these disadvantages, suggestions have been made to produce products with natural materials that can be preferred as an alternative, recyclable, less harmful to human health and environmentally friendly.

In addition, these natural materials will be able to provide significant gains in reducing carbon emissions, which is one of the important issues today. In this study, to compare the methods used in reducing the generator noise, in the second part, the definition of the generator and the sound pressure level of the noises it produces are given and acoustic solutions (passive and active methods) are mentioned. In the third part, the results obtained according to the literature review are given. In the fourth chapter, the sound pressure levels of the generators according to their types and the acoustic solutions developed to reduce these pressure levels are comparatively examined. In the last part, new solutions to be investigated to reduce generator noise are presented.

## 2. Material and Method

Generators are known as machines that can convert mechanical energy into electrical energy and work with the principle of electromagnetic induction (Faraday's Law) [32]. Vibration and noise during operation occur when the sound is above a certain level. Humans can hear sounds in the frequency range of 20-20000 Hz under normal conditions. [33]. In this case, the sound pressure level, which may differ according to the frequency ranges, is the response of people and objects to the sound in the air and

is often known as a concept that needs to be controlled, but depends on the sound source and measurement location. Sounds above 700 Hz begin to damage the ear [34]. In terms of these analyses, the analytics of the sound source can also be important. If we evaluate generators in this sense, it is understood that they produce different noise according to their size, capacity and design. Since these sounds at different frequencies and pressure levels directly affect the subjective concept of "noise level", they should be regulated by laws, not standards [27]. A sound level meter is used to measure the noise level [35]. The value obtained from this measurement is also expressed in dB (A) [36].

Our study aims to compile studies on noise in generators and to minimize the negative effects of noise on people. Therefore, it is also important to be protected from the harmful effects of noise, to create healthy and comfortable living spaces and to prevent occupational accidents in the workplace [37].

For this reason, insulation processes are also increasing in industrial areas and since using today's preferred technologies makes sound absorbing and sound-reducing insulation materials increasingly important [38], parameters such as which generators are more effective and how much sound insulation can be provided are analyzed.

Accordingly, in this study; first of all, the general structures of the generators and the elements in them are introduced. Then, the noises produced by the generators were examined and the studies in the literature for the acoustic masking method were given in detail. At the end, the results of these methods are compared and suggestions for new studies to be done are given.

### 2.1. Generator

Preferred methods are applied within the framework of these standards (Military facilities, etc.) in critical places in the form of power centers where network infrastructure costs are very high [39]. In addition, it must be of a quality to provide reliability, availability, voltage and frequency characteristics as well as being known as secondary electrical power [40]. Although it is classified according to fuel types (diesel, gasoline/LPG, natural gas, etc.) and working methods, it is widely used in factories, motorboats and trains [41, 42]. Generators also differ in size, shape and feature. Dimensional values of a diesel generator are given in Table 1 [43].

Dimensional values etc. of a diesel engine generator in Table 1 is seen. According to these data, the dimensions vary according to the generator types [43]. At the same time, the concept of power is among the issues that need to be analyzed. Because generators are mechanical devices, criteria such as maintenance and control are among the elements that should be evaluated in terms of efficient operation. In power systems, control is usually applied to

**Table 1.** Dimensional Values of Diesel Generator [43]

Generator Set, 50 Hz, 400 V			Room Size (metre, m)						Radiator Hot Air Outlet Window (meter, m)			Air Inlet Window Total Area (meter, m)	Room Door Size (meter, m)		Exhaust	
Engine Model	Model	Standby Power (kVA)	Dimensions (meter, m)			A	B	C	D	E	K*	L	M	Dia-meter (inch)	P (meter, m)	
			Lenght	Width	Height	Lenght	Width	Height								
S3.8-G6	AC 55	55	1.78	0.95	1.28	3	3	2.5	0.7	0.65	0.6	0.46	1.5	2	3	2
S3.8-G7	AC 66	66	2.15	1.05	1.52	3.5	3	2.5	0.7	0.7	0.7	0.5	1.5	2	3	2
6BTA5.9-G5	AC 110	110	2.2	1.05	1.63	4	3	2.5	1	1.1	0.5	1.1	1.5	2.2	3	2
6BTAA5.9-G6	AC 150	150	2.75	1.3	1.82	4.5	3.5	2.5	0.95	1.25	0.6	1.2	1.8	2.4	3	2.2
6BTAA5.9-G7	AC 170	170	2.75	1.3	1.82	4.5	3.5	2.5	0.95	1.25	0.6	1.2	1.8	2.4	3	2.2
QSL9-G5	AC 350	350	2.9	1.3	1.94	5	3.5	3	1.2	1.3	0.5	1.6	1.8	2.5	4	2.5
NTA 855-G4	AC 400	400	2.96	1.55	2.14	5	3.5	3.3	1.25	1.5	0.55	1.9	2	2.6	6	2.5
QSX15-G6	AC 500	500	3.38	1.55	2.1	5.5	3.5	3.3	1.7	1.6	0.45	2.8	2	2.6	8	2.5
QSX15-8G8	AC 550	550	3.38	1.55	2.1	5.5	3.5	3.3	1.7	1.6	0.45	2.8	2	2.6	8	2.5
VTA28-G5	AC 700	700	3.81	1.55	2.27	6	3.5	3.5	1.5	1.5	0.65	2.25	2	2.6	2*6	2.6
VTA28-G6	AC 825	825	3.81	1.55	2.27	6	3.5	3.5	1.5	1.5	0.65	2.25	2	2.6	2*6	2.6
QSK23-G3	AC 880	880	4	1.71	2.26	6.5	4	3.5	1.9	2	0.25	3.8	2.4	2.7	8	2.7
QST30-G4	AC 1100	1100	4.4	1.78	2.35	7	4.5	4	2.1	2	0.3	4.2	2.5	3	2*6	3.1
KTA38G5	AC 1100K	1100	4.4	1.78	2.37	7	4.5	4	2.1	2	0.3	4.2	2.5	3	2*6	3.1
KTA50-G3	AC 1410	1410	4.94	2.1	2.4	8	4.5	4	2.3	2.1	0.25	4.8	2.7	3	2*6	3.1
KTA50-G8 (GS8)	AC 1675	1675	5.45	1.95	2.45	8	4.5	4	2.25	2.25	0.2	5	2.7	3.5	2*8	3.6
QSK60-G4	AC 2250	2250	5.9	2.3	3	9	5	5	2.8	2.7	0.2	7.5	3.1	4	2*10	4

frequency, voltage, and other electrical parameters [44]. The power of the generator is also reflected in the sound during operation. This may be different depending on the type of fuel. Diesel engines have been found to have higher operating pressures and higher noise problems compared to gasoline engines [45]. At the same time, it is possible to talk about the advantages and disadvantages of generators relative to each other. While these provide advantages because gasoline generators can be supplied in a short time, they have a short usage period, and generators with natural gas are easier to find, as well as being low in cost and difficult to transport, etc. can be exemplified as [46].

## 2.2. Noises Produced by the Generator

During the operation of generators, different noises occur depending on the source. It is important to determine critical levels according to noise sources. For these critical levels, it is recommended by the World Health Organization (WHO) that it should not be above 70 dBA. View of a generator and sound pressure levels according to the noise sources in the generator is given in Fig. 1 [47].

In Fig. 1, it was seen that the measurements were usually made at a distance of 3 feet/1 meter. The area surrounding a machine has been defined as the "near field". In terms of designing the right solutions, the measurements were made at a distance of 3 feet / 1 meter and a height of 5 feet / 1.5 meters (typical ear height range). It is possible to

reduce these levels at the source. For example, the value of 120 -130 dB(A) before the silencer is used in the engine exhaust can be reduced by only 15 dB by using the silencer. The residence time at a sound level above 90 dB should not exceed 8 hours [9]. In older generators, the sound pressure level is higher [48]. On this subject, in the study of Lee (2007), generators with a power of 5250 Watt (W) that worked less than 10 hours on average in 1 year and generators of 2250 Watts (W) that worked more than 100 hours in more than 10 years were compared. It has been determined that the older one in W power gives more sound due to vibration. In the measurements, accelerometers were placed in the horizontal and vertical directions and the study was carried out. In both generator types, the vibration peaked around 60 Hz. It has been observed that the 5250 W generator has peaked at 60 Hz (vibration during the opening and closing of the generator due to the rotational speed of the motor), while it has peaks varying up to 100 Hz in the 2250W generator, while it is in the frequency range lower than 20 Hz. While the acceleration in the horizontal axis was greater than that measured in the vertical axis, it was observed that peaks occurred at a frequency of 100 Hz in the 2250 W generator, reaching the highest level at 60 Hz. The 2250W generator acceleration and displacement is more than three times its magnitude [49]. This situation arises due to mechanical systems. In this sense, it is known that in generators with diesel engines, noise occurs with the effect of vibrations caused by the crank connecting rod mechanism, mass and

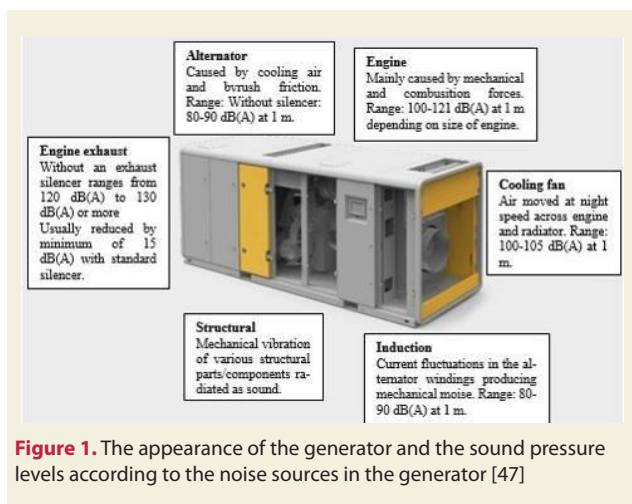


**Figure 1.** The appearance of the generator and the sound pressure levels according to the noise sources in the generator [47]

gas movements [50]. The fact that the vibration-induced noises are at the levels determined in the standards has become a situation that is expected to show parallelism in terms of the ergonomics of the working environment. Accordingly, motivation and health parameters are among the qualities to be considered. For example, the maximum allowable noise level in diesel generators was 75 dB(A) at 1 m from the closed surface in 2005 [51], in a later study it was found to be in the range of 100-110 dB without sound insulation [52]. In the study, it was determined to be 80 dB(A) at 1 m distance [53]. It has been stated that the engine room in a small ship is the loudest place in terms of the sound generated in the room where the generator is located and varies between 90-115 dB(A) and this level is usually caused by the high speed and the propeller during maneuvering [54]. The expected sound pressure level may differ depending on the type. In the standby generator, it is suggested that the sound pressure level by 56 dB LAeq, 1 hour [55]. There are also studies on generators used in different environments. In a study conducted for Nigeria, the sound pressure level in generators used in buildings was 87.4 dB [56], in another study conducted in houses/offices in Southern Nigeria, sound pressure levels were 70, 75 and 90 dB [57], again in the same country.

In the research on generators, the noise level was obtained as 91.2 -100.5 dB(A). It has been determined that these levels can be dangerous for human health because they are above the permissible limits [58].

Active and passive methods, etc., to be at the forefront of health risks, to minimize generator noise, etc. led to the development of alternative solutions. In the preference of these alternatives, OSHA (Occupational Safety and Health Administration), etc. The standards determined by the organizations are taken into account [59]. Preferred methods are applied within the framework of these standards.

### 2.3. Acoustic Solutions

The vibration occurs during the operation of generator engines. Therefore, it is recommended to wear ear-

plugs to prevent hearing loss. In addition, since carbon monoxide (CO) gas, known as a toxic gas, is colorless and odorless and has dangers that may cause the death of many people, generators should not be used indoors and ventilation should be provided in the environments where the generator is located [60]. In this regard, the fan can be described as an important device. Air transfer fans are preferred because heating occurs during the operation of engines and generators [61]. Silencer [62] etc. in pipes and ducts to reduce airborne noises. Sustainability is ensured through Life Cycle Evaluation Procedures of natural materials that can be an alternative to many synthetic materials [63].

The existence of materials with many properties in nature is an advantage. By taking advantage of the acoustic properties of these natural materials, the sound energy is reduced by transferring the acoustic pressure to the material movement [47]. In studies on this subject, it has been stated that acoustic insulation materials with up to 51 mm (2 inches) or different thicknesses and properties are used to reduce the sound pressure level [64]. In addition to the use of natural materials with acoustic properties, different studies are also carried out on the mechanical parts of the generator that cause vibration and noise. Active/passive noise and vibration control technologies are used in the design of generator engines [65]. Since the noise levels differ according to the environment where the generators are located, the studies on this subject also vary.

### 2.4. Passive Methods

Different passive methods are applied depending on the shape, size, and functional properties of generators. Parvathi and Navaneetha (2003) conducted an experimental study to prevent vibration-induced noise in portable generators with a sandwich made of rubber, fiber, polyurethane foam, wool felt, sand, cardboard, and two materials, which is one of these methods. They have reduced the pressure level by 10 dB(A) [66].

In another study, the sound pressure level in the generator was 76.3 -91.5 dB (reduction amount 15.2 dB) without taking any precautions, and these values were obtained as maximum 60.4-77.9 dB (17.5 dB decrease amount) in case of closing with a textile product [67]. Demirel et al. (2018), in the study they carried out in the generator room of an international airport, materials such as rock wool, polymer, rubber and plaster etc. It has been suggested that noise can be effectively reduced by layers that can be formed with materials [68].

In another study, where the vibration of the generator engine is reduced and quieter operation is ensured, the importance of reducing the sound pressure level without increasing the cost is mentioned. Not just the 10 dB reduction cost but 500 Hz. The cost of reducing the noise above and below also varies. Because in general, single materials 500 Hz. sound absorption capacity is very low. Ma-

terial properties are important in this regard. Therefore, it is important to reduce the sound pressure level without increasing the cost. To achieve this efficiently, some strategies are implemented. Noise reduction strategies vary depending on whether the generator is indoors or outdoors. Low-frequency noises are difficult to reduce, and high-frequency noises with rigid barriers are tried to be controlled with materials such as acoustic foam. In generators with a power up to 2,000 kW, sheet metal, etc. They apply sound reduction process by preserving them with materials such as However, special sound-insulated enclosures are used in generators with a power of more than 2,000 kW. Accordingly, in noise reduction strategies; acoustic barriers (usually steel sheet on the outer surface, a blocky sandy surface or cast wall is used on the inner walls), acoustic insulation material (acoustic foam is known to be effective in high-frequency noises), vibration isolation (with proper design of flexible fuel lines and evenings on the exhaust), vibration can be reduced), exhaust mufflers, etc. materials can be used [69].

In another study, acoustic materials are preferred because the barriers used in sections such as air inlet, exhaust and heat output in most power generators can pass noise. To obtain the sound pressure level, which is measured as 73.5 dB(A) on average in this type of generator, below 68 dB(A), the sound pressure level is obtained as 67.0 dB(A) by using an acoustic barrier applied to the polyester surface of the acoustic foam with aluminized. has been done. It has been stated that although the noises originating from the engine and exhaust have a low frequency in the range of 250 -315 Hz according to the noise source, there are high-frequency noises in the range of 1250-2000 Hz in the airflow, fan and alternator [70]. In terms of acoustics, glass wool is one of the most preferred products. Accordingly, Schnitta (2010), in his study on the production of an acoustic barrier made of 2" (2 inches= 5.08 m) thick glass wool to prevent noise in generators, measured 72.3 dB at 0.9144 meters and approximately 60 dB at 3.66 meters. doubling the distance according to the inverse square rule in a "quiet" AC capacitor, approximately 6 dB at this value, at a maximum distance of 0.9144 m from a 1.524 m tall condenser, the noise level at the barrier window is approximately 6.6 dB at 125 Hz, at a height of 10 m. found that the noise level is reduced by approximately 14.1 dB at 125 Hz when the barrier is used [71].

It is possible to reduce the noise at the desired level by producing the materials with acoustic properties mentioned above in different thicknesses. In this sense, the acoustic material in the sponge structure used effectively is given in Fig. 2. This material can be produced in different thicknesses such as 1 cm, 2.5 cm, and 5 cm [72].

The noise can be reduced by 48-85 dB(A) at a distance of 1 m when high-density stone wall-filled perforated sheet metal is used as acoustic material [73].

203.2-micron thick neoprene coated, fiberglass reinforced, aluminized polyester white or foil film (1.5 mil/38.1 micron) coating and 48 kg/m<sup>3</sup> density glass fiber in 25 mm and 50 mm thicknesses, with 25 mm thick material and Noise Reduction Coefficient (NRC) as 0.75, with 50 mm thick material, the NRC was obtained as 0.94 [74]. The NRC curves here are a report for noise criteria and are characterized by a degree of interference measured by SIL. The graph showing the NRC curves is given in Fig. 3 [75].

The relative humidity of the air causes frequency-dependent sound absorption. It reaches its highest value when the frequency increases and for relative humidity in the range of 10 -30%. Below 4kHz, the worst moisture reduction corresponds to 0.1dB/m. The reduction coefficient (%) at 20°C relative humidity for frequencies between 2 kHz-12.5 kHz is given in Fig. 4 [76].

A different material developed is made of galvanized, stainless steel mesh and rock wool, providing a 19 dB reduction in sound pressure level. The related image is given in Fig. 5 [77].

In another study to reduce noise in generators, an ultrasonic design was made. In this design, a reduction in noise in the range of 12 dB(A)-20 dB(A) is achieved by using an acoustic sponge [78]. In another study carried out to reduce noise, a casing box in which the generator



Figure 2. Acoustic material in sponge structure [72]

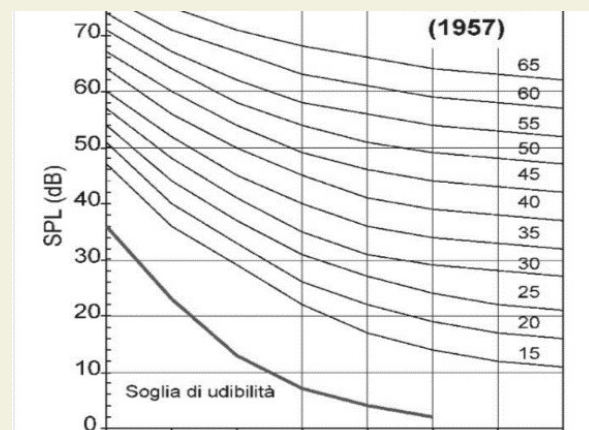


Figure 3. Graph showing NRC curves [75]

can be placed has been produced. When the inner surface of this box is also covered with an acoustic sponge, the noise is reduced by 75% in the 15-20 dB range [79]. It is also possible to place the generator in a closed environment. Standard modular acoustic panels, which are produced as closed boxes, are produced in various thicknesses and materials according to the noise control level to be provided. These materials are; It can be in the form of glass wool or mineral wool between the inner and outer steel material [80]. Ghorbani et al. (2016)'s work on reducing noise with generators working with natural gas, measurements were made by placing the generator in a 20 mm thick, steel-framed plywood material with elastomeric foam on its inner surface. Experimental operations were carried out with the generator in this box when its lid is open, with the simple enclosure

(SE), the semi-closed improved box (SME, the semi-covered modified enclosure) and the fully closed box (FME, fully covered modified enclosure). As a result of the operations performed by creating an air gap between the generator and the inner surface of the box, the generator sound

level was 93.2 dB(A) for SE, 87.2 dB(A) for SME and 87.2 dB(A) for FME before acoustic measures were taken. It was determined to be 86.1 dB(A). Measurements were made at frequencies above 800 Hz for SE, and above 250 Hz for modified ones (SME and FME). Covering the generator with plywood is given in Fig. 6 [81].

Different processes can also be applied as passive methods. As can be seen in Fig. 7, the panel system can also be used to reduce/prevent noise [82].

Ölmez et al. In the study of (2019), a solid model with a thickness of 1.5 mm and outer surfaces of 3 mm was designed for the diesel generator in 3D and using a material such as a mesh, at frequencies of 63, 100, 125 and 160 Hz, vibration related noise points were generally found in the cooling air. It has been determined that it is concentrated in the entrances and exits, doors, sound-insulated enclosure upper surfaces, and also chassis upper surfaces. Due to this situation, the wall thickness of the outer structure was increased to minimize these noises [83]. In the study of Elancheliyan (2013), for two different generators with 360-kilovolt ampere (KVA) power, one of the diesel generators used in the construction sector, 360 (generator named G1) and 500 (generator named G2); at a distance of 1 m; 103.7 dB(A) for G1 and 104.3 dB(A) for G2, when this distance is increased to 10 m, 87.7 dB(A) for G1 and 90.1 dB(A) for G2, respectively. If there is an

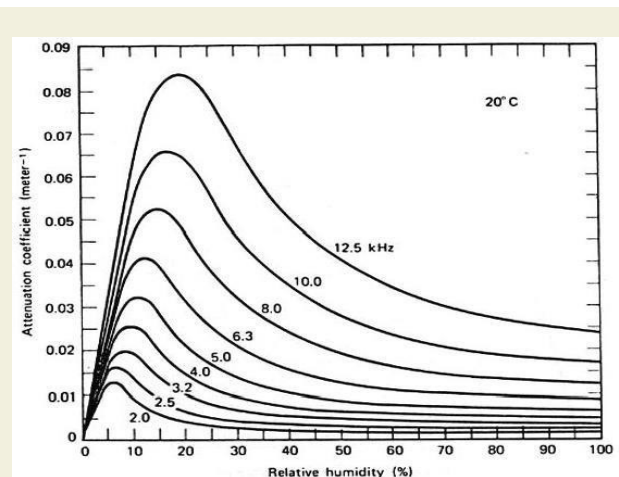


Figure 4. Reduction coefficient (%) at 20°C relative humidity for frequencies between 2 kHz-12.5 kHz [76]

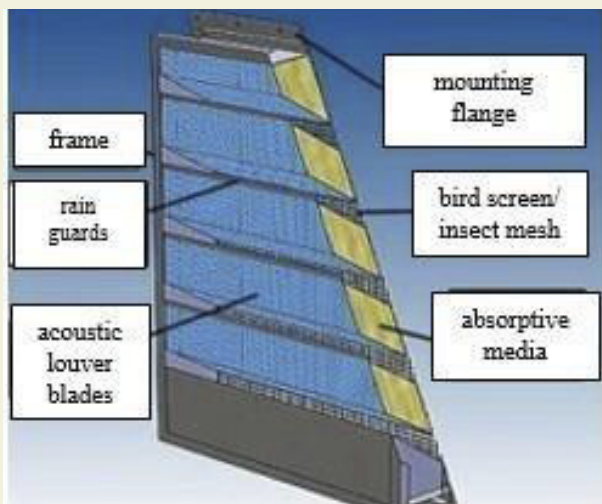


Figure 5. Design obtained from galvanized, stainless steel mesh and acoustic material [77]

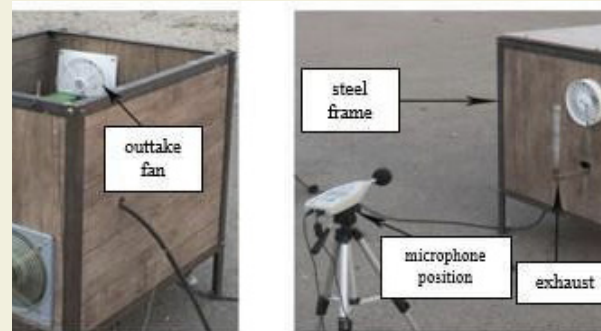


Figure 6. Covering the generator with plywood [81]

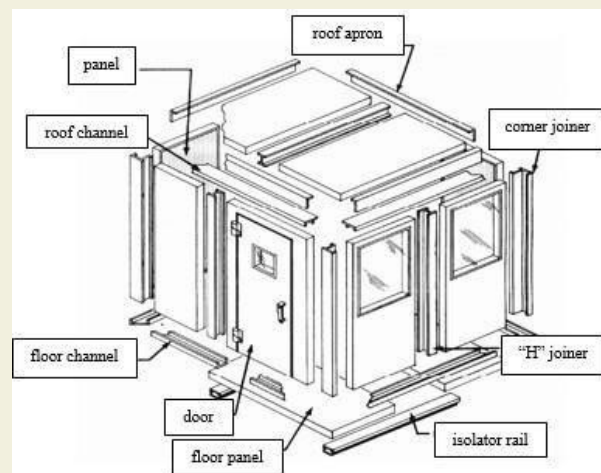
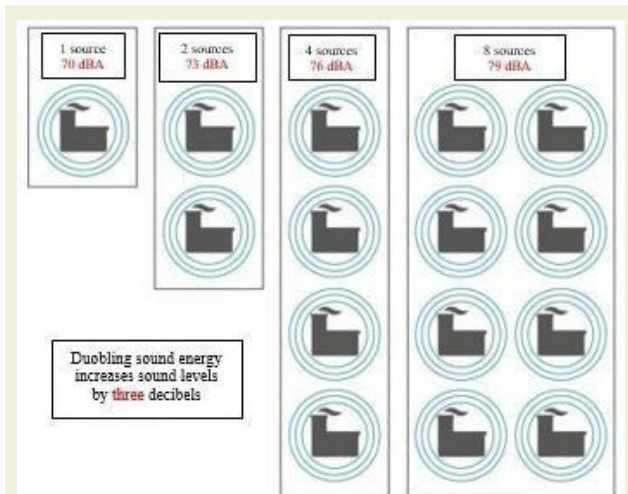


Figure 7. Panel system [82]

acoustic barrier between the generator, which is the sound source, and the measuring device, these values are; He determined that 87.6 dB(A) for G1 and 89.3 dB(A) for G2, when this distance is increased to 10 m, it is 79.9 dB(A) for G1 and 81.8 dB(A) for G2, respectively. This shows that the sound pressure level decreases as the distance to the generator increases [84].

## 2.5. Active Methods

Acoustic sensors, etc., are based on micro-electro-mechanical systems (MEMS) technology. Acoustic measurement applications are widely used in fields such as industrial, military, scientific and medical. It is also used in mass production and widely used in mobile devices such as laptops and smartphones, with lower cost and higher performance [85]. In addition, different applications have been developed for reducing the sound pressure level. By halving the number of sources, the sound pressure level is reduced by 3 dB(A). Accordingly, the change in sound pressure level is given in Fig. 8 [86].



**Figure 8.** Change in sound pressure level when the number of sound sources is halved [86]

According to Figure 8, each generator produces a factory 70 decibels of sound. If a second generator is turned on next to this generator, the sound pressure level increases by 3 dB(A) to 73 dB(A). If the number of generators increases to four, the sound pressure level rises to 76 dB(A) [86].

According to Doğru (2016), the logarithmic average of daily personal noise exposure in diesel+electric trains and generator wagon (electricity) workers is 74.62 dB(A), this value is 77.1 dB(A) in generator wagons of mainline trains and 73.8 dB(A) on average in the region where the generator car workers are located. It has been stated that the noise can be reduced by about 30 dB at low frequency with the active noise method [87]. Another application inactive control methods is the use of silencers in the generator. In a study on this subject, pre- and post-design mufflers (old and new) were compared. Ac-

cordingly, although the measurement at a distance of 1 m was 120 dB at a distance of 1 m, a measurement of 109 at a distance of 2 m and 106 dB at a distance of 3 m in the old muffler, these values were obtained as 85 dB at a distance of 1 m, a measurement of 80 dB at a distance of 2 m and a measurement of 106 dB at a distance of 3 m. distance measurement was obtained as 70 dB. They obtained optimal results in the range of 1000-2000 Hz when a silencer was used [88]. In the study of Wei and Luo (2019), it was determined that the (A) weighted noise level in diesel generators was reduced from 92.2 dB to 59.7 dB with square mufflers [89].

Ishimitsu et al. (2000) stated that active control methods were preferred to reduce the vibrations between the wall and the ground due to the wave in their study on the ship, which is an environment other than the building [90].

The sound pressure level in the engine rooms of the ships is 110 -115 dB, which is the highest value compared to other sections, and it can cause hearing damage. To prevent this negative situation, the A-weighted sound pressure level of the engine has been reduced by 3 dB by designing mechanisms such as the use of low noise engine types (gas) and components, gear hammering, improved design of engine covers and engine top casing. With new designs, it is aimed to reduce it by 5 dB [91].

Vibration and noise were analyzed in generators that are also used in yachts and ships. In the study of Jordan and Elliott (2016), loudspeakers and microphones were used in the yacht cabin by increasing the control points from 7 to 19 in the application of the active noise control system, since noise and vibration are also disturbing for yacht manufacturers. The response to noise between speaker 1 and microphone 1 is given in Fig. 9 [92].

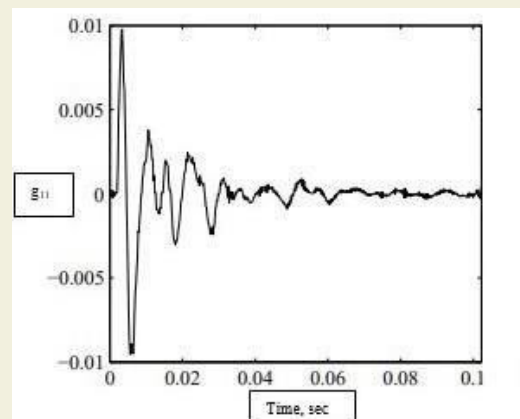


**Figure 9.** Response to noise between speaker 1 and microphone 1 [92]

As can be seen in Fig. 9, it can be seen from these results that the acoustic environment is relatively well damped with a reverberation time of about 180 ms and is characterized by multiple modes due to the size of the cabinet. As a result, it has been observed that the noise level can

be reduced up to 23 dB at frequencies of 50 Hz and above [92]. Noise sources on a ship; diesel generator engine exhaust, ventilation inlet/outlet, pumps, cooling systems etc. known as. If the sound power level from the engine is 142 dB(A) (permissible value is 135 dB(A), the sound from the exhaust is 28 -35 dB, the sound power level of the coolers is approximately 90 dB(A), 25-30 dB for radial fans, for axial fans, this value is 25-35 dB. To reduce these sound levels, it has been suggested to reduce the noise-causing components and cover them with an insulating material from the outside [93]. Therefore, there are studies on this subject in the literature, one of which is the study of Bayraktar (2006) who stated that irregularity of the fan blades may affect the acoustic properties, therefore, the fan design can be effective by analyzing it with the Finite Element Method [94].

During the operation of generators, materials known as vibration wedges are used to prevent noise caused by vibration, which is one of the problems encountered. These materials prevent the formation of low-frequency noise caused by vibrations caused by unbalanced forces in the diesel engine [95]. In another study on the prevention of vibration, the sound level was measured as 108 dB at 50 Hz frequency in a generator with a maximum output power of 8 kVA (kilo volt-ampere). To reduce this noise level caused by vibration when an experimental study was conducted with insulating materials used in the form of three separate wedges at different angles to the engine, it was understood that the one placed at an angle of 90 ° was effective in preventing the noise caused by vibration [96].

In the study of Fuller (2012) on a portable (portable) generator with 2kW (kilowatt) power, to minimize the globally radiated noise, when working on active and passive noise control, sound pressure in the frequency range of 50-600 Hz It has been seen that a reduction of 10 -13 dB can be achieved at the level [97]. In another study on portable generators, the sound pressure level was reduced by up to 3 dB(A) by applying limited layer damping to the cooling fan cover to reduce noise. When precautions are taken in many parts of the generator, it has been determined that there is a decrease of 8.5 dB(A) in the sound pressure level [98]. To solve the noise problem in generators, the image of the silencer material used is given in Fig. 10 [99].

In the study, in which both active noise control and passive noise control were applied in the diesel generator, it was reduced between 5-10 dB by the feedback control method performed on a diesel generator with a power of 45 kVA (kilo volt-ampere, 36 kW). According to the feedforward control results obtained by using the acoustic reference sensor, it was observed that the sound pressure level was obtained on average 1.0 dB(A) and better results were obtained with the feedback method [100].

With the rapid advancement of technology in re-

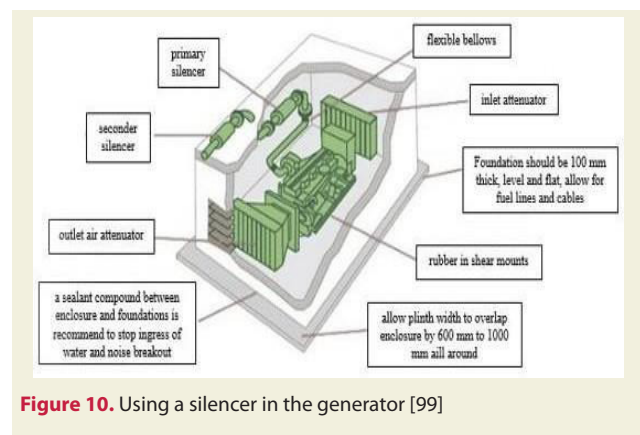


Figure 10. Using a silencer in the generator [99]

cent years, the variety of applications has increased. Regarding this, Gang et al. (2019) preferred to apply Vortex Generator (VG) Technology to the wind turbine blade in their study. In these turbines, it is requested that the sound pressure level should not exceed

44 dB when the sound speed is 8 m/s and 42 dB when the sound speed is 6 m/s. The maximum noise before adding VG is 107 dB, which corresponds to a frequency of 41 Hz (Hertz). After adding VG, the maximum noise is 83 dB, corresponding to a frequency of 45 Hz.

The sound pressure level decreases by approximately 20 dB at the frequency of 2000-4000 Hz [101]. In another study, it was stated that Acoustic Emission (with AE signals) methods could be effective in measuring vibrations caused by cylinder pressure of diesel engines [102]. According to the working principle, the noise factor can exhibit different behaviors. In this sense, it can be given as an example that electric vehicles differ from conventional internal combustion vehicles in terms of noise behavior, frequency and sound pressure level [103]. In addition, it is known that the noise in electric vehicles is less than that in internal combustion vehicles. In addition, in a study performed by producing artificial engine sound for the modification of acoustic characteristics, mechanical and combustion sounds were combined and an engine sound of gasoline and diesel vehicles were analyzed to reduce it by more than 10 dB after 1 kHz for diesel vehicles. Because as a result of the comparison, it has been determined that the diesel engine sound has a higher amount of noise after 1 kHz compared to the gasoline engine [104]. In another study by Narayan (2014), it was stated that the parameters that determine engine performance such as injection process, torque and power in diesel engines are controlled. For this, the use of filtering was preferred in the examination of injection effects by using air source motor acoustic signals and capacitors [105]. In addition to filtering, microphones can also be used in active noise and vibration control, while creating the second field of equal size, opposite to the first field [106]. According to these applied methods, there are differences in the amount of reduction in the sound pressure level. One of the examples that can be given to this situation is the reduction in sound

pressure level of at least 25 dB(A) by using a silencer in the exhaust [107].

According to the data obtained from the literature review, it has been seen that many methods can be applied by the design of the generators in noise control [108].

### 3. Results

By investigating how sensitive the human ear is to which frequencies, a chart called equal loudness contours has been developed [109]. The graph of Fletcher-Munson Loudness Curves is given in Fig. 11 [110]. It is known that an important factor regarding the speech transmission index (STI) relates to the objective parameter of speech intelligibility for voice transmission channels. Robust ergonomics studies gain importance especially for “Special buildings” sensitive to sound characteristics. The private building is divided into 4 groups depending on the behavior and effectiveness against sound. While [AG1] shows “clave buildings” whose main function is directly related to sound, [AG2]; its main function is not related to sound, it is used as warning and guidance. [AG3]; the sound is considered as ambient noise. [AG4]; These areas are very sensitive to sound. Sound level control should be provided with special techniques.

Frequency analysis is very important for noise control in such buildings. In this article, buildings are divided into 5

groups for vibration [111].

The Fletcher-Munson Loudness Curves plot shown in Figure 11a shows the human ear’s perceptual capacities of sound pressure levels at different frequencies. For sound and vibration transmission from the ground, the acceleration and deceleration period according to the frequency, noise and vibration sound pressure level (SPL) difference of Ankara Metro Railway is analyzed and given in Fig. 11b.

The graph about the vibration and noise effects on the side buildings of the Ankara Metro Rail System and the ANKARAY Light Rail system line and the high noise and vibration caused by the subway rails at the entrance to the tunnel is given in Fig. 11 b, c, d. In this sense, especially the train horn, while the noise and vibration accelerate, but the noise and vibration decrease for the deceleration period [112].

In experimental studies on audio signals distorted by impact noise, efficient results can be obtained, especially for low noise ratios, when analyzes are made by suggesting algorithms [113].

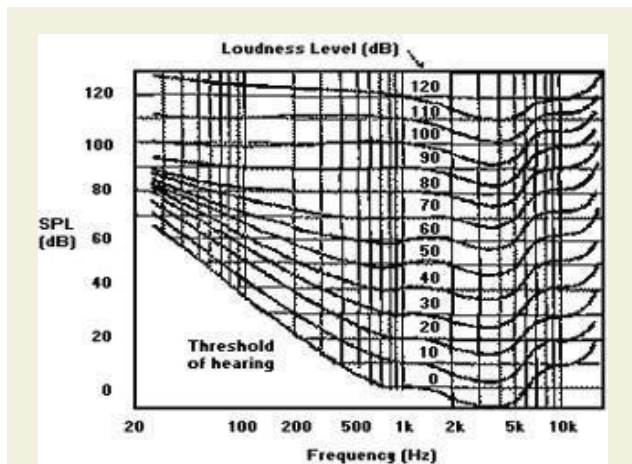


Figure 11a. Fletcher-Munson Loudness Curves [110]

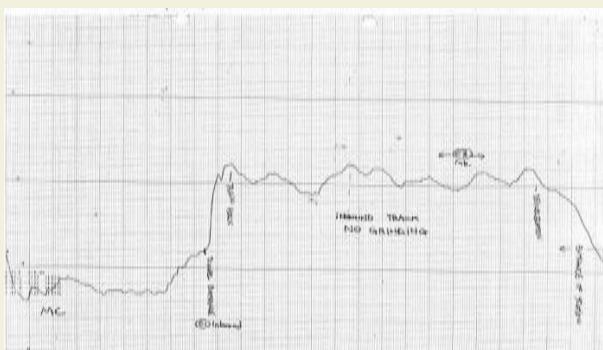


Figure 11b. SPL differences in terms of acceleration and deceleration period noise and vibration [112]

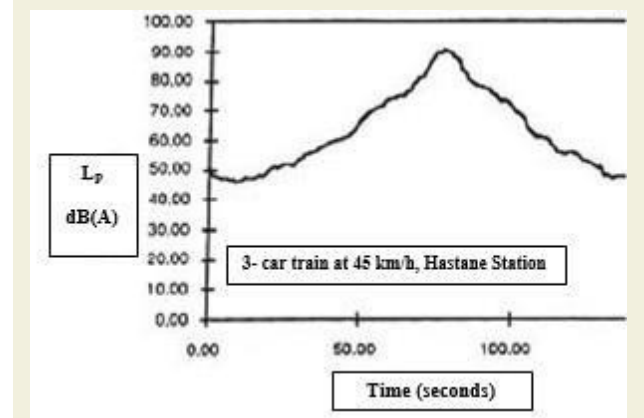
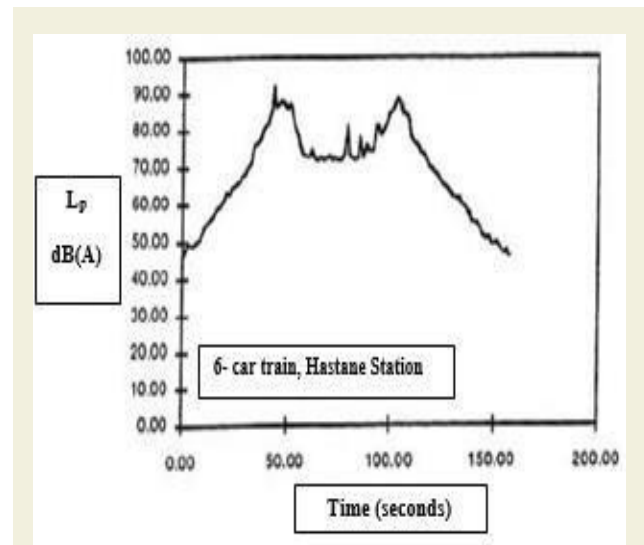


Figure 11 c, d; The subway rails cause high noise and vibration at the entrance to the tunnel, and especially the train horn accelerates the noise and vibration, but the noise and vibration are also reduced for the on period [112]

Depending on the design and condition of a vehicle's suspension/damping system, the human body has different pain thresholds. Depending on the structure and condition of the vehicle's spring / shock absorber system, sometimes painful stress may occur in the human body. However, not only the spring/damping system but also other appropriate technical protection methods for the vehicle are important. The results measured during road movement of a truck are measured in Intermediate Bulk Container (IBC) vibration tests [114].

Working committees in some countries on noise are concerned with the standardization of test methods in building acoustics. In addition to national standardization, committees actively use their influence at the European and international level. In general, much of the low interest in industrial noise and standardization in the near future is concerned with the maintenance and updating of existing standards [115].

Hydroacoustic performance analysis was performed in open water conditions by applying the TVI (Type Vortex Index) technique to estimate the noise from tip eddy cavitation for a marine propeller. In this sense, the effects of blade number, cavitation number and propagation coefficient on the propeller tip eddy cavitation noise were investigated [116]

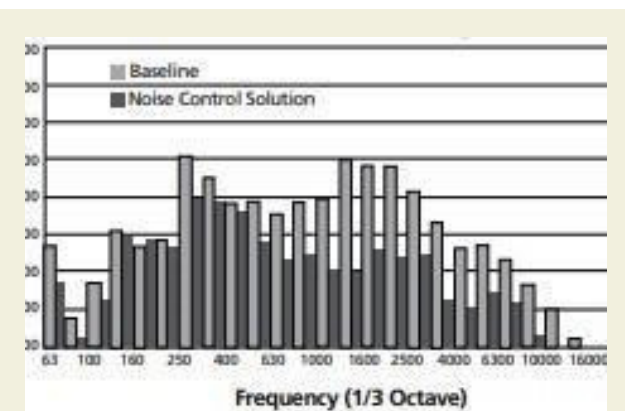


Figure 12. The sound pressure level obtained before and after using the acoustic barrier depending on the frequency [70]

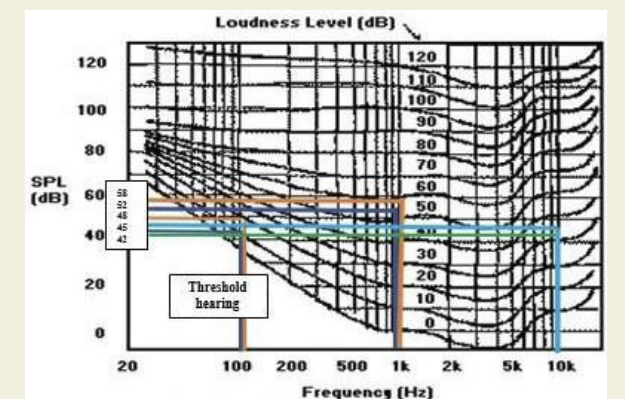


Figure 13. Comparison of the values obtained before and after using the acoustic barrier in the graph of Fletcher-Munson Loudness Curves

### 3.1. Example of Passive Method

The sound pressure values obtained before and after using acoustic barriers in sections such as air inlet, exhaust and heat output in most of the power generators are given in Fig. 12 [70].

According to Fig. 12, the sound pressure level, which was measured as 73.5 dB(A) on average, was obtained as an average of 67 dB(A) after this barrier was obtained, according to the measurements made at 8 different points before using an aluminized acoustic barrier on the polyester surface of the acoustic foam.

According to the data in Fig. 12, the sound pressure levels obtained at 100 Hz, 1k Hz and 10k Hz frequencies before and after using the acoustic barrier were compared, and the graph of Fletcher-Munson Loudness Curves is given in Fig. 13.

Sound pressure levels at 100, 1k and 10k Hz frequencies are shown in Fig. 13. According to Fig. 13; Before using the acoustic barrier, values of 48 dB at 100 Hz, 58 dB at 1k Hz, and 45 dB at 10k Hz were obtained. After using the acoustic barrier, it was obtained as 42 dB at 100 Hz and 50 dB at 1k Hz. It was observed that there was no perceived at 10k Hz. Depending on the barrier usage, the values obtained at different frequencies are given in detail in Table 2.

**Table 2.** Sound pressure levels according to frequencies before and after using acoustic barrier

Frequency (Hz)	Before Acoustic Barrier			After Acoustic Barrier		
	100	1k	10k	100	1k	10k
Sound Pressure Level (dB)	48	50	52	42	0	0
	30	58	52	52	50	50
	10	-	45	0	0	0

According to this; before using the acoustic barrier, 48 dB at 100 Hz, 50 dB at 1k Hz, 52 dB at 10k Hz, 40 dB at 1k Hz and 30 dB at 10k Hz after acoustic barrier use. has been obtained.

### 3.2. Example of active method

The data in Fig. 14 were obtained when the noise of the engine exhaust of the generator with a power of 500 kW was measured in the frequency range of 25-2548 Hz, without using a muffler [88].

According to Figure 14, sound pressure levels are approximate without the use of a silencer; 113 dB at 30 Hz, 109 dB at 60 Hz, 119 dB at 90 Hz, 111 dB at 180 Hz, and 105 dB at 270 Hz. The values obtained from the measurement results after using the silencer are given in Fig. 15 [88].

According to Fig. 15, the sound pressure levels are approximately; 71 dB at 30 Hz, 61 dB at 60 Hz, 45 dB at 90 Hz, 62 dB at 180 Hz, 58 dB at 270 Hz.

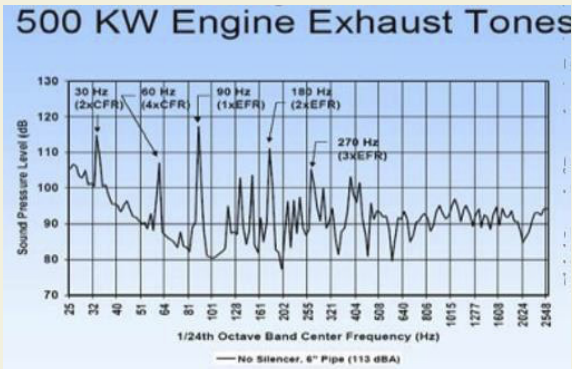


**Figure 14.** Frequency-sound pressure level graph obtained from the engine exhaust of 500 kW generator without using a silencer [88]

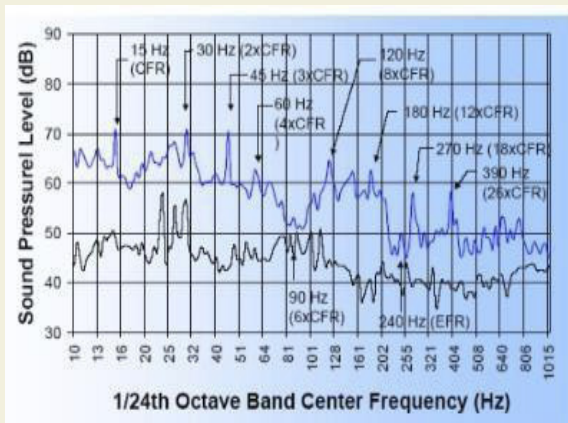


**Figure 15.** Frequency-sound pressure level graph obtained by using a silencer of the engine exhaust of a 500 kW generator [88]

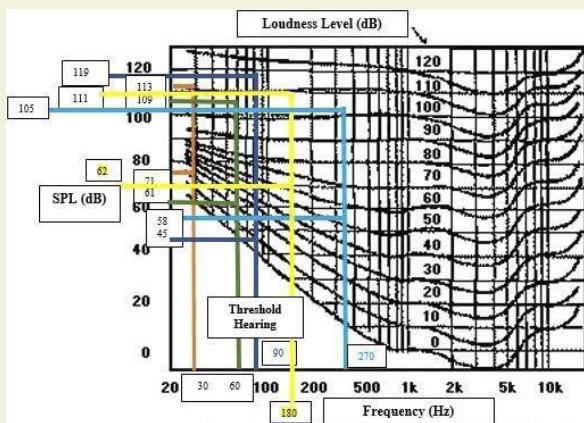


**Figure 16.** Comparison of the frequency values of the sound pressure values obtained before and after the muffler is installed in the Fletcher-Munson Loudness Curves graph

A comparison of the frequency values of the sound pressure values obtained before and after the muffler is installed in the Fletcher-Munson Loudness Curves graph is in Fig. 16.

Sound pressure levels at 100, 1k and 10k Hz frequencies are shown in Fig. 16. According to Figure 13; Before using the acoustic barrier, values of 48 dB at 100 Hz, 58 dB at 1k Hz, and 45 dB at 10k Hz were obtained. After using the acoustic barrier, it was obtained as 42 dB at 100 Hz and 50 dB at 1k Hz. It was observed that there was no

perceived at 10k Hz. Depending on the barrier usage, the values obtained at different frequencies are given in detail in Table 3.

**Table 3.** Sound pressure levels according to frequencies before and after using acoustic barrier

Frequency (Hz)	SPL (Sound Pressure Level) Before Acoustic Barrier, dB				SPL After Acoustic Barrier, dB			
	SPL	100	1k	10k	SPL	100	1k	10k
30	113	110	110	113	71	71	70	72
60	109	100	100	100	61	60	60	52
90	119	119	120	120	45	45	40	30
180	111	110	110	112	62	60	70	72
270	105	100	100	100	58	30	50	40

According to this; Before using the acoustic barrier, 48 dB at 100 Hz, 50 dB at 1k Hz, 52 dB at 10k Hz, 40 dB at 1k Hz and 30 dB at 10k Hz after acoustic barrier use. has been obtained. When the literature review is examined, silencer, acoustic sponge, glass wool etc. are used to prevent generator noise. It has been observed that materials with many sound-absorbing properties are used. As a result of the studies examined in this study, the measures taken to minimize the noise in the generator and the changes in the sound pressure level are given in Table 4.

When the data in the table are examined, it is seen that active and passive control methods are used. Although it is common to use a silencer in active methods, there is a need for improvement due to the intense fan noise. With the rapid progress of technology, felt, rock wool, etc., which have sound-absorbing and insulating properties. The use of materials is also increasing day by day. With the expansion of the product range, the preferability can be moved to better levels. As a result, more practical solutions can be developed to minimize noise.

### 4. Conclusions

In Table 2 given in the Results section, it has been observed that the sound pressure level in the generators is above 70 dB on average. This value varies according to the fuel type. In diesel generators, it was determined as 100-110 dB (92.2 dB in some models, 74 dB in diesel-electric generators, 93.2 dB in natural gas generators and 91.2-100.5 dB in electric generators).

The distance can also be effective in analyzing the noise factor in generators. Regarding this, noise levels for generators were determined to be 70 dB(A) at 7 meters and 80 dB(A) at 1 meter.

The above-mentioned values can be logarithmic or arithmetic, which is the perceived value of the human ear as a result of the measurements. Accordingly, it was obtained as 93 dB when measured logarithmically at a distance of

**Table 4.** Measures taken to minimize the noise in the generator and the amount of change in sound pressure level [52, 87, 88, 81, 66, 67, 92, 84, 93, 69, 58, 70, 89, 71, 98, 97, 72, 77, 99, 91, 101, 107]

Sequence No	Product	Sound Pressure Level Before Action dB (A)	Action taken	Sound Pressure Level After Precautions dB (A)	Explanation
1	Diesel generator	100-110	-	-	One measurement at a distance of m
		5.8			Noise exposure in the mainline engine room
2	Diesel+electric	74.62	Application of active control method	Approximately 30 dB reduction was achieved.	Generator car of the mainline trains
		77.1			Generator car of the mainline trains
		73.8			Region of employees
3	Generator	1 m at 120, the second metric at 109, 3 mt at 106.	Using a silencer	1 mt at 85, 2 mt at 80, 3 mt at 70.	-
4	In the natural gas generator	93.2	930 * 670 * 2 mm thickness, 750mm 3 in size, plywood used for closing and acoustic foam box with steel-framed boxes	88.4	-
5	Generator	-	Rubber, fiber, polyurethane foam, wool felt, sand, cardboard, 32 mm thick sand layer	A reduction of 10 dB	-
6	Generator	Max.91.5-Min.76.3, decrease 15.2	As a result of covering the generator with a textile material	Max.77.9- Min. 60.4, decrease 17.5	While outdoors
7	The generator used on a luxury yacht	-	In case of active control	50 Hz of over 23 dB 'e up is reduced.	-
8	Diesel generator	1 mt from approximately 104 dB, 10 mt approximately from 90 dB.	In the case of using barrier	1 m from 89.3 to about 10 metric tons to about 80 from.	-
9	The generator used on board	-	To reduce these noises, it has been suggested to reduce the components and to cover them with an acoustic material from the outside.	-	The noise level of the coolers is 90 dB (A), the Engine power level is 135 dB (A).
10	Generator	-	When using a quieter and less vibrating motor	In the amount of 10 dB reduction is achieved.	-
11	Electric generator	91.2-100.5	-	-	Gas emissions
12	Power generator	73.5dB(A)	In the case of using the barrier obtained by using aluminized on the polyester surface of the acoustic-foam.	67dB(A)	-
13	Diesel generator	92.2	Design in the structure of the muffler.	59.7	-
14	Generator	-	In the case of an acoustic barrier made of glass wool around the generator.	If the height of the acoustic barrier is 0.9144 m, 72.8 is obtained, and if it is 3.66 m, 60 is obtained. If it is 10 meters, 14.1 dB reduction is achieved.	-
15	Generator	-	In case of damping operation to the cooling fan cover.	3dB(A) reduction is achieved.	-
16	Generator	-	In the case of active-passive control operation .	10-13dB(A)	-
17	Generator	-	In the case of using acoustic sponges of different thicknesses.	Approximately 80% until reduction is provided.	-
18	Generator	-	In the case of using galvanized, stainless steel mesh and rock wool material.	19 dB (A) reduction is achieved.	-
19	Generator	-	In the case of using an acoustic reference sensor.	1 according to the forward feed method, 5-10 according to the feedback method.	-
20	Generator	-	Different designs of engine covers.	A reduction of 3 dB was achieved.	-
21	Vortex Generator	In the 42-107 dB range.	In the case of different designs on wind turbine blades.	A reduction of up to 20 dB was achieved.	-
22	Generator	-	In the case of using a muffler on the exhaust.	Provide a minimum of 25 dB(A) is gone.	-

7 m, and as 90.5 dB when measured arithmetically. It has been determined that the logarithmic measurement of the sound pressure level gives healthier results.

In the material method section, the definition of generators and the noise they produce are given. Acoustic solutions are analyzed under the heading of active and passive methods.

When passive methods are examined in Chapter 2, it is seen that the values measured as approximately 104 dB at a distance of 1 m (meter) and 90 dB at a distance of 10 m are reduced to 89.3 and 80 dB, respectively, in the case of using a barrier. This provides significant advantages. In case the natural gas generator is closed with a 2 mm thick plywood and steel framed box and acoustic sponge is used in this box; the sound pressure level is from 93.2 to 88.4 dB, (approximately 4.8). Rubber, fiber, polyurethane foam, wool felt, sand, cardboard, the barrier obtained as a 32 mm thick sand layer is 10 dB when the generator is closed with a textile material, the values are 60.4, 76.3-91.5 (the difference between the minimum-maximum values is 15.2 dB). It can be reduced from 73.5 dB (A) to 67 dB (A) if a barrier is formed on the polyester surface of the acoustic foam by using aluminized. It has been understood that if a different acoustic sponge is used, it can be reduced by 80%.

When the active methods are examined in Chapter 2, it is 92.2 to 59.7 dB with the design made in the silencer used in the diesel generator, 3 dB (A) with the damping process on the cooling fan cover, 10-13 dB (A) in the case of active-passive control, acoustic reference 1 according to the forward feed method, 5-

10 dB according to the feedback method, 3 dB with different design of engine covers, 20 dB in case of different designs in Vortex Generator, wind turbine blades, minimum 25 dB(A) in case of using silencer in exhaust amounts were decreased.

In diesel-electric generators, with the application of active control methods, approximately 30 dB, in case of using a silencer, values that are 120 at 1 m, 109 at 2 m, 106 dB at 3 m, 85 at 1 m, 80 at 2 m. It has been understood that it can be reduced to 70 dB at 3 meters, 3 dB with the different design of the engine covers, 10 dB with the use of a quieter and less vibrating engine, and 20 dB with the different designs of the wind turbine blades in the Vortex Generator.

According to these results, it has been seen that it is reduced by approximately 36 dB by using a silencer compared to active control methods, therefore it is a more successful method. Because, by using mufflers in sections where noise is intense, such as exhaust, a reduction in sound pressure level up to 25 dB can be achieved. In addition, no disadvantages of the silencer in terms of human health were encountered.

It has also been concluded that materials such as acous-

tic-sponges, which are preferred in passive control methods, are not as effective as active methods in terms of sound pressure level. In addition, while the use of acoustic sponges with a porous structure and sound absorption capacity, which are described as open cells, provides an advantage, it can be a disadvantage due to its synthetic content. Because in nature, nature-friendly and recyclable materials can be preferred to reduce carbon gas emissions from artificial materials.

## 5. References

- [1] Binaların Gürültüye Karşı Korunması Hakkında Yönetmelik (2017). Access address: E.T: 06.07.2021, <https://www.resmigazete.gov.tr/eskiler/2017/05/20170531-7.html>.
- [2] İzoder (2018). Binaların Gürültüye Karşı Korunması Yönetmeliği, Açıklama ve Uygulama Kılavuzu. E.T: 07.06.2021, Access address: <https://www.izoder.org.tr/dosyalar/binalarin-gurultuye-karsi-korunmasi-yonetmeliği-aciklama-ve-uygulama-klavuzu.pdf>.
- [3] Caliskan, M., Belgin, E. (2004). Noise at Work and Protection of Business, Part II Noise: Concept and Approach, Middle East Technical University Department of Mechanical Engineering, First Edition, Turkish Medical Association Publications, p. 7.
- [4] Adams, W. (2010). Noise. New Community Plan, Draft EIR. Taha 2010-074. E.T: 07.07.2021, [www.planning.lacity.org/eir/westadams/deir/index.html](http://www.planning.lacity.org/eir/westadams/deir/index.html).
- [5] Origer, T., & Associates. Southeast Greenway General Plan Amendment and Rezoning, Revised Draft Eir, City of Santa Rosa, January 28, 2019. E.T. 07.07.2021, <https://srcity.org/DocumentCenter/View/22895/Revised-Draft-EIR-Southeast-Greenway-Project>.
- [6] Keet, J. (2004). City of Tshwane Metropolitan Municipality, City of Tshwane Noise Management Policy (Second Draft), by: Calyx Prepare Environmental.
- [7] Özkan, M. O., Çiftçi, S. E., Öztürk Akbaş, A., Postalcioglu Bozcan, F. E. Guide to Combating Noise in Working Life, T.C. Ministry of Family, Labor and Social Services, General Directorate of Occupational Health and Safety. Access address: E.T: 06.07.2021, <https://www.csgeb.gov.tr/medias/12239/calismayasamindagurultuilemucadelerehberi.pdf>
- [8] Alauda, A. (2012). Noise Element, Historic Overview, Town Of Woodside General Plan. P:232. E.T. 08.07.2021, <https://www.woodsidesidetown.org/planning/general-plan-2012-0>.
- [9] International Labour Office Staff. (1984). Protection of workers against noise and vibration in the working environment pp: 64. International Labour Organisation. ISBN 92-2-101709-5.
- [10] Aciri, A., Offner, G., Nijman, E. & Corradi, R. (2015). Numerical transfer path analysis for the assessment of air-borne noise in internal combustion engines. In Proceedings of ICoEV 2015, International Conference on Engineering Vibration: Ljubljana, (pp. 7-10), Ljubljana: Faculty for Mechanical Engineering.
- [11] Gerges, S., Sehrndt, G. A. (2001). 5 Noise Sources. Occupational Exposure to Noise: Evaluation, Prevention and Control. Federal University of Santa Catarina, Mechanical Engineering Department, Noise and Vibration Laboratory.

- [12] British Standards Institution Publication, BS 5228-1:2009+A1:2014. Code of practice for noise and vibration control on construction and open sites-Part 1: Noise Licensed copy: Warrington Borough Council, 24/08/2018, Uncontrolled Copy, © BSI, ISBN 978 0 580 77749 3.
- [13] Valley A. Noise. (2000). A technical assistance series prepared by: Maine State Planning Office Maine Department of Environmental Protection, Technical Assistance Bulletins. E.T: 08.07.2021, <https://www.maine.gov/dacf/municipalplanning/docs/groundwatertabulletin.pdf>
- [14] Berger, E. H., Neitzel, R., Kladden, C. A. (2015). Noise navigator TM sound level database with over 1700 measurement values EAR 88-34/HP 3M Personal Safety Division E-A-RCAL Laboratory, Univ. of Michigan, Dept. of Environmental Health Science, Ann Arbor, MI June 26, Version 1.8. E.T: 20.12.2021, <https://studylib.net/doc/18168222/noise-navigator-sound-level-database>.
- [15] Fıçıcı, F., Dursun, B., Gökçöl, C. (2007). Investigation of Noise Originating from Wind Energy Systems, SAU. Journal of Science, II. skin, I. Number, 54-62.
- [16] Victoria, E. (2011). Noise From Industry in Regional Victoria Recommended Maximum Noise Levels from Commerce, Industry and Trade Premises in Regional Victoria. Publication 1411 October 2011 Authorised and published by EPA Victoria, 200 Victoria Street, Carlton. E.T: 05.07.2021, [www.epa.vic.gov.au](http://www.epa.vic.gov.au).
- [17] Wabarakatuh, A.W & Sejahtera, S. (2007). Guidelines for Environment Noise Limits and Control, hereby Published by the Department of Environment is a new publication to supersede the previously published Planning Guidelines for Environmental Noise Limits and Control.
- [18] Çalışkan, M., Bakırcı, E. (2011). Mapping the Environmental Noise Emitted from the Highway and Determining Its Effect on the Exterior of Buildings, 9th National Acoustics Congress, METU Culture and Congress Center, Ankara.
- [19] Technical assistance project for the capacity to implement the environmental noise Directive Europe Aid/131352/D/SER/TR Technical Assistance Project for the Capacity to Implement the Environmental Noise Directive, (2015). Turkey Annex A: Catalog of Possible Noise Reduction Measures, Output 8.1, APPENDIX A: Possible noise reduction measures Catalog 28 August 2015. E.T: 24.07.2021, [www.kmo.com.tr](http://www.kmo.com.tr).
- [20] Noise Mapping Guide, (2008). Harmonization and Implementation of EU Directives on Environmental Noise Assessment and Management European Union Twinning Project. TR/2004/IB/EN/ 02 Noise Mapping Guide.
- [21] Hermes, M. (2016). Understanding commercial and industrial generator noise, Generac Power Systems, 1-3, E.T: 08.07.2021, [https://www.generac.com/industrial/generac-industrialpower/media/library/Whitepapers/PDFs/Generac-Industrial-Power\\_Whitepaper\\_Commercial-Industrial-Generator-Noise.pdf](https://www.generac.com/industrial/generac-industrialpower/media/library/Whitepapers/PDFs/Generac-Industrial-Power_Whitepaper_Commercial-Industrial-Generator-Noise.pdf).
- [22] Toprak, R., & Aktürk, N. (2002). Raylı ulaşım sistemlerinin neden olduğu gürültü ve çevresel etkileri. Türkiye Mühendislik Haberleri, 417, 33.
- [23] Reclamation, managing water in the west, Resource Management Plan Navajo Reservoir Area Colorado and New Mexico Final Environmental Assessment and Finding of No Significant Impact US, Department of the Interior Bureau of Reclamation Upper Colorado Region Western Colorado Area Office Grand Junction - Durango, Colorado, E.T: 08.07.2021, <https://www.usbr.gov/uc/envdocs/ea/navajo/NavajoResRMP-FEA.pdf>
- [24] Teiche, K., Planner S. (2020). City of larkspur staff report. Honorable Mayor Way and the Larkspur City Council. City Council Meeting.
- [25] Diesel Generators Technical Specification. UNHCR The UN Refugee Agency, March 2017. E.T: 20.07.2021, <https://www.coursehero.com/file/94547820/Annex-A-Diesel-Generators-TORpdf/>.
- [26] Rosborough, R. (2016). Generator Sound Pressure Level Calculations Electric Power, Caterpillar Inc. LEXE1169-01, E.T: 20.07.2021, <https://www.petersonpower.com/sites/power/files/2017-10/Generator-Sound-Levels.pdf>.
- [27] Arevalo, E. What is the allowable noise level and the distance of dB measurement for generator sets? E.T: 05.07.2021, [www.powercity.ph](http://www.powercity.ph).
- [28] Noise and vibration, (2014). Environmental Impact Analysis Noise and Vibration, Environmental Impact Report, City of Malibu, Malibu Civic Center Wastewater Treatment Facility Project, ICF 00123.13.
- [29] International Standard ISO 8528-10. Reciprocating internal combustion engine driven alternating current generating sets. Part 10: Measurement of airborne noise by the enveloping surface method, First Edition 1998-10-01.
- [30] Ministry of environment and forestry, environmental noise action plan 2019-2020. E.T: 24.06.2021, [www.cevreorman.gov.tr](http://www.cevreorman.gov.tr).
- [31] Diesel engine generator group installation recommendations manual, Aksa Generator. E.T: 06.06.2021, [www.diesel.aksa.com.tr](http://www.diesel.aksa.com.tr).
- [32] Karataş, M. Y., Erçetin, R. (2018). Scada Applications in Diesel Generators. Journal of Istanbul Aydın University, 10(4); 113-126.
- [33] İstanbulluoğlu, H., & Kır, T. (2016). Mesleki gürültü maruziyeti (Askeri personel örneği). TAF Preventive Medicine Bulletin, 15(4).
- [34] Bies, A. D., Hansen, C. H. (2003). Engineering noise control, theory and practice, 3th. London and New York: Spon Press, 2003.
- [35] De Bow, S. (2008). Town of brook line Massachusetts, November 18, Special Town Meeting, Special Town Meeting Article 3-Supplement No. 1 Page 1.
- [36] Industrial generators the 10 key points which make the difference, 6kVA-830kVA, 5kW-750kW, 50HZ-60HZ Power Products, Kohler SDMO, PPR-GC-DO-EN-71. E.T: 6.06.2021. <http://www.kohler-sdmo.com>.
- [37] Why should we have sound insulation?, E.T: 05.06.2021, [www.izoder.org.tr](http://www.izoder.org.tr).
- [38] Koçyiğit, F. B. (2014). Comparative Study on: Acoustic Properties of Renovated Historic School Buildings and New School Buildings. Atılım University Publications.
- [39] Korkmaz, K., Generator Selection Criteria, E.T: 05.06.2021, [www.emo.org.tr](http://www.emo.org.tr).
- [40] Department of Airports, Airport Electrical Systems, Publication No: HAD/T-26, ISBN: 978-975-493-076-4, Septem-

- ber 2016, Ankara. E.T: 05.06.2021, [www.shgm.gov.tr](http://www.shgm.gov.tr).
- [41] Moore, D.J. (2013). Condition monitoring of diesel engines faculty of engineering and physical sciences school of mechanical, A thesis submitted to The University of Manchester for the degree of Doctor of Philosophy in the Faculty of Engineering and Physical Sciences, Aerospace and Civil Engineering.
- [42] Demir, B.T. (2015). Generator selection and synchronization. IV. Electrical Installation National Congress and Exhibition, Security in Electrical Facilities, Chamber of Textile Engineers İzmir Branch, 21-24 October 2015, Tepekule Congress and Exhibition Center, İzmir.
- [43] Aksa Power Generation. Diesel engine generator assembly installation recommendations handbook. E.T: 20.07.2021, [www.aksa.com.tr](http://www.aksa.com.tr).
- [44] Nanahara, T., Yamashita, K., Inoue, T., Iramina, A., & Asato, S. (2005). Identification of system characteristics of a power system with time series data. Identification of frequency fluctuation characteristics of a small-scale isolated system. *Electrical Engineering in Japan*, 150(3), 23-31.
- [45] Narayan, S. (2013). Effect of dwell time on noise radiated from diesel engine. *International Journal of Applied Engineering Research*, 8(11), 1339-1347.
- [46] Electricity Generator. E.T: 20.07.2021, <https://electricinfo.com/generator-nedir/>.
- [47] White paper, Silencing and sealing in gensets: a comprehensive approach. Recticel Flexible Foams. E.T: 21.07.2021, [www.recticelflexiblefoams.com](http://www.recticelflexiblefoams.com).
- [48] Howe, B., & Principal, P. E. (2010). Low frequency noise and infrasound associated with wind turbine generator systems: a literature review. Ontario: Ministry of the Environment RFP, 1-51.
- [49] Lee, A. (2007). Portable generator vibration measurements, U.S. Consumer Product Safety Commission Directorate for Engineering Sciences.
- [50] Kangasperko, A. (2018). Mitigation of diesel generator vibrations in nuclear applications, Thesis (Master's). Aalto University School of Engineering.
- [51] Bhawan, P., & Nagar, E. A. (2020). Central Pollution Control Board, Determination of Environmental Compensation to be recovered for violation of Hazardous and Other Wastes (Management and Transboundary Movement) Rules, 2016
- [52] Teksan, maintenance and operation manual diesel generator sets, reliable power always with you. E.T: 24.07.2021, [www.teksan.com](http://www.teksan.com)
- [53] Bala, S. S. (2014). Noise and emission limit for in-use generator sets. Central Pollution Control Board, Ministry of Environment. Forests, Govt. of India, 20th November, 2014B-12013/30/2009/PCI-I 2014.
- [54] Gloza, I. Underwater ship passport, Naval University of Gdynia. E.T: 25.07.2021, [www.yadda.icm.edu.pl](http://www.yadda.icm.edu.pl).
- [55] Cockcroft, P., Lyons, R., Canham, R. (2016). Noise surveys and assessment for relocation of stand by generator and noise limits for proposed M&E Plant, Christie's, WBM Acoustic Consultants, London.
- [56] Wahab, A. (2018). Characterization and Effects of Noise Levels of Portable Generators Used in Residential Buildings in Ibadan Metropolis, Nigeria: A Case Study. *Journal of Sustainable Architecture and Civil Engineering*, 22(1), 49-63.
- [57] Ibadode, O., Tenebe, I. T., Emenike, P. C., Adesina, O. S., Okougha, A. F. & Aitanke, F. O. (2018). Assessment of noise-levels of generator-sets in seven cities of South-Southern Nigeria. *African Journal of Science, Technology, Innovation and Development*, 10(2), 125-135.
- [58] Yesufu, L. A., Ana, G. R. E. E., & Umar, O. Z. (2013). Knowledge and perception of noise induced health hazards associated with generator use in selected commercial areas in Ibadan, Nigeria. *International Journal of Collaborative Research on Internal Medicine & Public Health*, 5(9), 581-595.
- [59] Froehlich, P. (2013). Noise Pollution in the Laboratory, Parker Hannifin Corporation, 1-4.
- [60] Using portable generators safely, OSHA Fact Sheet. E.T: 05.06.2021, [www.osha.gov](http://www.osha.gov).
- [61] Design guide for heating, ventilating, and air conditioning systems, reclamation managing water in the west. Design guide for heating, ventilating, and air conditioning systems, February 29, 2000, 8:09 -Last Rev: September 21. E.T: 24.07.2021, <https://www.usbr.gov/tsc/techreferences/mands/mands-pdfs/HVACManl.pdf>, (2006).
- [62] Noise, Caterpillar, application and installation guide. E.T: 09.07.2021, <http://www.scribd/document/481933784/NOISE-LEBW4973-03-pdf>.
- [63] Asdrubali, F., Schiavoni, S., & Horoshenkov, K. V. (2012). A review of sustainable materials for acoustic applications. *Building Acoustics*, 19(4), 283-311.
- [64] The Midwest's most trusted generator distributor. E.T: 24.06.2021. [http://ps.buckeyepowersales.com/wp-content/uploads/2020/06/KD800\\_SS\\_20.pdf](http://ps.buckeyepowersales.com/wp-content/uploads/2020/06/KD800_SS_20.pdf)
- [65] Krishna, C. R., J.E. Wegrzyn (1999). Survey of noise suppression systems for engine generator sets. (No. BNL-67163; 400403209). Brookhaven National Lab. (BNL), Upton, NY (United States).
- [66] Parvathi, K. & Gopalakrishnan, A. N. (2003). Studies on control of noise from portable power generator. In *Proceedings of the Third International Conference on Environment and Health*, Chennai, India, 328-338.
- [67] Hammad, U., Aizaz, A., Khan, A. A. & Qurehi, T. (2013). Design and development of noise suppression system for domestic generators. *European Scientific Journal*, ES, 4(special), 526-533.
- [68] Demirel, F., Gorkem, M., & Ozcetin, Z. (2018). Noise control and vibration insulation study for an international airport building generator room. *International Journal of Scientific and Technological Research*, 4(5), 11-21.
- [69] Bloxsom, W. (2019). Understanding and Implementing Generator Set Noise Control Sound Science. MTU Onsite Energy. Understanding Generator Set Noise Control. ©2019/ // / MTU Onsite Energy. E.T: 25.07.2021, [https://www.mtu-solutions.com/content/dam/mtu/download/technical-articles/20210\\_Sound\\_Science\\_WP.PDF/\\_jcr\\_content/renditions/original./20210\\_Sound\\_Science\\_WP.PDF](https://www.mtu-solutions.com/content/dam/mtu/download/technical-articles/20210_Sound_Science_WP.PDF/_jcr_content/renditions/original./20210_Sound_Science_WP.PDF)
- [70] Gries, D. (2004). Noise control solutions for standby power generators. Aero EAR Specialty Composites, Indianapolis, IN, 1-7.

- [71] Schnitta, B. Special mounts, Acoustic blankets, and properly sized barriers are all part of the solution. Soundproofing Outdoor Generators and Condensers, November 2010. E.T: 07.02.2021, <http://www.soundsense.com/wp-content/uploads/2013/06/JLC-article-Nov-2010-Soundproofing-Outdoor-Generators-and-Condensers.pdf>
- [72] Adetaş, E.T: 05.06.2021, <https://www.adetasyapi.com/jenerator-odasi-ses-izoolasyon>.
- [73] Power electrics expands hybrid fleet with £2m investment, E.T: 07.06.2021, <http://power-electrics.com/blog/5-ways-to-make-make-your%20generator-quiter>.
- [74] Kinetics noise control. E.T: 07.06.2021, <https://kineticsnoise.com/industrial/s4.html>.
- [75] Cirillo, E., d'Alba, M., & Martellotta, F. (2006). Rumore e attività lavorativa negli uffici. *La Medicina del Lavoro*, 97(6), 749-761.
- [76] Chen, Z., & Maher, R. (2004). Atmospheric sound propagation considerations for the Birdstrike Project. Montana State University Proprietary.
- [77] dB Noise Reduction offers a wide range of custom designed products and services to meet the specific needs of your application, E.T: 05.06.2021, [http://www.dbnoisereduction.com/tecnical\\_data\\_and\\_specifications/tds04\\_acoustic\\_louvers.php](http://www.dbnoisereduction.com/tecnical_data_and_specifications/tds04_acoustic_louvers.php).
- [78] Generator sound insulation cover: ALPHAfon- IC, E.T: 07.06.2021, <https://alphacoustic.com/en/product/generator-sound-insulation-cover/>.
- [79] Nitrogen generator noise reduction enclosure. E.T: 07.06.2021, <http://www.msnoise.com/nitrogen-generator-noise-reduction-enclosure.html>.
- [80] eNoise control, acoustic blankets, specializing in acoustics, noise & vibration control, 317 -774-1900. E.T: 07.06.2021, [www.enoise.control.com](http://www.enoise.control.com).
- [81] Hassan-Beygi, S. R., & Ghobadian, B. (2016). Noise reduction of a portable generator set driven by small natural gas engine using an acoustic enclosure. *Agricultural Engineering International: CIGR Journal*, 18(3), 159-170.
- [82] eNoise control. Steel Sound Enclosure Installation Manual. E.T: 24.06.2016, [https://www.enoisecontrol.com/wp-content/uploads/2019/01/Installation\\_Instructions-eNoise\\_Steel\\_Sound\\_Enclosure.pdf](https://www.enoisecontrol.com/wp-content/uploads/2019/01/Installation_Instructions-eNoise_Steel_Sound_Enclosure.pdf)
- [83] Ölmez, U., Bayhan, N., Doğan, H., & Uysal, M. (2019). Detection of Structural Vibration-Induced Noises with Modal Analysis in Diesel Generators. *Electrica*, 19(1), 72-84.
- [84] S, Elanchelian. (2013). Noise effects of generator sets at construction sites. *International Journal of Occupational Safety and Health*, 3(2), 12-17.
- [85] Toro, K. A. A. (2019). Modernizing infrasound systems: characterization and analytics approaches for next generation sensors (Doctoral dissertation, University Of Hawai'i At Mānoa).
- [86] Jarrett Smith, A., Claffin, A., Kuskie, M. A Guide to noise control in minnesota acoustical properties, measurement, analysis, and regulation minnesota pollution control agency, November 2015. E.T: 08.06.2021, <https://pca.state.mn.us/sites/default/files/p-gen6-01.pdf>.
- [87] Doğru, Ö. (2016). Investigation of noise exposure in train workers. T.R. Ministry of Labor and Social Security, General Directorate of Occupational Health and Safety, Occupational Health and Safety Specialization Thesis, ANKARA.
- [88] Uddin, M. N., Rahman, M. A., & Sir, M. (2016). Reduce generators noise with better performance of a diesel generator set using modified absorption silencer. *Global Journal of Research In Engineering*, 16(1), 41-54.
- [89] Wei, L., & Luo, Y. (2019). Simulation-based structural design of diesel generator mufflers and their performance analysis. *International Journal of Simulation and Process Modelling*, 14(1), 64-71.
- [90] Ishimitsu, S., Kitagawa, H., Hagino, N., & Horihata, S. (2000). Active control of the room noise of ship by the correlation analysis of measured wavelet, internoise.
- [91] Lamula, L., Saine, K., Saarinen, K., & Hyrynen, J. (2008). Cylinder pressure generated noise of medium speed diesel engine. *Proceedings of Joint Baltic-Nordic Acoustics*, 1-5.
- [92] Cheer, J., & Elliott, S. J. (2016). Active noise control of a diesel generator in a luxury yacht. *Applied Acoustics*, 105, 209-214.
- [93] Register, O. D. S. (2010). Noise from ships in Ports: Possibilities for Noise Reduction. Danish Environmental Protection Agency.
- [94] Bayraktar, S. (2006). Theoretical and experimental investigation on centrifugal fan with a special interest on fan noise.
- [95] Doğan, H., Uysal, M. Noise control solutions in diesel generator sets. *Teksan, Article/Diesel Generator*, E.T: 24.07.2021, <https://www.teksan.com/Files/noise-control-solutions-for-diesel-generator-sets.pdf>
- [96] Hündürel, M. (2011). Optimum isolation of vibrations of a single cylinder diesel generator. Istanbul University, Doctoral dissertation, Institute of Science and Technology, Department of Mechanical Engineering.
- [97] Fuller, C. R., Papenfuss, C., & Saux, T. D. (2012). Active-passive control of portable generator set radiated noise. In *Proceedings of Acoustics*, pp. 21-23.
- [98] Tandon, N., Nakra, B. C., Ubhe, D. R., & Killa, N. K. (1998). Noise control of engine driven portable generator set. *Applied acoustics*, 55(4), 307-328.
- [99] Aaberg, D. Generator Set Noise Solutions. E.T: 09.06.2021, <https://800nonoise.com/tutorials/generator-set-noise-solutions/>.
- [100] Boone, A. J. (2006). Active minimization of acoustic energy density to attenuate radiated noise from a diesel generator. Brigham Young University.
- [101] Gang, L., Zhengtao, Z., & Pingguo, Z. (2019, December). Numerical study on noise reduction of wind turbine blade vortex generator. In *IOP Conference Series: Earth and Environmental Science* (Vol. 358, No. 2, p. 022026). IOP Publishing.
- [102] Lowe, D. P. (2013). Characterisation of combustion related acoustic emission sources for diesel engine condition monitoring (Doctoral dissertation, Queensland University of Technology).
- [103] Pallas, M. A., Kennedy, J., Walker, I., Chatagnon, R., Bérenghier, M., & Lelong, J. (2015). Noise emission of electric and hybrid electric vehicles. Final report of FOREVER WP2, CEDR.

- [104] Min, D., Park, B., & Park, J. (2018). Artificial engine sound synthesis method for modification of the acoustic characteristics of electric vehicles. *Shock and Vibration*.
- [105] Narayan, S. (2014). Analysis of Combustion Noise in Diesel Engines. *Acta Mechanica Slovaca*, 18(3-4), 28-34.
- [106] Winberg, M. (2005). Noise and vibration control of combustion engine vehicles (Doctoral dissertation, Blekinge Institute of Technology).
- [107] Bhawan, P., Nagar, E. A. (2019). Noise Regulations In India, Central Pollution Control Board Ministry of Environment&Forests, Pollution Control Law Series: PCLS/06no-oo-O I.
- [108] Feth, L. L. (1970). A pseudorandom noise generator for use in auditory research. *Behavior Research Methods & Instrumentation*, 2(4), 169-171.
- [109] Ufuk Önen ile Ses Kayıt ve Müzik Teknolojileri, E.T: 08.06.2021, <http://www.ufukonen.com/en/fletcher-ve-munson-egrileri.html>.
- [110] Koçyiğit, F. B. (2021)..Acoustic lecture notes,
- [111] Koçyiğit, F. B. (2009). Analysis of frequency band factor for sound ergonomics in three different types of special buildings. *Technology*, 12(4): 245-257.
- [112] Koçyiğit, F.B. (2010). Railway vibrations transmitted through the ground and the effect of vibrations on building case study from Ankara. *Technology*, 13(2): 71-83.
- [113] Awad, A. (2019). Impulse noise reduction in audio signal through multi-stage technique. *Engineering Science and Technology, an International Journal*, 22(2), 629-636.
- [114] Erhard, A., Goedecke, T., Pöttsch, M., & Nitsche, M. (2010). Vibrations-und Stoßbelastungen an IBCs und Tankfahrzeugen. *Materials Testing*, 52(1-2), 63-70.
- [115] Schmitt, M. (2006). Normung von Prüfverfahren in der Bauakustik. *Materials Testing*, 48(3), 78-79.
- [116] Sezen, S., Doğrul, A., & Bal, Ş. (2018). An empirical approach for propeller tip vortex cavitation noise. *Sigma Journal of Engineering and Natural Sciences*, 36(4), 1127-1139.

# Comparison of pure-hydrogen production performances of blast furnace slag, and metal powders in sodium borohydride hydrolysis reaction

Feride Cansu İskenderoğlu<sup>1</sup>, Mustafa Kaan Baltacıoğlu<sup>2\*</sup>

<sup>1</sup>İskenderun Technical University, Faculty of Engineering and Natural Science, Mechatronics Engineering Department, Hatay, 31200, Turkey

<sup>2</sup>İskenderun Technical University, Faculty of Engineering and Natural Science, Mechanical Engineering Department, Hatay, 31200, Turkey

**Orcid:** F.C. İskenderoğlu (0000-0003-4083-677X), M.K. Baltacıoğlu (0000-0002-4082-902X)

**Abstract:** In this study, hydrolysis reaction performances of raw BFS powder and metal powders (which are ingredients of BFS) that are used as a catalyst are compared. Hydrogen generation by hydrolysis reaction of the Al and Fe<sub>2</sub>O<sub>3</sub> Nano&Granule powders with sodium borohydride (NaBH<sub>4</sub>) addition in water was studied by using different catalysts amounts at reaction vessels. The measured values of reaction temperatures and hydrogen flow rates were measured by using high-precision equipment. As a result of the obtained data, it was determined that Fe<sub>2</sub>O<sub>3</sub> and Al catalysts have advantages over hydrogen production rate and fuel conversion, also, these experiments show a very high success in different parameters, and create promising effects in the reactions. Among the Al catalyst samples, the highest efficiency performances are achieved with Al Nanocatalyst samples at 85.31 °C preheat with an instantaneous hydrogen generation rate of approximately 11.226 L / min for 33 minutes. Among the Fe<sub>2</sub>O<sub>3</sub> catalyst samples, the highest efficiency performances are achieved with Fe<sub>2</sub>O<sub>3</sub> Nanocatalyst samples at 50 °C preheat with an instantaneous hydrogen generation rate of approximately 29.91 L / min for 12 minutes.

**Keywords:** Metal powders, NaBH<sub>4</sub>, Hydrogen production, Nano Material, Blast Furnace Slag

## 1. Introduction

Today most of our energy needs are provided by fossil fuels. Fossil fuel sources are limited as they are non-renewable energy sources, also, are rapidly being depleted with the increase in industrialization. Although fossil fuels seem useful to meet energy needs, serious damage is caused to the environment during the extraction and transportation process, thus, creating very harmful environmental effects of the fossil fuel resources. Since the main component of fossil fuels is carbon, they emit greenhouse gases (CO<sub>2</sub>, CH<sub>4</sub>, N<sub>2</sub>O) that are harmful to the atmosphere when they are combusted. Due to this, air pollution problems arise [1]. Due to the decrease in the reserves of fossil energy resources and the damage they cause to the environment, a search for new energy resources has been started. As a result of this search, renewable energy resources have increased interest in them. These resources are the most ideal energy sources for continuous energy needs and clean energy [2].

Opportunities of rapid technological change such as renewable energy sources, which are more environmentally

friendly and more efficient, will come into play for energy production in a sustainable future. One of these sources is hydrogen, which can be used as an energy raw material in today and the future. As one of the renewable energy sources, hydrogen is a great hope to reduce the ever-growing energy need and environmental pollution. Although hydrogen gas has many advantages, its biggest disadvantage is storage difficulty. Due to its low density, it must be stored in high-pressure tanks to provide sufficient fuel to the systems, thus increasing the storage cost [3]. Hydrides have been preferred in recent years due to their high hydrogen volume and reliability. Many types of hydrides such as metal hydrides and chemical hydrides are used in obtaining hydrogen. Examples of the most popular chemical hydrides are NaBH<sub>4</sub>, NH<sub>3</sub>, and MgH<sub>2</sub>. Borohydrides such as NaBH<sub>4</sub> are preferred due to their environmental friendliness, non-flammability, and stability in alkaline solutions [4]. A popular way to obtain hydrogen is using sodium boron hydride (NaBH<sub>4</sub>) which is a purposive hydrogen carrier. Therefore, among the chemical hydrides, NaBH<sub>4</sub> is the most studied and researched [5].

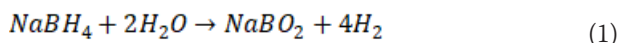
\* Corresponding author.  
Email: mkaan.baltacioglu@iste.edu.tr



Some of the main advantages of  $\text{NaBH}_4$  can be listed as;

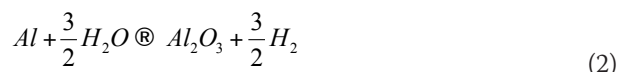
- i) High ability to produce hydrogen at room temperature,
- ii) It is a hydrogen reservoir and has a high hydrogen density (About 10%),
- iii) It has a high reduction,
- iv) It has easy storage and transportation features.

As shown in Equation 1, hydrogen gas and Sodium Metaborate ( $\text{NaBO}_2$ ) are released end of the reaction of  $\text{NaBH}_4$  with water,  $\text{NaBH}_4$  can be synthesized from  $\text{NaBO}_2$  which is a by-product. As a result of the study done by Schlesinger, it was observed that  $\text{NaBH}_4$  hydrolysis was slow at room temperature [6]. Adding catalysts to the hydrolysis reaction increases hydrogen production by reducing the activation effect [5,7]. Most of the  $\text{NaBH}_4$  hydrolysis studies are based on more efficient and faster hydrogen gas generation than the hydrolysis reaction. The various chemicals used during hydrolysis reactions, it is aimed to produce hydrogen gas in a faster and more sustainable manner.



In the literature, the effect of the catalyst used in the hydrolysis of  $\text{NaBH}_4$  depends on the large area of the surface, high conductivity or high degree of graphitization, a suitable pore structure to ensure mass transport, and the number of metal particles. Metal-containing catalysts used as catalysts in hydrogen production reactions from  $\text{NaBH}_4$  have high catalytic activity. Noble metal-based catalysts such as Ru, Pd, and Pt are used in the hydrolysis reaction of  $\text{NaBH}_4$  [7–9]. These catalysts have been observed to greatly increase the catalytic activity of the reaction, but their use is limited due to their rare and costly properties in the industrial field. In studies where transition metals such as Co, Ni, Fe, and Cu are used, it is expected that these metal catalysts will be used as high-efficiency catalysts, considering the high catalytic activity of Ni and Co metal catalysts and because they are less costly than noble metals. Efforts to synthesize cheaper catalysts are quite popular. Therefore, metal powders are produced from industrial wastes such as  $\text{Al}_2\text{O}_3$  [10],  $\text{SiO}_2$  [11],  $\text{TiO}_2$  [12], activated carbon [13] or metal-rich clays [14,15], zeolite [16,17] scanning electron microscope (SEM) and ceramics [18]. New catalysts can be synthesized for use in hydrogen production reactions [14]. İskenderoğlu et al. examined the catalytic activity of the raw BFS powder in hydrolysis reactions. The hydrogen production of raw BFS catalyst, which is used with 10%  $\text{NaBH}_4$  by weight in the reaction at  $50^\circ\text{C}$ , is  $54.63 \text{ L}/\text{min}_{\text{catalyst}}$  [19].

Also, Al and water react to hydrogen generation, and the hydrogen gas can be released by the reaction shown in equation 2 at a high temperature or high pressure [20].



The results of Zhu et al.'s study show that for Al powder with 7%  $\text{NaBH}_4$  addition by weight, the maximum hydrogen volume concentration obtained by using steam is approximately 21,000 ppm at  $650^\circ\text{C}$  [21].

In this study, the effects of both BFS powder and Al and  $\text{Fe}_2\text{O}_3$  metal powders in the content of BFS powder on the hydrolysis reaction of Nano and Granule forms were examined and the results of the experiments were compared. The fact that these metal powders have not been used in studies in the literature before, and the effect of metal powders used in different amounts in the experiments, the effect of BFS powder or HCl acid addition on the test results, makes this study different from its counterparts. As a result, it is aimed to produce efficient hydrogen gas by using a cheaper, more environmentally friendly catalyst material than other catalysts, like many catalyst articles in the literature. In addition to all these, another factor that makes this article special is that the catalyst used is a product that can be obtained from waste product without requiring any processing and by considering the use of zero waste. According to the results obtained as a result of the experiments, it has been proven that the addition of HCl acid to  $\text{Fe}_2\text{O}_3$  metal powder, which has not been used in hydrolysis experiments before, has a noticeable efficiency effect on hydrogen production.

## 2. Materials & Experimental Methods

The 98.5% pure  $\text{NaBH}_4$  that contains 0.05% Si and 0.005% Fe was supplied from a commercial company.  $\text{Fe}_2\text{O}_3$  was also obtained from a commercial company. Nanosize  $\text{Fe}_2\text{O}_3$  has 99.55% purity and contains 0.003% Ca, 0.015% Cr, 0.14% Mn, 0.05% Al and 0.091%  $\text{SiO}_2$ . Al Nano supplied from ZAG Kimya company is 99% pure and 0-150  $\mu\text{m}$  in size. Al Granule supplied from Nanokar Company is 98.5% pure and 2 mm in size. The Cobalt (Co) Micron powder was supplied from the Nanografi company. The Cobalt (Co) Micron Powder is 99.99% pure and has a size of 1  $\mu\text{m}$ . BFS was supplied from Iskenderun Iron and Steel factory. the steel BFS, which produced in Turkey, is assumed to consist of  $\text{SiO}_2$  (39.66 %),  $\text{Fe}_2\text{O}_3$  (1.58 %),  $\text{Al}_2\text{O}_3$  (12.94 %), CaO (34.20 %), MgO (6.94 %),  $\text{Na}_2\text{O}$  (0.20 %), K<sub>2</sub>O (1.44 %),  $\text{SO}_3$  (0.72 %) [22].

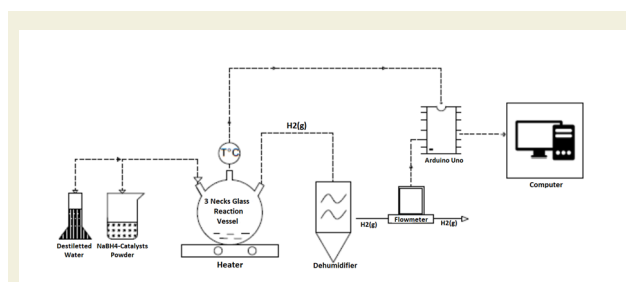


Figure 1. Experimental installation

The schematic view of the experimental setup is shown in Figure 1. It consists of a 4-port reactor, heater, moisture trap, Alicat Scientific brand flow meter, DS18B20 temperature sensor, MTOPS MS300HS brand heater, and Arduino Uno. The amount of  $\text{NaBH}_4$  was kept constant as 2 g for all experiments. Then, in the hydrolysis reaction of  $\text{NaBH}_4$ , BFS powders, and  $\text{Fe}_2\text{O}_3$ , Al Nano&granule powders were weighed one by one in the analytical balance as 0.2 gr, 0.5 gr, 1 gr, and 2 gr together with distilled water.

The effect of the catalytic activity performances of these powder samples on the hydrolysis reaction of  $\text{NaBH}_4$  was investigated. These catalytic hydrolysis reactions were carried out in a four-necked round bottom flask reactor. Solid  $\text{NaBH}_4$  was weighed on an analytical balance and metal powder samples which used as catalysts were transferred to the reactor. Distilled water was added to the solid powder in the reactor by using a measuring cylinder. The reaction temperature was measured by a thermocouple that connected to the Arduino Uno. The hydrogen gas produced as a result of the reaction was passed through a desiccant to separate it from the water vapor contained in it. The volume of hydrogen gas produced was measured by a high precision Alicat Scientific brand flowmeter. The measured data were simultaneously transferred to the microprocessor and saved to the computer.

### Hydrogen Production

Hydrogen production took place in a three-necked round bottom flask reactor as shown in Figure 1. The three-necked were used as water and catalyst inlet, thermocouple outlet, and hydrogen outlet connections. All connections of the reactor were wrapped with gas Teflon tape to prevent possible hydrogen leakage, providing a high sealing environment. The catalyst mixture prepared from the water and catalyst inlet and 20 ml of distilled water measured with the aid of a measuring cylinder were transferred into the reactor. Then, with the aid of a heater, the reactor was heated to  $50^\circ\text{C}$ . The hydrogen gas produced as a result of the hydrolysis reaction taking place in the reactor was passed through the desiccant and conveyed to the flow meter. The flow rate of hydrogen and the reaction temperature with the thermocouple in the reactor were measured by the flow meter. Using Arduino Uno, data from both the thermocouple and the flow meter were simultaneously recorded in an Excel file.

## 3. Results and Discussions

### 3.1. Effect of BFS powder on Hydrolysis Reaction

Experiments were carried out using three different amounts of 2 g, 3 g, and 4 g for the BFS catalyst, 20 ml of distilled water was used for all three experiments and

the reaction vessel was heated up to  $50^\circ\text{C}$ . The results obtained from the experiments are shown in Figures 2a and 2b. The experiment using 2 g BFS lasted for 27 minutes and the maximum temperature was up to  $59.13^\circ\text{C}$ . In the experiment, the total flow reached 142.44 L and the maximum flow amount was measured as 0.23 L/min.gcatalyst. The instantaneous flow rate of the reaction was measured as 5.275 L/min. The experiment using 3 g BFS lasted 22 minutes and the maximum temperature was up to  $62.88^\circ\text{C}$ . In the experiment, the total flow reached 146.25 L and the maximum flow amount was measured as 0.28 L/min.gcatalyst. The instantaneous flow rate of the reaction was measured as 6.647 L/min. The experiment using 4 g BFS lasted for 25 minutes and the maximum temperature increased up to  $63.81^\circ\text{C}$ . In the experiment, the total flow reached 216.88 L and the maximum flow amount was measured as 0.28 L/min.gcatalyst. The instantaneous flow rate of the reaction was measured as 8.675 L/min. Among the three reactions, the longest-lasting reaction was the one using 2 g of BFS, and it lags behind the others in terms of total hydrogen produced. The temperatures and maximum flow values reached in the experiments using 3 and 4 gr BFS are approximately the same. In terms of instantaneous flow rate and the total amount of hydrogen produced, the experiment using 4 g of BFS is quite efficient.

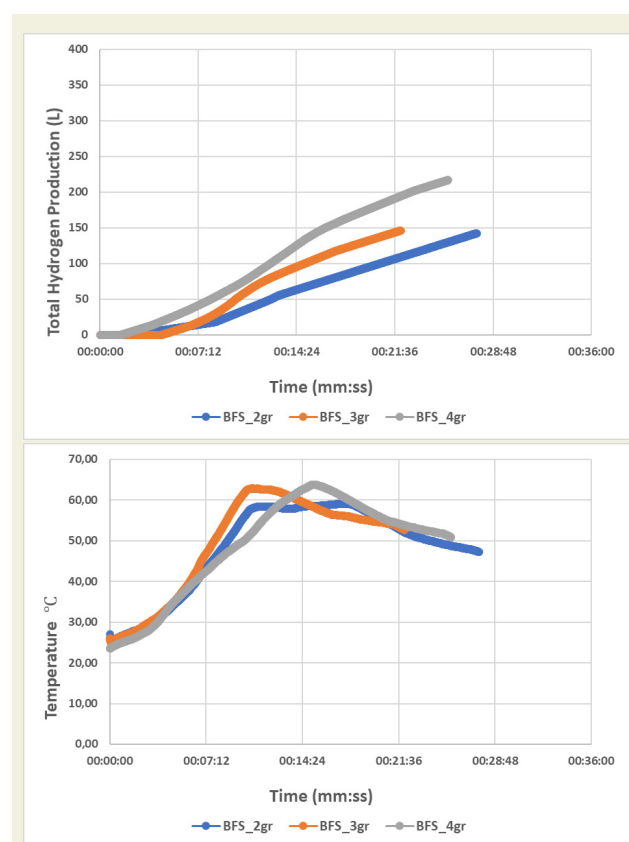


**Figure 2.** a) The Total Hydrogen Production of Different Amounts of BFS Powders, b) The Temperature Effect of Different Amounts of BFS Powders

## 3.2. Effect of Granule and Nanoparticles on Hydrolysis Reaction

### 3.2.1. Effect of Granule particles on Hydrolysis Reaction

#### *Al Granule powders:*

When 0.2 gr and 0.5 gr of Al Granule metal powder were used, hydrogen gas output could not be measured because of very low levels. Therefore, experiments were carried out using two different amounts, 1 g, and 2 g, and 20 ml of distilled water and 2 g of NaBH<sub>4</sub> were used for both experiments and the reactor was heated up to 50. The results of total hydrogen production and reaction temperatures obtained from the experiments are shown in Figures 3a and 3b. According to these Figures, the experiment using 1 gr Al Granule lasted 26 minutes and the maximum temperature was up to 67.62 °C. The total flow amount measured in the experiment is 166.3 L and the maximum flow rate was measured as 0.18 L/min.g<sub>catalyst</sub>. The instantaneous flow rate of the reaction was measured as 6.396 L/min. The experiment using 2 gr Al Granule lasted 26 minutes and the maximum temperature was up to 67.19 °C. The total flow amount measured in the experiment is 172.92 L and the maximum flow rate was measured as 0.28 L/min.g<sub>catalyst</sub>. The instantaneous flow rate of the reaction was measured as 6.065 L/min. Test times and maximum temperatures attained for both catalyst quantities are approximately the same. When the amount of hydrogen produced was compared,

it was observed that when 2 g of Al granule was used, there was 6 L more production.

#### *Fe<sub>2</sub>O<sub>3</sub> Granule powders:*

Fe<sub>2</sub>O<sub>3</sub> Granule catalyst was used in 3 different amounts, 0.2 gr- 0.5 gr-1 gr. In all experiments, hydrolysis reactions were carried out using 20 ml of distilled water and 2 g of NaBH<sub>4</sub>, and the reaction vessel was heated up to 50°C and closed. The results obtained from the experiments are shown in Figures 4a and 4b. In the experiment performed with 0.2 gr Fe<sub>2</sub>O<sub>3</sub> catalyst, the reaction time, the maximum temperature reached by the reaction, the maximum flow rate of the reaction, the instantaneous flow rate of the reaction, and the total flow rate were 12 minutes, 88.25 °C, 1.99 L/min.g<sub>catalyst</sub>, 28.47 L/min, and 341.65 L, respectively. In the experiment where 0.5 g Fe<sub>2</sub>O<sub>3</sub> catalyst was used, the reaction time, the maximum temperature reached by the reaction, the maximum flow rate of the reaction, the instantaneous flow rate of the reaction, and the total flow rate were 12 minutes, 87.06°C, 2.52 L/min.g<sub>catalyst</sub>, 28.26 L/min, and 339.21 L, respectively. The last experiment, which used 1 g Fe<sub>2</sub>O<sub>3</sub> Nano-powder, ended at 19 minutes, and the highest temperature reached by the reaction was measured as 90.25 °C. The total flow in the experiment is 304.37 L, the maximum flow amount is 4.33 L/min.g<sub>catalyst</sub> and the instantaneous flow amount in the reaction is 33.81 L/min.

In the experiments of Fe<sub>2</sub>O<sub>3</sub> Granule with 0.2 gr- 0.5 gr

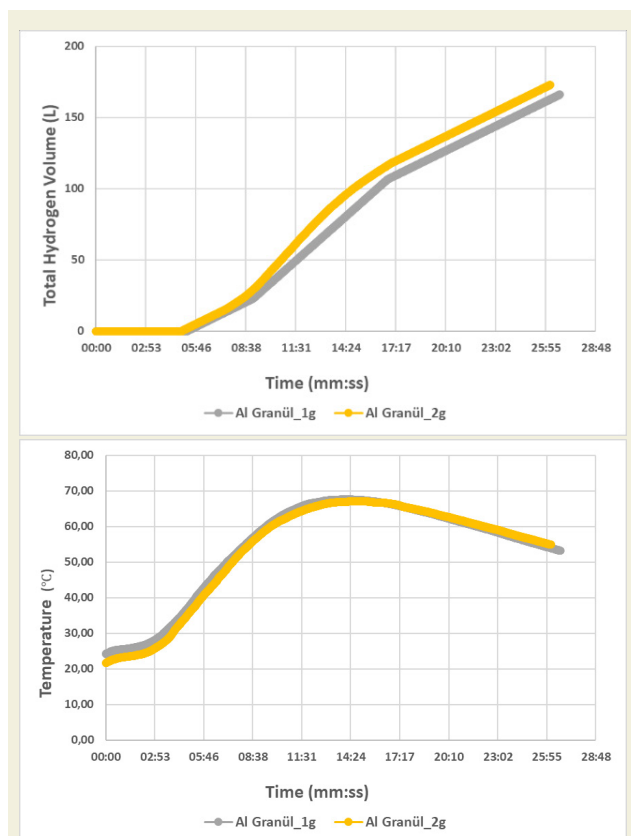


**Figure 3.** a) The Total Hydrogen Production of Different Amounts of Al Granule Powders, b) The Temperature Effect of Different Amounts of Al Granule Powders

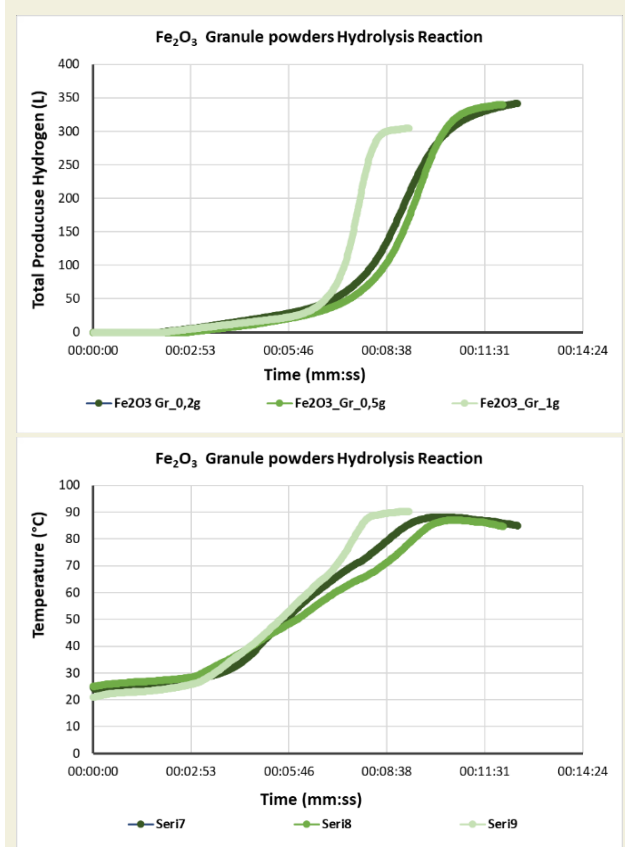


**Figure 4.** a) The Total Hydrogen Production of Different Amounts of Fe<sub>2</sub>O<sub>3</sub> Granule Powders, b) The Temperature Effect of Different Amounts of Fe<sub>2</sub>O<sub>3</sub> Granule Powders

-1 gr, the reaction temperature, maximum flow amount and instantaneous flow amount are approximately close to each other. However, the experiment in which the total flow was the highest in these experiments according to the nanosize was the experiment using 0.2 gr  $Fe_2O_3$  Granule.

### 3.2.2. Effect of Nanoparticles on Hydrolysis Reaction *Al Nano Powders:*

Experiments were carried out using 4 different amounts of metal powder of Al Nano as 0.2 gr, 0.5 gr, 1 gr, and 2 gr. For all experiments, 20 ml of distilled water, and 2 g of  $NaBH_4$  were used and the reaction vessel was heated to 50 °C. The results obtained from the experiments are shown in Figures 5a and 5b. The experiment using 0.2 gr Al Nano lasted 26 minutes and the maximum temperature was up to 58.44 °C. The total flow in the experiment was 184.05 L and the maximum flow amount was measured as 0.28 L/min.gcatalyst. The instantaneous flow rate of the reaction was measured as 7.078 L/min. The experiment using 0.5 g Al Nano lasted 31 minutes and the maximum temperature was up to 73 °C. The total flow in the experiment was 316.11 L and the maximum flow amount was measured as 0.42 L/min.gcatalyst. The instantaneous flow rate of the reaction was measured as 10.197 L/min. The experiment using 1 gr Al Nano lasted 28 minutes and the maximum temperature was up to 84.31 °C. The total flow in the experiment was 366.81 L and the maximum flow amount was measured as 0.62 L/min.gcatalyst. The instantaneous flow rate of the reaction was measured as 13.100 L/min.

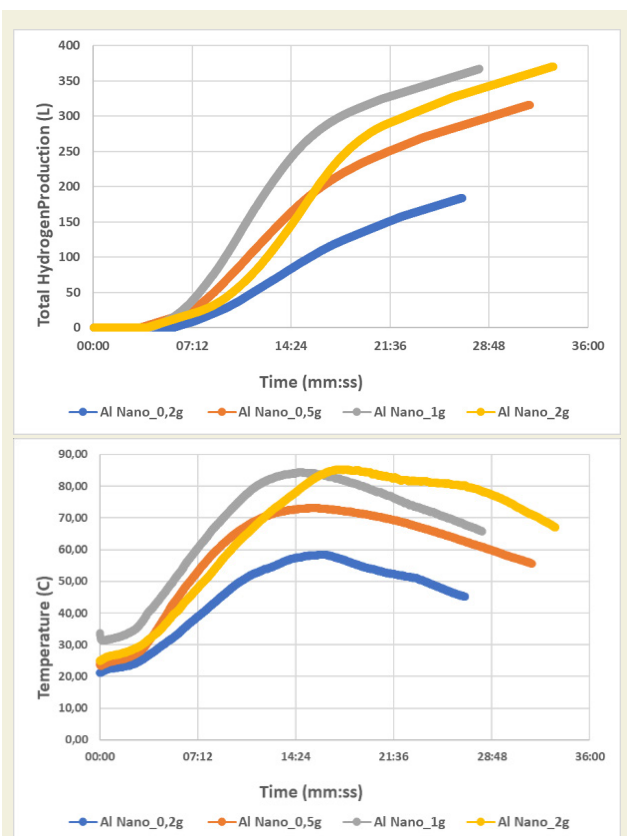


Figure 5. a) The Total Hydrogen Production of Different Amounts of Al Nano Powders, b) The Temperature Effect of Different Amounts of Al Nano Powders

The experiment using 2 gr Al Nano lasted 33 minutes and the maximum temperature was up to 85.31 °C. The total flow in the experiment was 370.46 L and the maximum flow amount was measured as 0.52 L/min.gcatalyst. The instantaneous flow rate of the reaction was measured as 11.226 L/min. For Al Nano, the reaction time and temperature increased as the amount of catalyst increased. In addition, the total amount of hydrogen produced and the instantaneous flow rates have also increased. If we examine Figures 5a and 5b, we can say that the most efficient is 2 gr Al Nano.

### *Fe<sub>2</sub>O<sub>3</sub> Nano Powders*

$Fe_2O_3$  Nanocatalyst was used in 3 different amounts, 0.2 gr -0.5 gr -1 gr. In all experiments, hydrolysis reactions were carried out using 20 ml of distilled water and 2 g of  $NaBH_4$ , and the reaction vessel was heated up to 50 °C and closed. The results obtained from the experiments are shown in Figures 6a and 6b. In the experiment performed with 0.2 gr  $Fe_2O_3$  catalyst, the reaction time, the maximum temperature reached by the reaction, the maximum flow rate of the reaction, the instantaneous flow rate of the reaction, and the total flow rate were measured at 26 minutes, 79.19 °C, 0.57 L/min.gcatalyst, 12.55 L/min, and 339.07 L, respectively. In the experiment where 0.5 g  $Fe_2O_3$  catalyst was used, the reaction time, the maximum temperature reached by the reaction, the maximum flow rate of the reaction, the instantaneous

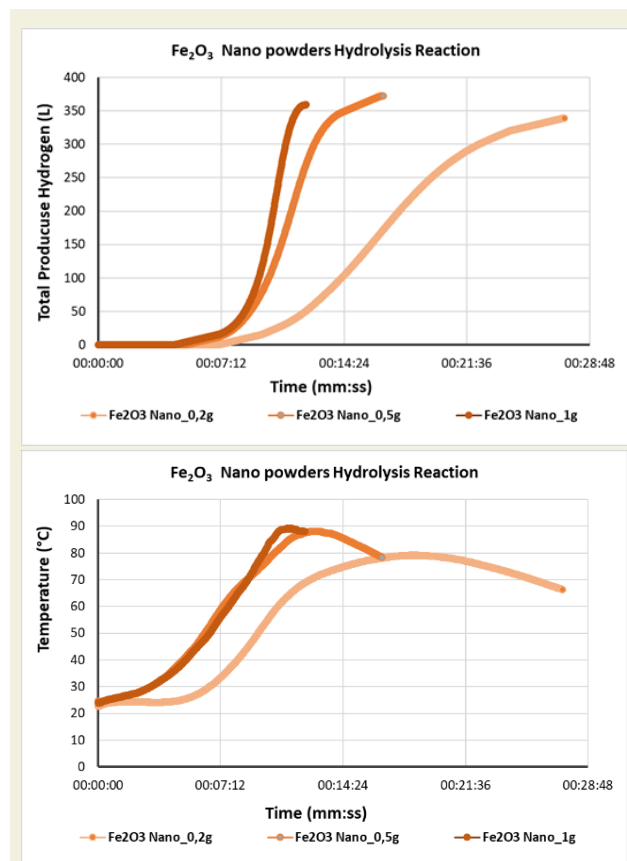


Figure 6. a) The Total Hydrogen Production of Different Amounts of  $Fe_2O_3$  Nano Powders, b) The Temperature Effect of Different Amounts of  $Fe_2O_3$  Nano Powders

flow rate of the reaction, and the total flow rate were 16 minutes, 88.12°C, 1.5 L/min.gcatalyst, 23.28 L/min, and 372.5 L, respectively. The last experiment, which used 1 g Fe<sub>2</sub>O<sub>3</sub> Nano, ended in 12 minutes and the highest temperature reached by the reaction was measured as 89.25 °C. The total flow in the experiment is 358.97 L, the maximum flow amount is 2.53 L/min.gcatalyst and the instantaneous flow amount in the reaction is 29.91 L/min.

0.2 gr- 0.5 gr-1 gr Fe<sub>2</sub>O<sub>3</sub> In nano experiments, the highest temperature, maximum flow amount, and total flow values were seen in the experiment performed with 1 gr Fe<sub>2</sub>O<sub>3</sub>. The experiment with the highest total flow amount is the value made with 0.5 gr Fe<sub>2</sub>O<sub>3</sub> Nano. The longest experiment was the experiment using 0.2 gr Fe<sub>2</sub>O<sub>3</sub> Nano. As a result, with the increase in the amount of catalyst used in hydrolysis reactions, the total amount of hydrogen gas produced increases in direct proportion.

### 3.2.3. Comparison of Nano and Granule particles

As seen in Figure 7, it is more efficient than Al Granule in experiments where Al Nano is used as a catalyst. The amount of hydrogen produced is approximately 2 times higher. This is because the surface area width of Al Nano is more than Al Granule. This is because the solution formed in the hydrolysis reaction comes into contact with more catalyst surface area. In this case, it causes an increase in the reaction time. If two different amounts of Al Granule are compared, it can be observed that 1 gr Al Nano gives better results in experiments using Al Nano, although they are approximately the same efficiency.

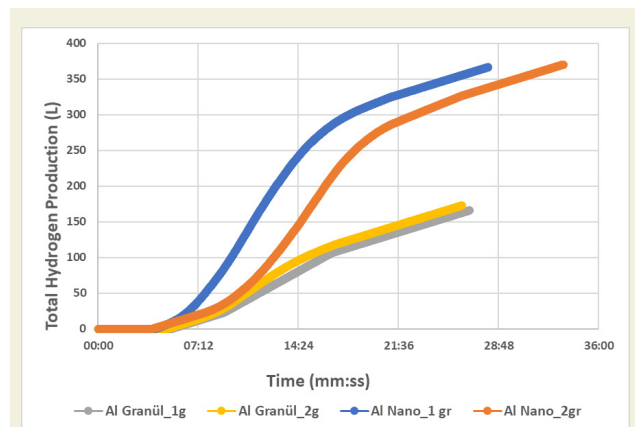


Figure 7. Time-Dependent Total Hydrogen Produced in Al Nano and Al Granule

In 0.2 gr experiments, Fe<sub>2</sub>O<sub>3</sub> Granule produced more hydrogen than Fe<sub>2</sub>O<sub>3</sub> Nano and reached higher temperatures. As seen in Figure 8, Fe<sub>2</sub>O<sub>3</sub> Granule gave better results at maximum flow rate and instantaneous flow rate. In the 0.5 g experiment, Fe<sub>2</sub>O<sub>3</sub> Nano produced more hydrogen and increased to a higher temperature. Fe<sub>2</sub>O<sub>3</sub> Granule reached a higher value at maximum flow amount and instant flow rate. In 1 gr experiments, Fe<sub>2</sub>O<sub>3</sub> Granule has the highest temperature value and Fe<sub>2</sub>O<sub>3</sub> Nano has the highest amount of hydrogen produced. Fe<sub>2</sub>O<sub>3</sub> Granule

has higher values at maximum flow amount and instant flow rate.

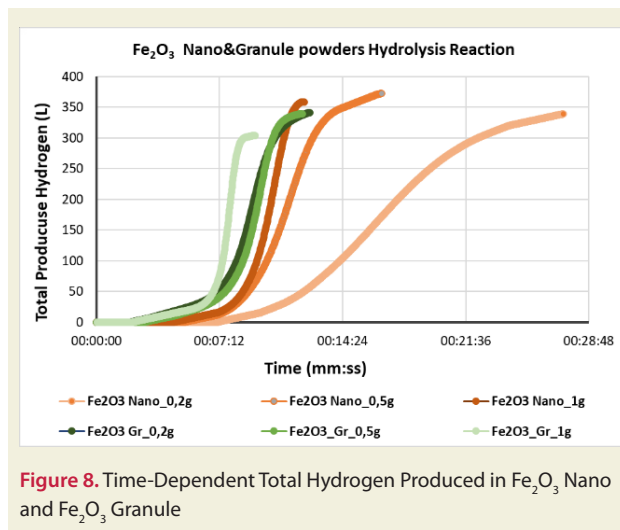


Figure 8. Time-Dependent Total Hydrogen Produced in Fe<sub>2</sub>O<sub>3</sub> Nano and Fe<sub>2</sub>O<sub>3</sub> Granule

## 3.3. Adding BFS To The Hydrolysis Experiment

### 3.3.1. Effect of Al Nano and BFS on Hydrolysis Reaction

1 g and 2 g of Al nano metal powder, 1 g of BFS, and 2 g of NaBH<sub>4</sub> were reacted. For both experiments, 20 ml of distilled water was used and the reaction vessel was heated to 50 °C. The results obtained from the experiments are shown in Figures 9a and 9b. The experiment using 1 gr Al Nano lasted 28 minutes and the maximum temperature was up to 71°C. The total flow in the experiment was 189.18 L and the maximum flow amount was measured as 0.28 L/min.gcatalyst. The instantaneous flow rate of the reaction was measured as 6.756 L/min. The experiment using 2 gr Al Nano lasted 25 minutes and the maximum temperature was up to 71°C. The results obtained from the experiments are shown in Figures 9a and 9b. The total flow in the experiment was 216.45 L and the maximum flow amount was measured as 0.28 L/min.gcatalyst. The instantaneous flow rate of the reaction was measured as 8.538 L/min.

The addition of BFS to the Al Nano metal powder kept the reaction time of 1 g Al Nano the same as in the BFS-free experiment. However, it reduced the maximum temperature reached by the reaction by 13 °C. It reduced the instantaneous flow rate of the reaction by 7 L/min and the total hydrogen flow amount by 177 L. For 2 gr Al Nano, it extended the reaction time by 8 minutes. With this; It decreased the maximum temperature value by 14 °C, the total hydrogen flow amount by 154 L, and the instantaneous flow rate by 3 L/min, respectively.

### 3.3.2. Effect of Fe<sub>2</sub>O<sub>3</sub> Nano&Granule and BFS on Hydrolysis Reaction

In this experiment, in addition to 20 ml distilled water, 2 gr NaBH<sub>4</sub> and 0.5 gr Fe<sub>2</sub>O<sub>3</sub> Granule powder, 2 gr BFS was used. The reaction was completed in 18 minutes and

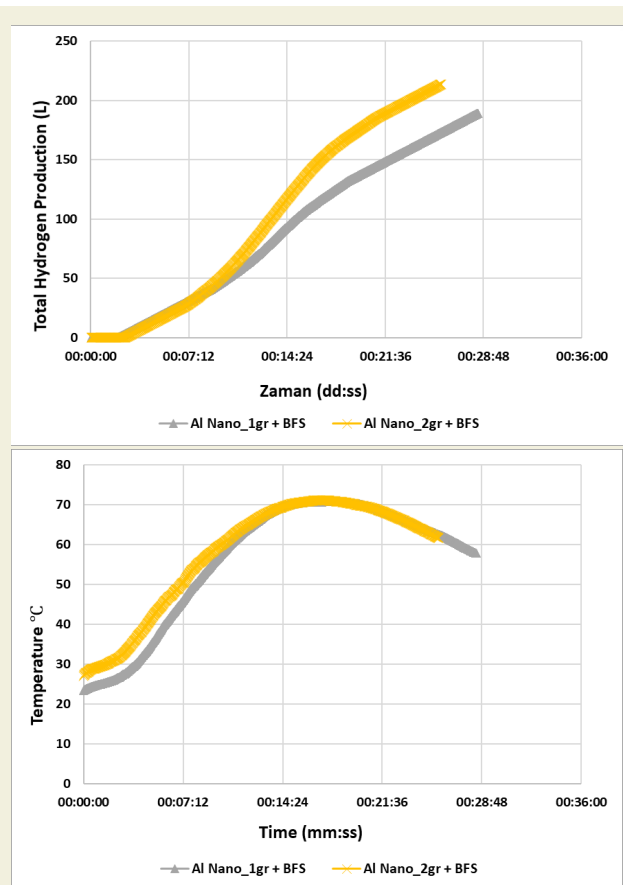


**Figure 9.** a) The Total Hydrogen Production of Different Amounts of Al Nano&BFS Powders, b) The Temperature Effect of Different Amounts of Al Nano&BFS Powders

the maximum temperature was measured as 84.62°C. The results obtained from the experiments are shown in Figures 10a and 10b. In this experiment, a total of 290.08 L of hydrogen is produced, the maximum flow is 1.01 L/min. catalyst, and the instantaneous speed of the experiment is 16.11 L/min. These reaction results gave lower values than the 0.5 g Fe<sub>2</sub>O<sub>3</sub> Granule test without BFS.

In this experiment, in addition to 20 ml distilled water, 2 gr NaBH<sub>4</sub> and 0.5 gr Fe<sub>2</sub>O<sub>3</sub> Nanopowder, 2 gr BFS was used. The experiment lasted 19 minutes and the maximum temperature was 82.06°C. In this experiment, a total of 262.9 L hydrogen was produced, and the maximum flow was measured as 0.67 L/min. catalyst. The instantaneous velocity of the experiment is 13.83 L/min. These values gave lower results than the 0.5 gr Fe<sub>2</sub>O<sub>3</sub> Nano experiment without BFS.

### 3.3.3. Comparison of Fe<sub>2</sub>O<sub>3</sub> Granule, Fe<sub>2</sub>O<sub>3</sub> Nano, and Al Nano Experiments Using BFS

The BFS, Al Nano, Al Nano + BFS powders used in the same amounts were compared according to Figure 11. The catalyst that produces the least hydrogen compared to other amounts is 2 g of BFS. The experiment in which Al Nano and BFS powder are used together is more efficient than the experiment in which only BFS powder is used. For this reason, although the BFS powder harmed the Al Nano experiment, it was observed that the Al Nanopow-

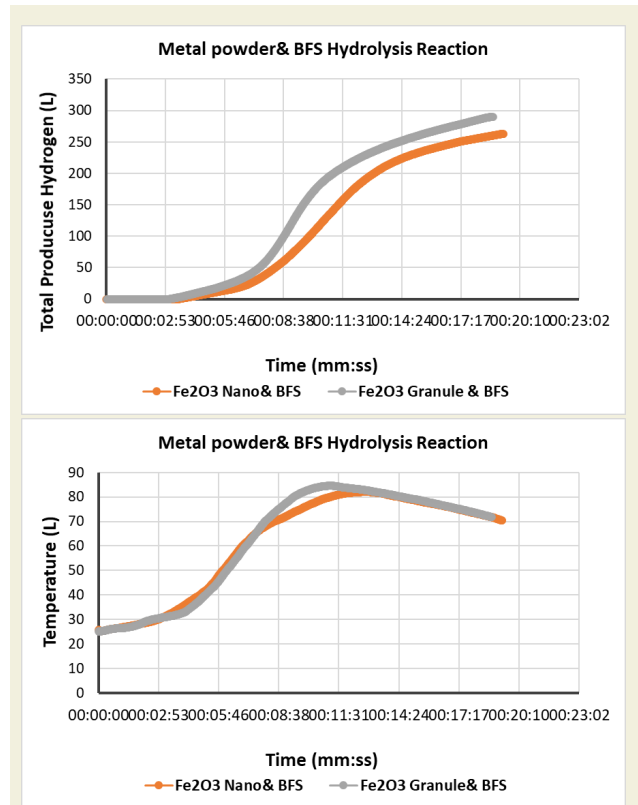


**Figure 10.** a) The Total Hydrogen Production of Different Amounts of Fe<sub>2</sub>O<sub>3</sub> Nano&BFS Powders, b) The Temperature Effect of Different Amounts of Fe<sub>2</sub>O<sub>3</sub> Nano&BFS Powders

der had a positive effect on the hydrolysis experiments in which the BFS was used.

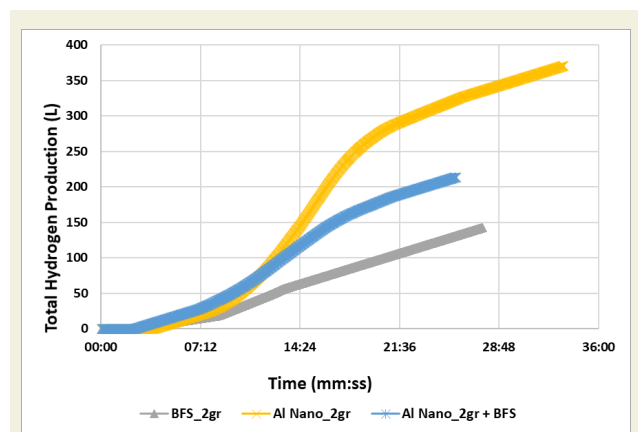


**Figure 11.** Effect of Al Nano + BFS Powder on Hydrolysis Reaction

The BFS, Fe<sub>2</sub>O<sub>3</sub> Granule, Fe<sub>2</sub>O<sub>3</sub> Nano, Fe<sub>2</sub>O<sub>3</sub> Nano + BFS, and Fe<sub>2</sub>O<sub>3</sub> Granule + BFS powders used in the same amounts were compared according to Figure 12. The 0.5 gram Fe<sub>2</sub>O<sub>3</sub> Granule test with BFS gave better results than the BFS Fe<sub>2</sub>O<sub>3</sub> Nano test. The BFS Fe<sub>2</sub>O<sub>3</sub> Nano experiment lasted longer than the experiment using granules.

### 3.4. Adding HCl Acid to the Hydrolysis Reaction

#### *Al Metal Powders*

In addition to the experiments above, the effect of HCl

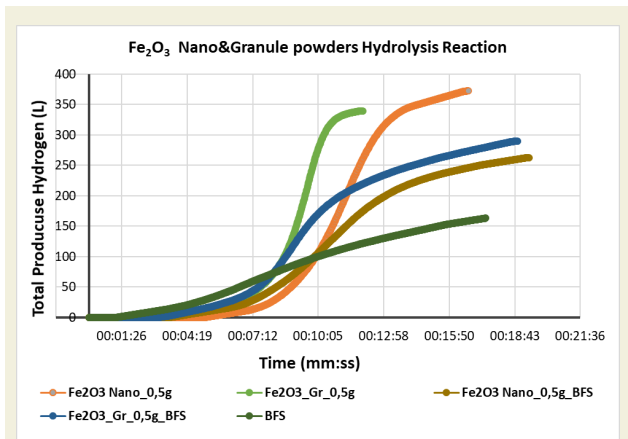


**Figure 12.** Effect of 0.5 gr  $\text{Fe}_2\text{O}_3$  Nano,  $\text{Fe}_2\text{O}_3$  Nano+BFS,  $\text{Fe}_2\text{O}_3$  Granule,  $\text{Fe}_2\text{O}_3$  Granule+BFS Powder on Hydrogen Production

acid in experiments using Al Metal powders is examined in this section. In addition to 2 gr Al Granule or 2 gr Al Nanopowders, 1 ml HCl acid was added to the reaction using 2 gr  $\text{NaBH}_4$ . For both experiments, 20 ml of distilled water was used and the reaction vessel was heated to 50 °C. The results obtained from the experiments are shown in Figure 12. The experiment using 2 gr Al Granule and 1 ml HCl acid took 4 minutes and the maximum temperature was up to 80.87°C. In the experiment, the total flow was 332.25 L and the maximum flow amount was measured as 11.18 L/min.gcatalyst. The instantaneous flow rate of the reaction was measured as 80.562 L/min. The experiment using 2 gr Al Nano and 1 ml HCl acid took 11 minutes and the maximum temperature was 70.44°C. The total flow in the experiment was 234.52 L and the maximum flow amount was measured as 5.75 L/min.gcatalyst. The instantaneous flow rate of the reaction was measured as 23.452 L/min. Adding HCl acid to Al Granule metal powders decreased the reaction time by 22 minutes compared to the experiment without adding HCl acid. The maximum temperature reached by the reaction increased by 13 °C, the instantaneous flow rate of the reaction increased by 74 L/min, and the total hydrogen flow rate by 150 L.

The addition of HCl acid to Al Nano metal powders de-

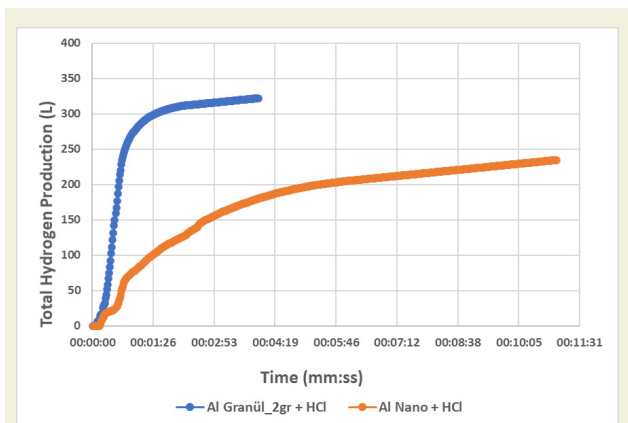


**Figure 13.** The effect of adding HCl Acid to the Hydrolysis Reaction with Al Nano and Granule catalysts

creased the reaction time by 22 minutes compared to the experiment without adding HCl acid. However, compared to the Al Granule experiments, it decreased the maximum temperature reached by the reaction by 15 °C and the total hydrogen flow amount by 140 L, respectively. However, it increased the instantaneous flow rate of the reaction by 12 L/min. This is due to the hydrogen gas released as a result of the reaction of HCl acid with water.

### $\text{Fe}_2\text{O}_3$ Metal Powders

In this experiment, in addition to 20 ml distilled water, 2 gr  $\text{NaBH}_4$ , 0.5 gr  $\text{Fe}_2\text{O}_3$  Granule or 0.5 gr  $\text{Fe}_2\text{O}_3$  Nanopowder, 1 ml of HCl acid was added to the reaction. The reaction vessel was heated to 50 °C. In the experiment using 0.5 gr  $\text{Fe}_2\text{O}_3$  Granule and 1 ml HCl acid, the reaction time, the maximum temperature reached by the reaction, the maximum flow rate of the reaction, the instantaneous flow rate of the reaction, and the total flow rate were 16 minutes, 77.62 °C, 3.36 L/min.gcatalyst, 18.11 L, respectively. It is measured as /min and 289.76 L. In the experiment using 0.5 gr  $\text{Fe}_2\text{O}_3$  Nano and 1 ml HCl acid, the reaction time, the maximum temperature reached by the reaction, the maximum flow rate of the reaction, the instantaneous flow rate of the reaction, and the total flow rate were measured 7 minutes, 87.62 °C, 4.53 L/min.gcatalyst, 69.49 L/min, and 416.95 L respectively. The addition of HCl acid to  $\text{Fe}_2\text{O}_3$  Granule metal powders increased the reaction time by 4 minutes compared to the experiment without adding HCl acid. The maximum temperature reached by the reaction increased by 9.4 °C, also increased the instantaneous flow rate of the reaction by 10.16 L/min, and decreased the total amount of hydrogen produced by 49.45 L. Addition of HCl acid to  $\text{Fe}_2\text{O}_3$  Nano metal powders increased the reaction time by 10 minutes compared to the experiment without adding HCl acid. However, according to the  $\text{Fe}_2\text{O}_3$  Granule ex-

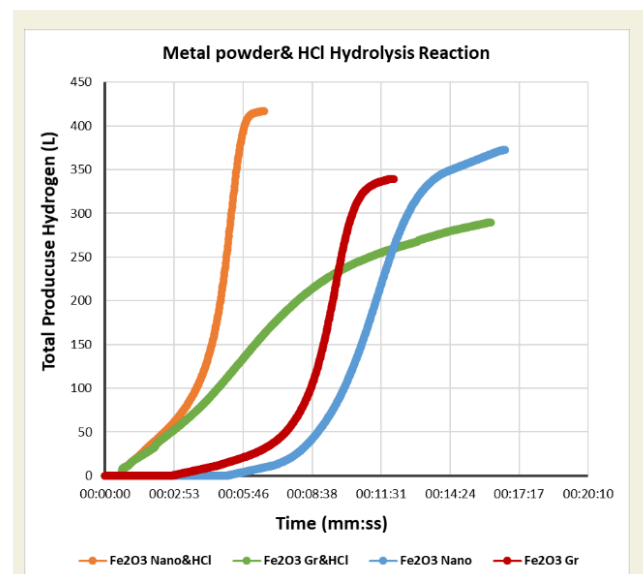


**Figure 14.** Effect of 0.5 gr  $\text{Fe}_2\text{O}_3$  Nano,  $\text{Fe}_2\text{O}_3$  Nano+HCl  $\text{Fe}_2\text{O}_3$  Granule,  $\text{Fe}_2\text{O}_3$  Granule+HCl Powder on Hydrogen Production

periments, the maximum temperature reached by the reaction is approximately the same, respectively, it increased the total hydrogen flow amount by 44.45 L and decreased the instantaneous flow rate of the reaction by 8.6 L/min.

### 3.5. Discussion

In this study, it has been proved by experiments that Al and  $\text{Fe}_2\text{O}_3$  catalysts can be used as efficient catalysts in  $\text{NaBH}_4$  hydrolysis reaction. In these experiments, the catalyst samples were made suitable for the  $\text{NaBH}_4$  hydrolysis reaction by various experiments in different amounts, BFS by-product, and HCl acid effect. In this study, the analysis of the hydrogen production reaction carried out under 5 different conditions with the Al and  $\text{Fe}_2\text{O}_3$  catalysts was made. It has been shown that both types of catalysts can be used efficiently in hydrolysis reactions when the experimental results of these metal powder catalysts are compared. According to the results of these optimization experiments, more effective test results are obtained by using different parameters and combinations.

In all experiments, hydrolysis reactions were carried out by using 20 ml of distilled water and 2 g of  $\text{NaBH}_4$  and the reaction vessel was preheated to 50 °C. Al and  $\text{Fe}_2\text{O}_3$  Nano metal powders catalyst were used in 3 different amounts as 0.2 g - 0.5 g - 1 g. During the experiments with 0.2 g, 0.5 g, and 1g of  $\text{Fe}_2\text{O}_3$  catalyst, the total flow rates were 339.07 L, 372.5 L, and 358.97 L, respectively. On the other hand, the total flow rate results of Al catalyst for 0.2 g, 0.5 g, and 1g usages were 184.05 L, 316.11 L, and 366.81 L, respectively. In the hydrolysis experiment in which  $\text{Fe}_2\text{O}_3$  metal powder was used together with BFS, approximately 45% more hydrogen production was observed compared to the experiment using only BFS. In the Al Nano experiment with the addition of BFS, approximately 30% more hydrogen production was observed compared to the experiment using only BFS. However, the use of BFS does not increase the yield in hydrolysis reactions where only Al and  $\text{Fe}_2\text{O}_3$  metal powders are used as catalysts. In hydrolysis reactions using HCl acid, total hydrogen production increased by 13% in the experiment where  $\text{Fe}_2\text{O}_3$  Nano and HCl acid were used together, while the total amount of hydrogen produced increased by 20% in the experiment where Al Nano and HCl acid were used together. It has been observed that adding HCl acid gives efficient results in the reaction. Therefore, it can be recommended to use HCl acid solutions with different molarities in reactions.

### 4. Conclusions

In this study, the yields of  $\text{Fe}_2\text{O}_3$  and Al catalysts were compared with the experiments conducted for hydrogen production from the catalytic hydrolysis of  $\text{NaBH}_4$  supported with BFS by-product and HCl acid. As a result of the obtained data, it was determined that  $\text{Fe}_2\text{O}_3$  and Al catalysts have advantages over hydrogen production rate

and fuel conversion. In line with the results obtained from the experiments, the  $\text{Fe}_2\text{O}_3$  catalyst and the  $\text{Fe}_2\text{O}_3$  catalyst & HCl acid experiments show a very high success in different parameters, and also  $\text{Fe}_2\text{O}_3$  catalysts create promising effects in the hydrolysis reactions of  $\text{NaBH}_4$ . Among the catalyst samples, the highest efficiency performances are achieved with  $\text{Fe}_2\text{O}_3$  Nanocatalyst samples at 50 °C preheat with an instantaneous hydrogen generation rate of approximately 29.91 L / min for 12 minutes. There is no study in the literature with  $\text{Fe}_2\text{O}_3$  catalysts in  $\text{NaBH}_4$  hydrolysis reactions. In addition, other metal catalysts used in these reactions are quite expensive and inefficient compared to  $\text{Fe}_2\text{O}_3$  catalysts. The use of  $\text{Fe}_2\text{O}_3$  catalysts as cheap and efficient catalysts in hydrolysis reactions has made a great contribution to literature studies.

### 5. Acknowledgements

This research was supported by Prof. Dr. Ertuğrul Baltacıoğlu. The BFS was provided by the İSTE Civil Engineering Department.

### References

- [1] Barbir, F., Veziroğlu, T.N., Plass, H.J., (1990). Environmental damage due to fossil fuels use. *International Journal of Hydrogen Energy*. doi: 10.1016/0360-3199(90)90005-J.
- [2] Panwar, N.L., Kaushik, S.C., Kothari, S., (2011). Role of renewable energy sources in environmental protection: A review. *Renewable and Sustainable Energy Reviews*. doi: 10.1016/j.rser.2010.11.037.
- [3] Yang, H., Lombardo, L., Luo, W., Kim, W., Züttel, A., (2018). Hydrogen storage properties of various carbon supported  $\text{NaBH}_4$  prepared via metathesis. *International Journal of Hydrogen Energy*. doi: 10.1016/j.ijhydene.2018.02.142.
- [4] Nabid, M.R., Bide, Y., Kamali, B., (2019). Hydrogen release from sodium borohydride by  $\text{Fe}_2\text{O}_3$ @nitrogen-doped carbon core-shell nanosheets as reasonable heterogeneous catalyst. *International Journal of Hydrogen Energy*. doi: 10.1016/j.ijhydene.2019.08.038.
- [5] Balbay, A., Selvitepe, N., Saka, C., (2021). Fe doped-CoB catalysts with phosphoric acid-activated montmorillonite as support for efficient hydrogen production via  $\text{NaBH}_4$  hydrolysis. *International Journal of Hydrogen Energy*. doi: 10.1016/j.ijhydene.2020.09.181.
- [6] Schlesinger, H.I., Brown, H.C., Finholt, A.E., Gilbreath, J.R., Hoekstra, H.R., Hyde, E.K., (1953). Sodium Borohydride, Its Hydrolysis and its Use as a Reducing Agent and in the Generation of Hydrogen. *Journal of the American Chemical Society*. doi: 10.1021/ja01097a057.
- [7] Lee, J., Shin, H., Choi, K.S., Lee, J., Choi, J.Y., Yu, H.K., (2019). Carbon layer supported nickel catalyst for sodium borohydride ( $\text{NaBH}_4$ ) dehydrogenation. *International Journal of Hydrogen Energy*. doi: 10.1016/j.ijhydene.2018.11.218.
- [8] Baydaroglu, F., Özdemir, E., Hasimoglu, A., (2014). An effective synthesis route for improving the catalytic activity of carbon-supported Co-B catalyst for hydrogen generation through hydrolysis of  $\text{NaBH}_4$ . *International Journal of Hydrogen Energy*. doi: 10.1016/j.ijhydene.2013.04.111.

- [9] Wei, Y., Wang, Y., Wei, L., Zhao, X., Zhou, X., Liu, H., (2018). Highly efficient and reactivated electrocatalyst of ruthenium electrodeposited on nickel foam for hydrogen evolution from NaBH<sub>4</sub> alkaline solution. *International Journal of Hydrogen Energy*. 43(2): 592–600. doi: 10.1016/j.ijhydene.2017.11.010.
- [10] Dai, P., Zhao, X., Xu, D., Wang, C., Tao, X., Liu, X., et al., (2019). Preparation, characterization, and properties of Pt/Al<sub>2</sub>O<sub>3</sub>/cordierite monolith catalyst for hydrogen generation from hydrolysis of sodium borohydride in a flow reactor. *International Journal of Hydrogen Energy*. 44(53): 28463–70. doi: 10.1016/j.ijhydene.2019.02.013.
- [11] Yang, C.C., Chen, M.S., Chen, Y.W., (2011). Hydrogen generation by hydrolysis of sodium borohydride on CoB/SiO<sub>2</sub> catalyst. *International Journal of Hydrogen Energy*. doi: 10.1016/j.ijhydene.2010.11.006.
- [12] Lu, Y.C., Chen, M.S., Chen, Y.W., (2012). Hydrogen generation by sodium borohydride hydrolysis on nanosized CoB catalysts supported on TiO<sub>2</sub>, Al<sub>2</sub>O<sub>3</sub> and CeO<sub>2</sub>. *International Journal of Hydrogen Energy*. doi: 10.1016/j.ijhydene.2011.11.105.
- [13] Zhang, X., Li, C., Qu, J., Guo, Q., Huang, K., (2019). Cotton stalk activated carbon-supported Co–Ce–B nanoparticles as efficient catalysts for hydrogen generation through hydrolysis of sodium borohydride. *Carbon Resources Conversion*. doi: 10.1016/j.crcon.2019.11.001.
- [14] Selvitepe, N., Balbay, A., Saka, C., (2019). Optimisation of sepiolite clay with phosphoric acid treatment as support material for CoB catalyst and application to produce hydrogen from the NaBH<sub>4</sub> hydrolysis. *International Journal of Hydrogen Energy*. doi: 10.1016/j.ijhydene.2019.04.254.
- [15] Tian, H., Guo, Q., Xu, D., (2010). Hydrogen generation from catalytic hydrolysis of alkaline sodium borohydride solution using attapulgite clay-supported Co-B catalyst. *Journal of Power Sources*. doi: 10.1016/j.jpowsour.2009.10.006.
- [16] Saka, C., Salih Eygi, M., Balbay, A., (2020). CoB doped acid modified zeolite catalyst for enhanced hydrogen release from sodium borohydride hydrolysis. *International Journal of Hydrogen Energy*. doi: 10.1016/j.ijhydene.2020.03.238.
- [17] Joydev, M., Binayak, R., Pratibha, S., (2014). Zeolite supported cobalt catalysts for sodium borohydride hydrolysis. *Applied Mechanics and Materials*.
- [18] Balkanlı, E., Figen, H.E., (2019). Sodium borohydride hydrolysis by using ceramic foam supported bimetallic and trimetallic catalysts. *International Journal of Hydrogen Energy*. doi: 10.1016/j.ijhydene.2018.12.010.
- [19] İskenderoğlu, F.C., Baltacıoğlu, M.K., (2021). Effects of blast furnace slag (BFS) and cobalt-boron (Co-B) on hydrogen production from sodium boron hydride. *International Journal of Hydrogen Energy*. doi: 10.1016/j.ijhydene.2020.12.219.
- [20] Dupiano, P., Stamatis, D., Dreizin, E.L., (2011). Hydrogen production by reacting water with mechanically milled composite aluminum-metal oxide powders. *International Journal of Hydrogen Energy*. doi: 10.1016/j.ijhydene.2011.01.062.
- [21] Li, F., Zhu, B., Sun, Y., Tao, W., (2017). Hydrogen generation by means of the combustion of aluminum powder/sodium borohydride in steam. *International Journal of Hydrogen Energy*. doi: 10.1016/j.ijhydene.2016.07.015.
- [22] Yazıcı, H., Yardımcı, M.Y., Yiğiter, H., Aydın, S., Türkel, S., (2010). Mechanical properties of reactive powder concrete containing high volumes of ground granulated blast furnace slag. *Cement and Concrete Composites*. doi: 10.1016/j.cemconcomp.2010.07.005.

# Thermo-hydraulic performance investigation of a heat exchanger tube inserted with twisted tapes modified with various twist ratio and alternate axis

Mahmut Uyanik<sup>1</sup>, Toygun Dagdevir<sup>1</sup>, Veysel Ozceyhan<sup>1\*</sup>

<sup>1</sup>Erciyes University, Faculty of Engineering, Department of Mechanical Engineering, Kayseri, Turkey

**Orcid:** M. Uyanik (0000-0002-5881-7115), T. Dagdevir (0000-0001-7388-3391), V. Ozceyhan (0000-0003-3829-9477)

**Abstract:** This paper presents a numerical investigation on a heat transfer enhancement by using various twisted tape inserted into a heat exchanger tube. The twist ratios of the twisted tapes are considered as 4, 6 and 8. Besides, the twisted tapes are modified with alternate axis for each twist period. The alternate axis is provided by connecting the twisted tapes having one twist with 90° connection angle. Water is selected as working fluid and turbulent flow condition corresponding to Reynolds number ranging from 5000 to 29,000 are considered in the study. The heat exchanger tube is under constant heat flux of 50 kW/m<sup>2</sup>. Numerical analysis results prove that the use of twisted tape improves thermal performance compared to the smooth tube. As the twist ratio decreases, the heat transfer performance and the friction loss penalty increase. Overall results are determined with thermohydraulic performance criteria (THP). The highest THP value is obtained as 1.21 for the tube inserted with the twisted tape which has the twist ratio of 4 and the alternate axis at Reynolds number of 5913.

**Keywords:** Heat transfer enhancement, flow characteristic, alternate axis, twisted tape, performance evaluation criteria.

## 1. Introduction

The effective use of energy has gained importance with the need for efficient use of energy, in recent. Since the usage of heat exchangers are widely employed in industry, it is extremely important to increase the performance of the heat exchangers. Heat transfer enhancement techniques are divided in two main categories: active and passive techniques. While active techniques require extra energy input to the system, the passive techniques do not demand any extra energy cost. Therefore, the passive techniques are generally preferred for increasing heat transfer due to reasons such as low-cost, ease of use and long-term maintenance [1][2]. Twisted tapes [3], helical screw tapes [4], wire coil [5], ring [6], etc. are inserted into the heat exchanger tube as passive techniques. The twisted tape is widely preferred due to induce effective heat transfer enhancement [7],[8]. However, using twisted tape in the tube increases the pressure drop penalty and thus causes an undesirable increase in the friction factor [9],[10]. For this reason, the researchers paid attention to increase heat transfer as much as possible but not to increase the friction factor too much while designing the twisted tape. In this scope, Li et al. [11] investigated the effect of the

centrally hollow narrow twisted tapes on the heat transfer enhancement characteristic. They recommended that the use of the cross hollow twisted tape is more effective under laminar flow conditions rather than turbulent flow conditions. Bhuiya et al. [12] investigated the thermal characteristics of triple twisted tape inserted heat exchanger tube under turbulent flow conditions. The heat transfer performance of their considered cases are found between 1.10 and 1.44 which the highest performance is obtained by the use of triple twisted tape insert. Skullong et al. [13] employed the staggered-winglet perforated tape to reduce the pressure drop penalty and to provide stronger fluid mixing. They found that the highest Nu and friction factor is obtained by the use of winglet perforated tape having largest winglet blockage ratio and lowest pitch length ratio. Dagdevir et al. [14] compared the performance of perforated twisted tape with dimpled twisted tape. They found that although the perforated twisted tapes induce stronger fluid mixing, the dimpled twisted tapes disrupt the boundary layer more effectively. In other research [15], they investigated the effect of the location of perforations and dimples on the twisted tape on the heat transfer and flow characteristics. They stated that

\* Corresponding author.  
Email: ozceyhan@erciyes.edu.tr



the perforations/dimples at the edge of the twisted tapes show better heat transfer and hydraulic performance rather than at the center of the twisted tapes. Changing the axis of twisted tape is another technique to enhance heat transfer by promoting the turbulence intensity, increasing swirl flow and disrupting the boundary layer. Ponnada et al. [16] compared the perforated twisted tapes whether they have alternate axis or not on the thermal performance. They found that the thermal performance factor is improved up to 1.433 and 1.396 by the use of perforated twisted tape having alternate axis and not having alternate axis, respectively. Wongcharee and Eiamsa-ard [17] carried out an experimental study on heat transfer enhancement by using twisted tape with alternate axis and CuO/water nanofluid. They found the maximum thermal performance factor of 5.53 by using the twisted tape with alternate axis, nanofluid volume fraction of 0.7% and at Reynold number of 1990. Wongcharee and Eiamsa-ard [18] investigated the effect of the twisted tape inserts with alternate axis on the friction factor and the heat transfer characteristic under laminar flow conditions. The twist ratio of the twisted tapes is considered as 3.0, 4.0 and 5.0 in their study. They found that the twist ratio of 3.0 provides the best heat transfer enhancement performance. Abolarin et al. [19] investigated that the effect of the alternating clockwise and counter clockwise twisted tape inserts on heat transfer and pressure drop characteristics under transitional flow regime. They considered the twist ratio of the twisted tapes of 5 and 12, and connection angles of 0°, 30° and 60°. They concluded that the increase in connection angle and decrease in twist ratio show better thermal performance.

According to the literature review, the twisted tape inserts having alternate axis promises good heat transfer enhancement performance. However, it is seen from the literature review that the effect of the twisted tape insert having alternate axis on the heat transfer and hydraulic performance have not been investigated with consideration of wide range twist ratios, connection angle of 90° and under turbulent flow conditions, yet. With this motivation, the twisted tape inserts which have alternate axis, connection angle of 90°, twist ratios of 4.0, 6.0 and 8.0, are numerically investigated under turbulent flow conditions.

## 2. Numerical Methodology

Ansys, Fluent 18.0 which solve the governing equations by finite element method is used to perform the numerical analyses for the present study. The SIMPLE (Semi-Implicit Method for Pressure-Linked Equation) algorithm is used to solve the governing equations by coupling the pressure and velocity gradients. Convergence criteria of the solution are selected as  $10^{-4}$  for continuity, velocities,  $k$  and epsilon and  $10^{-6}$  for energy.

The governing equations which are conservation of conti-

nunity, momentum and energy are given in Eqs. (1) to Eq. (3), respectively.

Mass conservation equation:

$$\nabla(\rho\vec{V}) = 0 \quad (1)$$

Momentum conservation equation:

$$\nabla(\rho\vec{V}\vec{V}) = -\nabla P + \nabla(\mu\nabla\vec{V}) \quad (2)$$

Energy conservation equation:

$$\nabla(\rho c_p \vec{V}T) = \nabla(k\nabla T) \quad (3)$$

Differential equations belong to the k-epsilon RNG turbulent model which is selected to simulate the turbulent flow through the tube are given in the following [20]:

$$\begin{aligned} \frac{\partial}{\partial t}(\rho k) + \frac{\partial}{\partial x_i}(\rho k u_i) &= \frac{\partial}{\partial x_j}(\alpha_k \mu_{eff} \frac{\partial k}{\partial x_j}) \\ &+ G_k + G_b - \rho \epsilon - Y_m + S_k \end{aligned} \quad (4)$$

$$\begin{aligned} \frac{\partial}{\partial t}(\rho \epsilon) + \frac{\partial}{\partial x_i}(\rho \epsilon u_i) &= \frac{\partial}{\partial x_j}(\alpha_\epsilon \mu_{eff} \frac{\partial \epsilon}{\partial x_j}) \\ &+ C_{1\epsilon} \frac{\epsilon}{k} (G_k + C_{3\epsilon} G_b) - C_{2\epsilon} \rho \frac{\epsilon^2}{k} - R_\epsilon + S_\epsilon \end{aligned} \quad (5)$$

### 2.1. Solution domain and boundary conditions

Solution domain adopted for the present study is schematically depicted in Fig. 1. Twisted tapes are inserted into a test section having length of 1 m. A fluid development section is placed before the test section to provide fully developed flow conditions. The length of the fluid development section is specified as 250 mm, which provides higher than ten times inner diameter [21]. In order to avoid from the reverse flow effect, an exit section with length of 150 mm is placed after the test section. Inner diameters of entire sections are same and dimension of 17 mm. The boundary conditions of the fluid development section and the exit section are determined as no-slip and adiabatic, while that of the test section is no slip and constant heat flux of 50 kW/m<sup>2</sup>. The velocity magnitude is calculated with considered Reynolds number ranging from 5000 to 35,000. Gauge pressure at the outlet is selected as 0 Pa, which provides the atmospheric conditions. Thermophysical properties of the working fluid is considered as temperature dependent. The thermo-physical properties of the working fluid are imported to the software by correlations with a form of Eq. (6) which their coefficients are given in Table 1. Temperature is in K unit in the correlations.

$$f(T) = a + bT + cT^2 + dT^3 \quad (6)$$

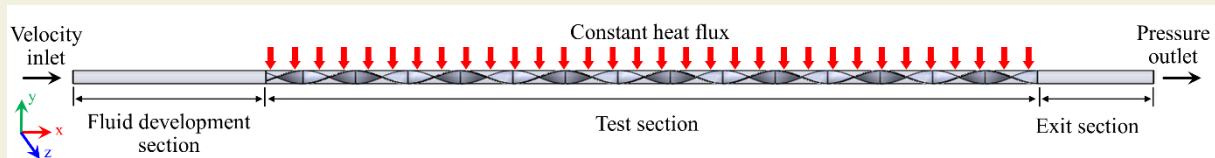


Figure 1. Solution domain and boundary types adopted in the present study

Table 1. Coefficients of the correlations belongs to the thermo-physical properties of the working fluid

Thermo-physical property	a	b	c	d
Density, $\rho$ [kg/m <sup>3</sup> ]	719.22	2.29643	-5.15E-03	1.91E-06
Specific heat capacity, $C_p$ [J/kgK]	6217.4	-15.2458	3.52E-02	-2.33E-05
Thermal conductivity, $k$ [W/mK]	-1.33612	1.29E-02	-2.67E-05	1.76E-08
Dynamic viscosity, $\mu$ [kg/ms]	0.0597994	-4.73471E-04	1.26033E-06	-1.12233E-09

Table 2. Definitions of the considered inserts with diameters

Definition	Pitch length (y) [mm]	Width (w) [mm]	Thickness (t) [mm]	Total length (L) [mm]	Connection angle of alternate axis
C-CC, y/w=4.0	68				
C-CC, y/w=6.0	102	17	1.0	1000	90°
C-CC, y/w=8.0	136				

## 2.2. Data Reduction

In order to evaluate the heat transfer and hydraulic performance of the considered tube configurations, Nusselt number ( $Nu$ ) and friction factor ( $f$ ) is used. Data used to calculate the  $Nu$  and the  $f$  are computed from Fluent by using surface integrals area-weighted averagely. Reynolds number ( $Re$ ) which defines the characteristic of the flow is given in Eq. 7. Density of the fluid, mean velocity magnitude of the flow, inner diameter of the tube and dynamic viscosity of the fluid are denoted by  $\rho$ ,  $U$ ,  $D_i$  and  $\mu$ , respectively.

$$Re = \frac{\rho U D_i}{\mu} \tag{7}$$

The  $Nu$  is calculated with Eq. (8). In this equation,  $h$  and  $k$  represent the convective heat transfer coefficient (Eq. (9)) and thermal conductivity of the fluid. Constant heat flux and wall temperature of wall and bulk temperature of the fluid are denoted with  $q''$ ,  $T_w$  and  $T_b$ .

$$Nu = \frac{h D_i}{k} \tag{8}$$

$$h = \frac{q''}{T_w - T_b} \tag{9}$$

The  $f$  is calculated with Eq. (10). In this equation,  $\Delta P$  and  $L$  represent the pressure drop penalty and length of the test tube.

$$f = \frac{\Delta P}{\frac{1}{2} \rho U^2 \frac{L}{D_i}} \tag{10}$$

## 2.3. Inserts

The twisted tapes are configured with different twist ratios ( $y/w$ ) of 4.0, 6.0 and 8.0, alternate axis (connection angle of 90°), in the present study. The considered twisted

tape inserts are designed to have three different twist pitch lengths ( $y$ ) of 68mm, 102 mm and 136 mm, thickness ( $t$ ) of 1 mm, width ( $w$ ) of 17 mm and total length ( $L$ ) of 1000 mm, respectively. Table 2 summarizes the dimension of the twisted tape configurations. The illustrations of the twisted tapes considered in the present study are given in Figure 2.

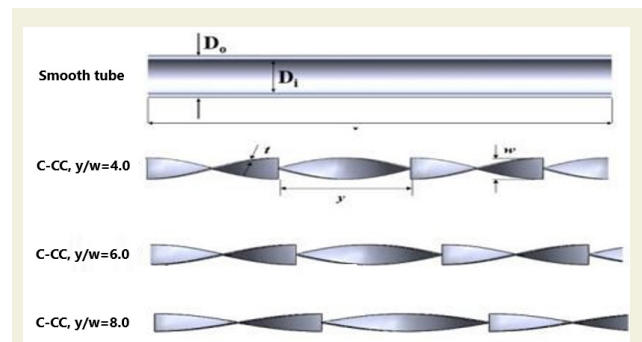


Figure 2. Considered tube configurations

## 3. Results and Discussions

### 3.1. Validation of the numerical methodology

Before the validation study, a grid independence study is performed to check a possible effect of the number of the elements on the results. A polyhedral grid structure having 2,955,760 (Fig. 3) is selected since the differences on the  $Nu$  and the  $f$  results are not higher than  $\pm 2.5\%$ .

In order to ensure the accuracy of the numerical methodology, a validation study is conducted by comparing the

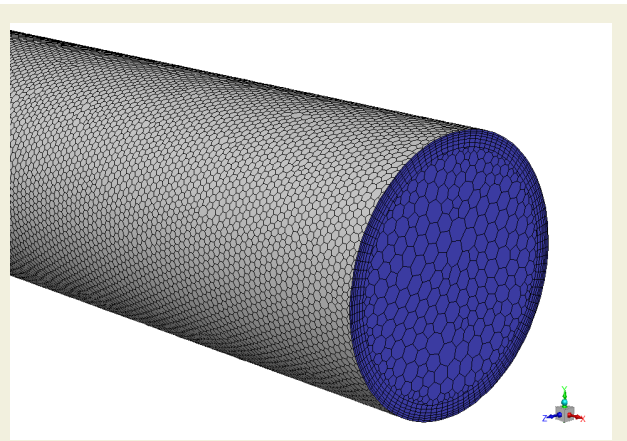


Figure 3. Grid structure used in the present study

results of the smooth tube with the correlations which are widely used in the literature. The used correlations are Dittus & Boelter Eq. (11) [22] and Blasius Eq. (12) [23]: for the Nu and the *f*, respectively.

$$Nu = 0.023Re_D^{0.8}Pr^{0.4} \tag{11}$$

$$f = 0.316Re_D^{-0.25} \tag{12}$$

The numerical results are compared with the literature in Fig. 4. As seen from this figure, a good agreement is obtained with the correlations.

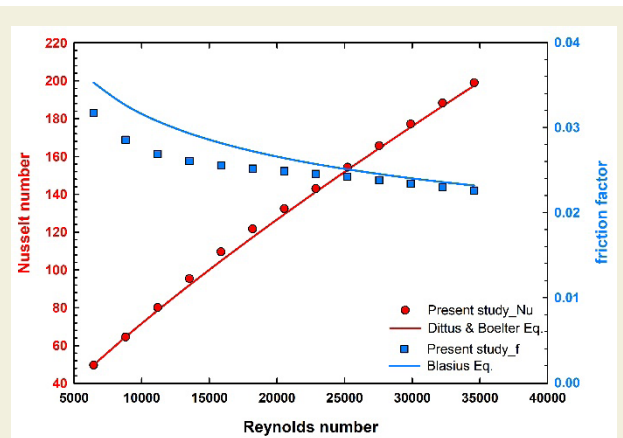


Figure 4. Comparison of the results of the Nu and the *f* belongs to the smooth tube with literature

### 3.2. Heat transfer performance

Fig. 5 shows the Nu number results versus Reynolds number for the considered tube configurations in the present study. It is concluded that Nu number increases with increasing Re number for all configurations. A higher Nu number was obtained when the tube configurations with twisted tape were compared to the smooth tube. In addition, with the increase in twist ratio of twisted tapes, there was a decrease in the thermal performance provided. The reason for this can be explained as the pipe with the twisted tape inserted approaching the smooth tube with the decrease in the twist ratio. In addition, with the increase of the twist ratio, the turbulence intensified and

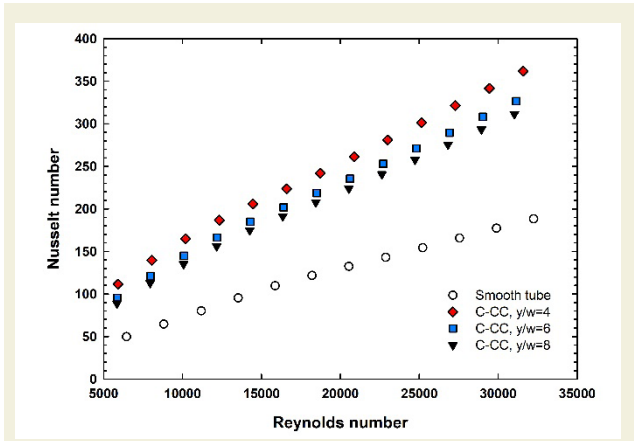


Figure 5. Variation of the Nu number according to the Reynolds number

the boundary layer was destroyed more effectively. The highest Nu value was obtained as 361.65 at Re 31,585 for the twisted tape configuration with a twist ratio of 4.0.

The temperature contours of the considered cases at Reynolds number of 15,000 are shown in Fig. 6a. It is seen from the figure that; the inserts effectively disrupt the thermal boundary layer and fluid having high temperature near the inner wall are mixed with the cold one at the center of the tube. It is a prove for the improvement of the heat transfer by using the twisted tape. When the effect of the twist ratios is examined, as the twist ratio decreases, the thermal boundary layer thickness decreases. Thus, decreasing the twist ratio has a positive role on heat transfer enhancement.

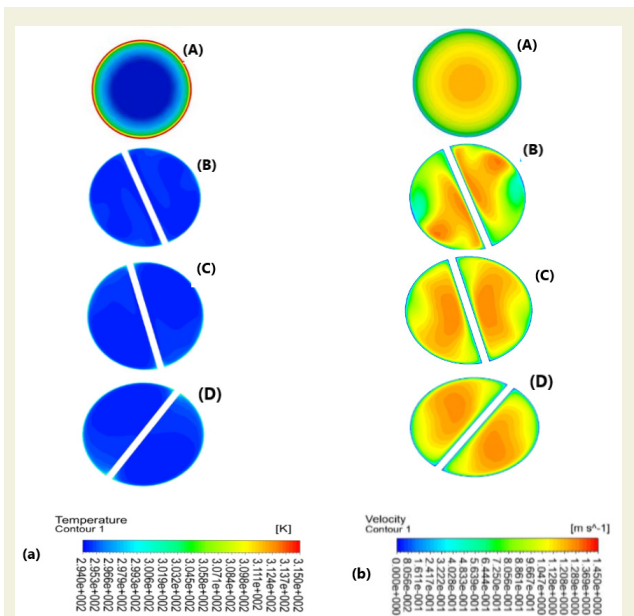


Figure 6. Temperature (a) and velocity (b) contours investigated tubes which are A) Smooth tube, B) C-CC\_y/w=4, C) C-CC\_y/w=6, D) C-CC\_y/w=8 at Reynolds number of 15000, respectively.

### 3.3. Hydraulic Performance

The distributions of the friction factor depending on Re for all investigated configurations are given Fig. 7. As ex-

pected, friction factor decreases with increasing Re number in all configurations. In the case of using twisted tape, the fluid in the tube encounters obstacle surfaces which causes increasing to friction factor. In addition, the increase in the twist ratio caused an increase in the friction factor. The highest friction factor value was obtained in Re 5913 as 0.2365 in the twisted tape configuration with a twist ratio of 4.

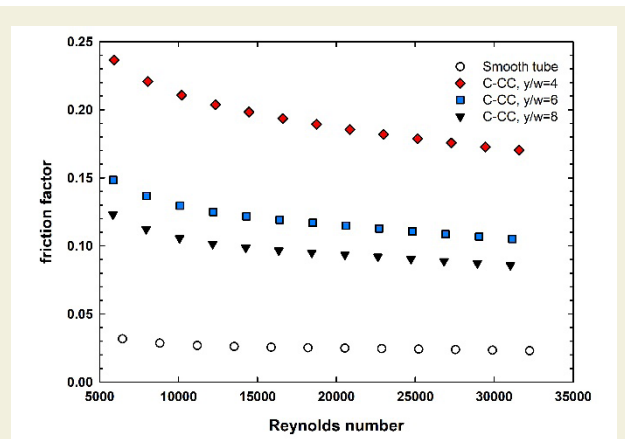


Figure 7. Change in friction factor depending on Re

The increase in the friction factor is directly related with the increase in pressure drop through the tube. As the twist ratio of the twisted tapes decreases, the pressure drop increases. Fig. 6b shows the velocity contours of the considered cases to observed the velocity distribution at the cross-section of the tube. An increase in the velocity gradient at the center of the tube attributes to the increase pressure drop. In addition to inserts increase the velocity gradient at the center of the tube, the decrease in the twist ratio is another parameter to increase the velocity gradient.

The velocity stream line contours obtained from the numerical analyzes are shown in Figure 8. When the stream lines of smooth tube and the tube with twisted tape are

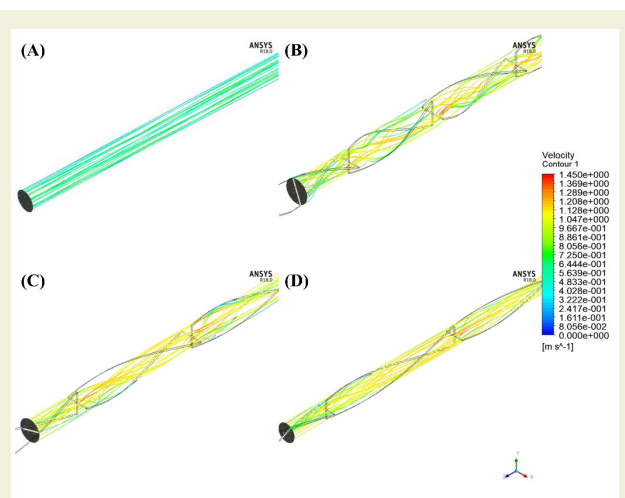


Figure 8. Velocity stream line contours investigated tubes which are A) Smooth tube, B) C-CC\_y/w=4, C) C-CC\_y/w=6, D) C-CC\_y/w=8 at Reynolds number of 15000, respectively

examined. It is seen that the flow in the smooth tube takes place axially, while the flow in the tube with twisted tape is swirling. The twisted tape placed in the tube ensures that the flow takes place by showing a swirl movement and ensures better mixing of the flow in the regions near the inner wall of the tube. Convection heat transfer occurs better in the regions near the inner wall of the tube, and in this case the placed twisted tapes increase heat transfer. In addition, when the contours are examined, it is seen that there is an increasing frequency of change in the flow direction with the decrement of the twist ratio, and alternate axis. This situation increases the turbulence intensity through the flow which has a positive effect on heat transfer enhancement.

### 3.4. Thermohydraulic Performance

Thermohydraulic performance criteria (THP) which is given in Eq. (13) is used to evaluate a heat exchanger system in terms of both thermal and hydraulic. The case where the THP value is 1 refers to the smooth tube. If the THP value is greater than 1, the method to be applied to the system will have a positive effect on the thermohydraulic performance of the system.

$$THP = \left( \frac{Nu_{TT}}{Nu_S} \right) / \left( \frac{f_{TT}}{f_S} \right)^{1/3} \tag{13}$$

The distribution of THP values based on Re are given in Figure 9. It can be resulted that the heat transfer enhancement results are more dominant than the friction loss results. The highest THP value of 1.21 is obtained by the case of y/w=4.0 at Re of 5913.

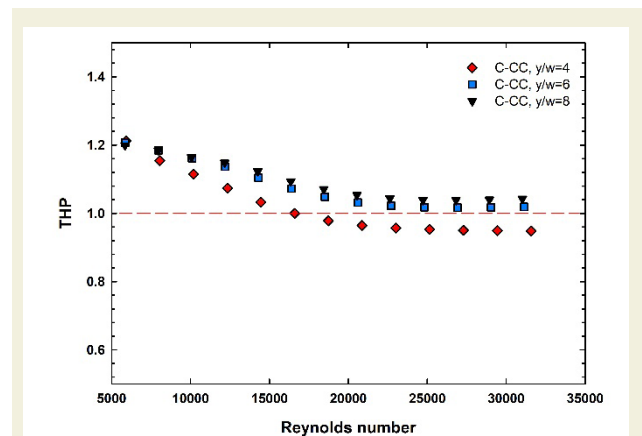


Figure 9. Thermohydraulic performance versus Reynolds number for all tube configurations examined

### 4. Conclusion

The performance of heat exchanger tube equipped with twisted tape inserts having alternate axis and various twist ratios are numerically investigated on the heat transfer and flow characteristics. Main conclusions obtained from the results are draw in below.

1. Decrease in the twist ratio generates more turbulent in-

tensity through the tube which induce the heat transfer enhancement.

2. The twisted tape with alternate axis allow to effectively mixing fluid through the tube. Thus, heat transfer is positively effective by this phenomenon. The highest Nusselt number of 361.65 is obtained by the case of twisted tape having the twist ratio of 4.0 at Re 31,585.

3. Decrease in the twist ratio and the alternate axis cause to the fluid encounter with larger obstacle surface which increase pressure drop penalty and friction factor. The highest friction factor of 0.2365 is observed in the case of twisted tape having the twist ratio of 4.0 at Reynolds number of 5913.

4. The highest THP value is obtained as 1.21 for the tube inserted with the twisted tape which has the twist ratio of 4 and alternate axis at Reynolds number of 5913.

## Acknowledgements

The authors acknowledge the financial, laboratory and infrastructure support provided by the Scientific Research Projects Coordination Unit, Erciyes University, Turkey (FDK-2020-10681).

## Nomenclature

### Abbreviations

$C_p$	specific heat capacity, (J/kgK)
C-CC	clockwise-counterclockwise alternate axis twisted tape
D	diameter, (mm)
h	convective heat transfer coefficient, (W/m <sup>2</sup> K)
f	friction factor, (-)
k	thermal conductivity, (W/mK)
L	total length, (mm)
Nu	Nusselt number, (-)
Pr	Prandtl number, (-)
$q''$	heat flux, (kW/m <sup>2</sup> )
Re	Reynolds number, (-)
THP	Thermohydraulic performance, (-)
t	thickness, (mm)
U	average velocity, (m/s)
w	width of the twisted tape (mm)
y	pitch length of the twisted tape (mm)
$\Delta P$	drop pressure, (Pa)

### Greek symbols

$\rho$	density, (kg/m <sup>3</sup> )
$\mu$	dynamic viscosity, (kg/ms)

### Subscripts

b	bulk
---	------

i	inner
s	smooth tube
TT	tube with twisted tape
w	wall

## References

- [1] Sheikholeslami, M., Gorji-Bandpy, M., Ganji, D.D., (2015). Review of heat transfer enhancement methods: Focus on passive methods using swirl flow devices. *Renewable and Sustainable Energy Reviews*. 49: 444–69. doi: 10.1016/j.rser.2015.04.113.
- [2] Dagdevir, T., Keklikcioglu, O., Ozceyhan, V., (2019). The Effect of Chamfer Length on Thermal and Hydraulic Performance by Using Al<sub>2</sub>O<sub>3</sub>-Water Nanofluid Through a Square Cross-Sectional Duct. *Heat Transfer Research*. 50(12): 1183–204. doi: 10.1615/HeatTransRes.2018025797.
- [3] Piriyarungrod, N., Eiamsa-ard, S., Thianpong, C., Pimsarn, M., Nanan, K., (2015). Heat transfer enhancement by tapered twisted tape inserts. *Chemical Engineering and Processing: Process Intensification*. 96: 62–71. doi: 10.1016/j.cep.2015.08.002.
- [4] Guo, J., Xu, M., Cheng, L., (2010). Numerical investigations of circular tube fitted with helical screw-tape inserts from the viewpoint of field synergy principle. *Chemical Engineering and Processing: Process Intensification*. 49(4): 410–7. doi: 10.1016/j.cep.2010.02.011.
- [5] Naphon, P., (2006). Effect of coil-wire insert on heat transfer enhancement and pressure drop of the horizontal concentric tubes. *International Communications in Heat and Mass Transfer*. 33(6): 753–63. doi: 10.1016/j.icheatmasstransfer.2006.01.020.
- [6] Banihashemi, S., Assari, M., Javadi, S., Vahidifar, S., (2022). Turbulent flow thermal characteristics in a pipe with ring insert: An experimental and numerical study. *Chemical Engineering and Processing - Process Intensification*. 172: 108780. doi: 10.1016/j.cep.2022.108780.
- [7] Bucak, H., Yilmaz, F., (2020). The current state on the thermal performance of twisted tapes: A geometrical categorisation approach. *Chemical Engineering and Processing - Process Intensification*. 153: 107929. doi: 10.1016/j.cep.2020.107929.
- [8] Rahimi, M., Shabaniyan, S.R., Alsairafi, A.A., (2009). Experimental and CFD studies on heat transfer and friction factor characteristics of a tube equipped with modified twisted tape inserts. *Chemical Engineering and Processing: Process Intensification*. 48(3): 762–70. doi: 10.1016/j.cep.2008.09.007.
- [9] Eiamsa-ard, S., Thianpong, C., Eiamsa-ard, P., (2010). Turbulent heat transfer enhancement by counter/co-swirling flow in a tube fitted with twin twisted tapes. *Experimental Thermal and Fluid Science*. 34(1): 53–62. doi: 10.1016/j.expthermflusci.2009.09.002.
- [10] Zhang, X., Liu, Z., Liu, W., (2012). Numerical studies on heat transfer and flow characteristics for laminar flow in a tube with multiple regularly spaced twisted tapes. *International Journal of Thermal Sciences*. 58: 157–67. doi: 10.1016/j.ijthermalsci.2012.02.025.
- [11] Li, P., Liu, Z., Liu, W., Chen, G., (2015). Numerical study on heat transfer enhancement characteristics of tube insert-

- ed with centrally hollow narrow twisted tapes. *International Journal of Heat and Mass Transfer*. 88: 481–91. doi: 10.1016/j.ijheatmasstransfer.2015.04.103.
- [12] Bhuiya, M.M.K., Chowdhury, M.S.U., Shahabuddin, M., Saha, M., Memon, L.A., (2013). Thermal characteristics in a heat exchanger tube fitted with triple twisted tape inserts. *International Communications in Heat and Mass Transfer*. 48: 124–32. doi: 10.1016/j.icheatmasstransfer.2013.08.024.
- [13] Skullong, S., Promvong, P., Thianpong, C., Pimsarn, M., (2016). Heat transfer and turbulent flow friction in a round tube with staggered-winglet perforated-tapes. *International Journal of Heat and Mass Transfer*. 95: 230–42. doi: 10.1016/j.ijheatmasstransfer.2015.12.007.
- [14] Dagdevir, T., Ozceyhan, V., (2021). An experimental study on heat transfer enhancement and flow characteristics of a tube with plain, perforated and dimpled twisted tape inserts. *International Journal of Thermal Sciences*. 159: 106564. doi: 10.1016/j.ijthermalsci.2020.106564.
- [15] Dagdevir, T., Uyanik, M., Ozceyhan, V., (2021). The experimental thermal and hydraulic performance analyses for the location of perforations and dimples on the twisted tapes in twisted tape inserted tube. *International Journal of Thermal Sciences*. 167: 107033. doi: 10.1016/j.ijthermalsci.2021.107033.
- [16] Ponnada, S., Subrahmanyam, T., Naidu, S.V., (2019). A comparative study on the thermal performance of water in a circular tube with twisted tapes, perforated twisted tapes and perforated twisted tapes with alternate axis. *International Journal of Thermal Sciences*. 136: 530–8. doi: 10.1016/j.ijthermalsci.2018.11.008.
- [17] Wongcharee, K., Eiamsa-ard, S., (2011). Enhancement of heat transfer using CuO/water nanofluid and twisted tape with alternate axis. *International Communications in Heat and Mass Transfer*. 38(6): 742–8. doi: 10.1016/j.icheatmasstransfer.2011.03.011.
- [18] Wongcharee, K., Eiamsa-ard, S., (2011). Friction and heat transfer characteristics of laminar swirl flow through the round tubes inserted with alternate clockwise and counter-clockwise twisted-tapes. *International Communications in Heat and Mass Transfer*. 38(3): 348–52. doi: 10.1016/J.ICHEATMASSTRANSFER.2010.12.007.
- [19] Abolarin, S.M., Everts, M., Meyer, J.P., (2019). Heat transfer and pressure drop characteristics of alternating clockwise and counter clockwise twisted tape inserts in the transitional flow regime. *International Journal of Heat and Mass Transfer*. 133: 203–17. doi: 10.1016/J.IJHEATMASSTRANSFER.2018.12.107.
- [20] Fluent., (2016). ANSYS Fluent User Guide.
- [21] Incropera, F. P., DeWitt, D. P., Bergman, T. L., & Lavine, A.S., (1996). *Fundamentals of heat and mass transfer*. 6th ed., New York: Wiley.
- [22] Dittus, F.W., Boelter, L.M.K., (1930). *Heat Transfer in Automobile Radiators of the Tubular Type*. University of California Publications on Engineering. 2.
- [23] Blasius, H., (1913). Das Aehnlichkeitsgesetz bei Reibungsvorgängen in Flüssigkeiten. *Mitt. Forschungsarbeiten Gebiete Ingenieurwesens*. 131.

# Estimation of three-point bending behavior using finite element method for 3D-printed polymeric sandwich structures with honeycomb and reentrant core

**Meltem Eryildiz<sup>1\*</sup>**

<sup>1</sup>Department of Mechanical Engineering, Faculty of Engineering and Architecture, Beykent University, Istanbul, 34398, Turkey

**Orcid:** M. Eryildiz (0000-0002-2683-560X)

**Abstract:** Sandwich structures are known as ultra-light porous materials. Because the structure has advantages in terms of acoustics, fatigue, and impact resistance that conventional stiffened plates cannot match, it has become a popular material in aerospace, automotive, marine, windmill, and architectural applications. One promising method for decreasing production waste and enhancing flexural stress is to employ additive manufacture (AM) technologies for sandwich structure manufacturing. In this study, polylactic acid (PLA), acrylonitrile butadiene styrene (ABS), and polyethylene terephthalate glycol (PETG) sandwich structures with reentrant and honeycomb cores were designed and then to compare the stress distributions in these sandwich composites, a finite element analysis (FEA) was used. According to the findings, higher flexure stresses and specific energy absorption were obtained in the reentrant sandwich structures compared to honeycomb sandwich structures. A minimum equivalent stress value was found in the ABS material, while a maximum equivalent stress value was found in the PLA material.

**Keywords:** Sandwich Structures, 3D printing, Finite Element Analysis, Three-point Bending

## I. Introduction

A sandwich structure is a porous ultra-lightweight material with a large specific surface area and high specific stiffness. Acoustics, fatigue, and impact resistance are all advantages of the sandwich structure that conventional stiffened plates cannot match. Therefore, sandwich structures have become a popular material in aerospace, automotive, marine, windmill, and architectural practices [1-2]. The application of additive manufacturing (AM) techniques for sandwich structure manufacturing is one promising technique for decreasing production waste and improving lateral stiffness. Additive manufacturing has been employed in industries that require a small number of complicated parts because AM can create net-shaped parts that would be impossible to build using traditional manufacturing methods. Moreover, AM has the ability to build interior geometries that would otherwise be impossible to achieve using a typical milling technique [3].

Sandwich structures contain a lightweight core between two thin solid face-sheets having strong flexural rigidity on top and bottom surfaces. The lightweight core connects the face-sheets with minimal weight gain, re-

sulting in high resistance to bending and buckling, as well as excellent energy absorption and shear stiffness. Transverse shear and compression loads are carried by the lightweight cores, whereas in-plane and flexure loads are carried by the solid face sheets [2]. A sandwich structure's structural and energy absorption capabilities, and also the failure mechanism, are all influenced by the geometrical parameters, material, and core design. Among all possible core designs, honeycomb and reentrant core have been extensively investigated. Castro et al. [4] examined the mechanical performance of three different 3D printed sandwich structure core designs. Chang et al. [5] studied the reentrant and the honeycomb sandwich structure experimentally and numerically. Zaharia et al. [6] investigated the mechanical behavior of 3D-printed sandwich structures having honeycomb, diamond-celled and corrugated core designs. Ingrole et al. [7] worked on the energy absorption and mechanical behavior of the 3D-printed sandwich structures having reentrant cores and compared them with the sandwich structures having honeycomb cores.

Honeycomb core is a popular choice for secondary structure applications due to its high mechanical properties.

\* Corresponding author.  
Email: meltemeryildiz@beykent.edu.tr



They are rigid and lightweight, and they can absorb a lot of energy when subjected to shockwaves and impact loads, which makes them ideal for sports equipment (e.g. helmets) and vehicles (e.g. bumpers). Several analytical, computational, and experimental studies showed that sandwich structures having honeycomb cores are rigid, lightweight, and when they are crushed, they absorb a lot of energy, especially in the out-of-plane direction [2,3,8]. Auxetic structures have lately gained a lot of interest since they have the uncommon property of thickening when stretched; that is, they have negative Poisson's ratios. One of these sorts of the core is reentrant core since it has a negative Poisson's ratio [8,9]. A negative Poisson's ratio coefficient for a material could result in increased indentation resistance, improved bending stiffness, shear resistance, and improved dielectric characteristics for microwave absorbers. Reentrant cores have a wide range of possible applications including engineering fields such as vibroacoustic, packaging, biomedicine, sensors, and automotive engineering [10-11]

In the literature, polylactic acid (PLA) is mostly used to make 3D printed sandwich structures. The choice of core material, on the other hand, has an impact on a sandwich structure's high stiffness, strong impact resistance, and great strength-to-weight ratio [3,12]. In the present study, polylactic acid (PLA), acrylonitrile-butadiene-styrene (ABS), and polyethylene-terephthalate-glycol (PETG) sandwich structures with reentrant and honeycomb cores are designed using CAD software. The stress distributions in these sandwich structures are then compared using a finite element analysis (FEA). In addition, the influence of the different core materials is examined and their potential in structural applications is indicated.

## 2. Materials and Method

The geometric features of the designed (by the CATIA V5 software) honeycomb and reentrant sandwich structures are given in Figure 1.

The finite element analysis (FEA) was performed using commercial software ANSYS to simulate the behavior of sandwich structures during three-point bending tests. The properties of materials used in the analysis are given in Table 1.

**Table 1.** Properties of PLA, ABS, and PETG

Properties\Material	PLA	ABS	PETG
Young's Modulus (Pa)	3,45E+09	2,39E+09	2,95E+09
Poisson's Ratio	0,39	0,399	0,33
Yield Strength (Pa)	5,41E+07	4,14E+07	5,3E+07
Tangent Modulus (Pa)	0,1	0,1	0,1
Shear Modulus (Pa)	1,241E+09	8,5418E+08	1,109E+09
Bulk Modulus (Pa)	5,2273E+09	3,9439E+09	2,89223E+09
Density (kg/m <sup>3</sup> )	1250	1040	1375

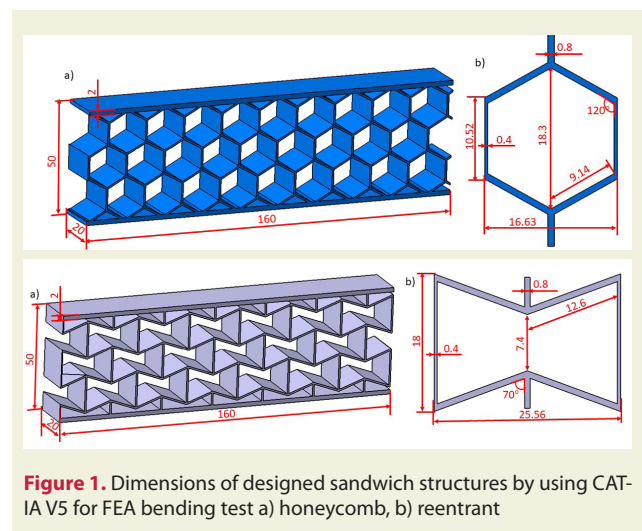


**Figure 1.** Dimensions of designed sandwich structures by using CATIA V5 for FEA bending test a) honeycomb, b) reentrant

Sandwich structures under a quasi-static three-point bending load were simulated in accordance with ASTM C393/393M-20 as shown in Figure 2. The load was applied by a center 10 mm diameter roller, the supports were two exterior 10-mm diameter cylindrical rollers, and the span length was 125 mm. In the FEA analysis, the bottom support rollers were fixed, and the central roller was given a displacement of 60 mm in the z-direction. Structural steel was chosen as the material of the rollers. The material properties of the sandwich structures in the geometry were assigned as PLA, ABS and PETG for each analysis and mesh structure were determined. The meshing was performed with quad/tri elements using an automatic methodology. Mesh model was given in Figure 2. The average element quality, aspect ratio and skewness for the reentrant model were 0.90324, 1.3409, 0.19042, respectively. The honeycomb model's average element quality, aspect ratio and skewness were, respectively, 0.93323, 1.3254, and 0.14108. For the reentrant model, the nodes and elements were 46073 and 37560, while for the honeycomb model, they were 62181 and 34560. The analysis was carried out in ANSYS 2021 R2 workbench and the results were received.

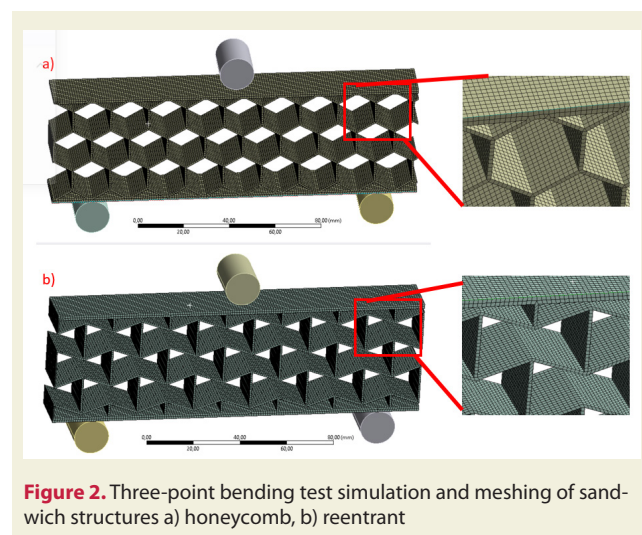


**Figure 2.** Three-point bending test simulation and meshing of sandwich structures a) honeycomb, b) reentrant

The highest stress experienced by the specimen under a given load is known as flexural stress. The maximum stress experienced in correspondence to the outer surface (at the midway) using the geometry, boundary conditions, and load configuration was estimated as:

$$\sigma = 3FL/2wd^2 \tag{1}$$

In Eq.(1), F is the load at the considered point and it is expressed in [N]. w is the width, L is the length and d is the height of the sandwich structure.

### 3. Results and Discussions

The force, flexure stress, equivalent von mises stress, and internal energy values after FEA analysis of the sandwich samples are given in Table 2. Specific energy absorption (SEA) is a significant measure for assessing the energy absorption of sandwich structures. It is defined as the sandwich structures' unit energy absorption efficiency, expressed as [13]:

$$SEA = \text{Absorbed Energy} / \text{Mass} \tag{2}$$

**Table 2.** FEA analysis of the sandwich structures

	Force Reaction (N)	Mass (g)	Flexure stress (MPa)	Equivalent (Von-mises)(MPa)	Specific energy absorption (J/g)
<b>PLA-reentrant</b>	2152,6	41,448	41,329	53,650	2,845
<b>ABS-reentrant</b>	3106,6	31,349	59,646	41,046	2,846
<b>PETG-reentrant</b>	2956,0	37,680	56,755	51,951	3,066
<b>PLA-honeycomb</b>	1234,6	38,120	23,704	54,053	2,197
<b>ABS-honeycomb</b>	1945,9	28,833	37,361	41,353	2,358
<b>PETG-honeycomb</b>	2591,6	34,655	49,758	52,938	2,604

The overall trend in Table 2 showed that higher specific energy absorption were obtained in the reentrant sandwich structures compared to honeycomb sandwich structures. By comparing the sandwich structures with reentrant and honeycomb core designs, it should be highlighted that the reentrant core absorbed more energy than the honeycomb core. One of the main reasons is that the inner density of the core in the reentrant was higher than in the honeycomb core design [13]. Moreover, SEA was increased from PLA to PETG. The reason for this is that PETG is a denser material that requires more effort to flexure and, as a result, absorbs more energy.

According to the three-point bending test results, the reentrant design showed increased flexure stresses, as shown in Figure 3. It can be observed that the reentrant core took the maximum amount of load under flexure. At reentrant sandwich structure, each layer of the cores fails one at a time under compression loading, leading up to a higher strain of failure of the samples. After the failure of each layer, the structures come to an equilibrium and can take

further loading until the failure of the next layer. This phenomenon is often referred to as snap-through instability. Due to this type of failure, this structure tends to have a higher flexure strength compared to honeycomb [8, 14]. The flexure stress of the PETG sandwich structure with reentrant core (~56 MPa) was the highest followed by the PETG sandwich structure with honeycomb core (~49 MPa).

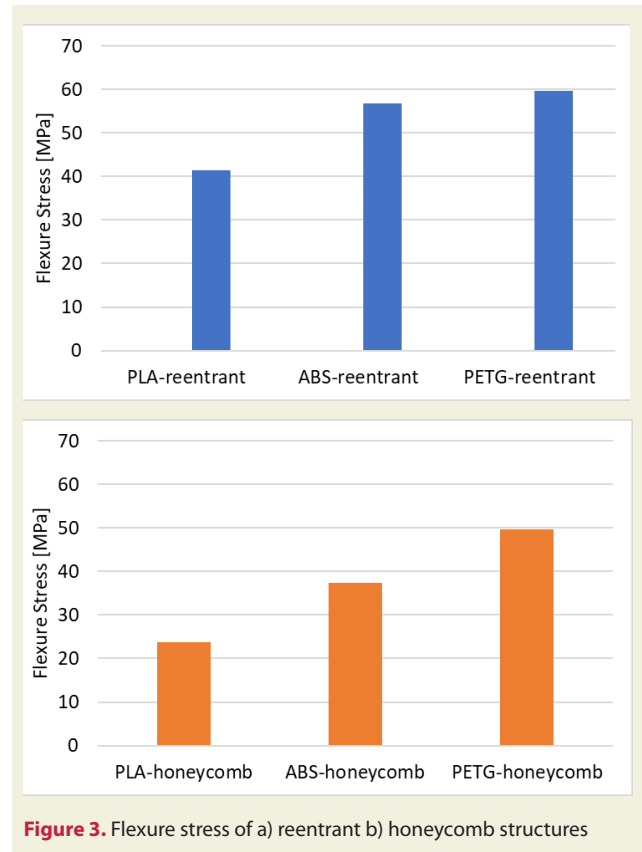


Figure 4 shows the equivalent (Von-Mises) stress values after the three-point bending test, which show that the highest Von-Mises stress occurred in the PLA sandwich structure, which was prone to failure. On the top and bottom layers of the core, the largest equivalent Von-Mises stresses were concentrated. In the light of these results, for reentrant core design, a minimum equivalent stress value of 41.046 MPa was found in the ABS material, while a maximum equivalent stress value of 53.65 MPa was found in the PLA material for reentrant core design. Similarly, for the honeycomb core design, the ABS material had a minimum equivalent stress value of 41.353 MPa, whereas the PLA material had a maximum equivalent stress value of 54.053 MPa. This can be because PLA is brittle material than ABS.

The filament type that is selected has a significant impact on the environment as well. PETG material is the most environmentally friendly, whereas ABS material is the least environmentally friendly. PLA have received widespread praise as a renewable, plant-based, and biodegradable replacement for plastics made from petroleum [15]. Furthermore, it is evident from the comparison (Figure 4)

that the PETG is appropriate for sandwich structures that need high flexure strength. PETG has a strong shock resistance and load carrying capacity because the resultant monomers are larger than the parent monomer ethylene glycol following the crystallization process [16].

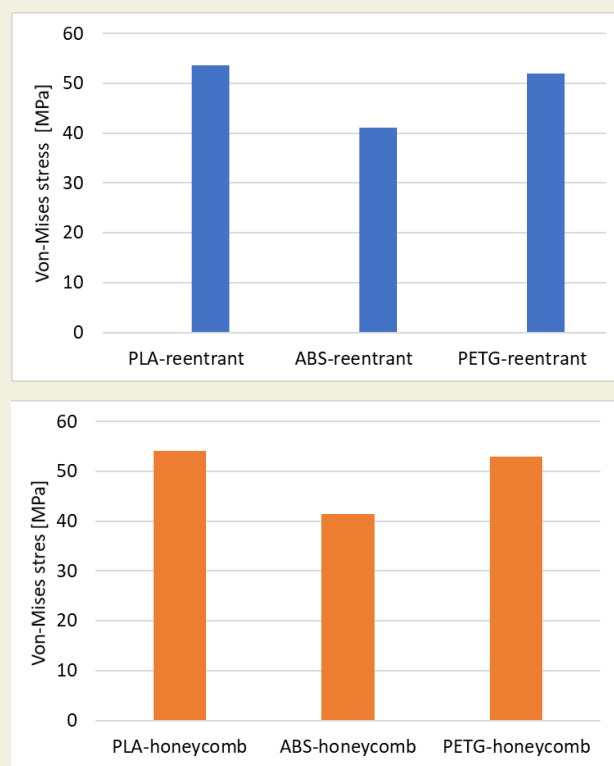


Figure 4. The equivalent (Von-Mises) stress a) reentrant b) honeycomb structures

As shown in Figure 5 and Figure 6, the reentrant core of the sandwich structure was attracted to the center of the panel due to the auxetic effect. The core material flew in a lateral direction towards the center, providing greater support for the flexure and resulting in a higher load level. The honeycomb core, on the other hand, showed no material concentration effect. The core in the central zone was compressed while those on the sides tended to expand away from the flexure center, indicating that the honeycomb core has a lower bending stiffness than the reentrant core. In addition, the auxetic reentrant core deformed consistently, distributing stress evenly [5-8].

Moreover, in the reentrant core design, the cores were more in a vertical position thus, the structure was stiffer. Many structural components in the three-point bending test are parallel to the z-axis direction of build orientation, and thus failure happens with loads orientated parallel to the z-axis. The honeycomb core had corners that are 120 degrees, whereas the reentrant core had corners that are 70 degrees. The reentrant core had fewer angle components in the z-axis direction. Thus, it may be concluded that it had a larger reinforcing effect in the loading direction and was, therefore, stiffer than the honeycomb core [8,17].

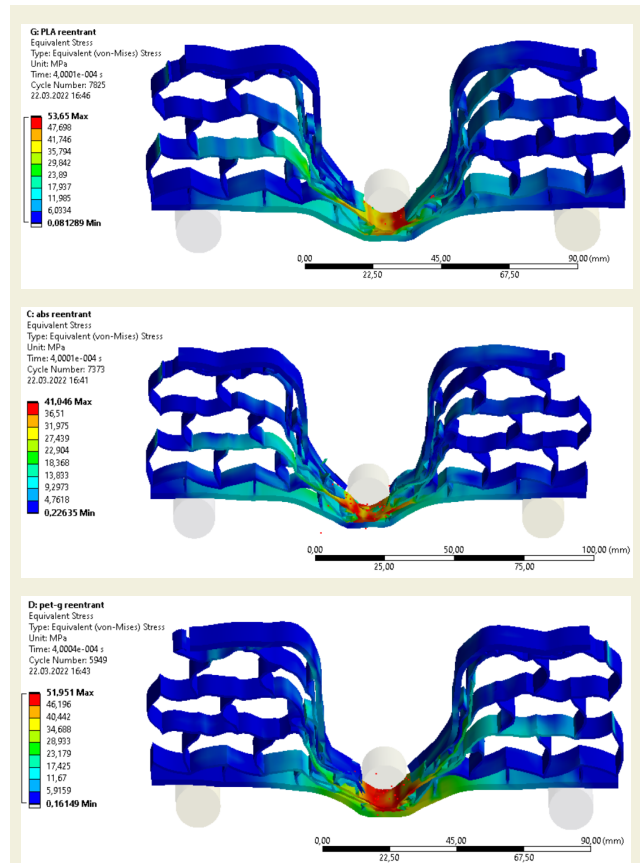


Figure 5. Equivalent stress distribution of sandwich structures with reentrant core a) PLA, b) ABS, c) PETG

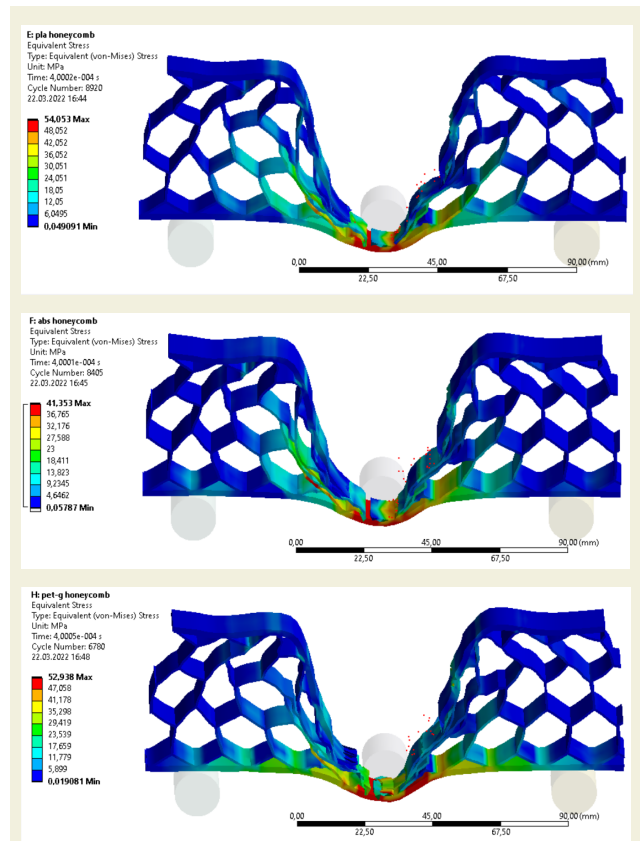


Figure 6. Equivalent stress distribution of sandwich structures with Honeycomb core a) PLA, b) ABS, c) PETG

## 4. Conclusions

PLA, ABS, and PETG sandwich structures with reentrant and honeycomb cores were designed using CATIA V5 software in this study, and then ANSYS finite element analysis software was used to compare the stress distributions in these sandwich composites. According to the results:

- Higher flexure stresses and specific energy absorption were obtained in the reentrant sandwich structures compared to honeycomb sandwich structures.
- The equivalent (Von-Mises) stress values after the three-point bending test showed that the highest Von-Mises stress occurred in the PLA sandwich structure, which was prone to failure.
- Minimum equivalent stress value of 41.046 MPa was found in the ABS material, while a maximum equivalent stress value of 53.65 MPa was found in the PLA material for reentrant core design.
- For the honeycomb core design, the ABS material had a minimum equivalent stress value of 41.353 MPa, whereas the PLA material had a maximum equivalent stress value of 54.053 MPa.

## References

- [1] Xie, S., Feng, Z., Zhou, H., & Wang, D. (2021). Three-point bending behavior of Nomex honeycomb sandwich panels: Experiment and simulation. *Mechanics of Advanced Materials and Structures*, 28(18): 1917-1931, DOI:10.1080/15376494.2020.1712751
- [2] Sarvestani, H. Y., Akbarzadeh, A. H., Mirbolghasemi, A., & Hermenean, K. (2018). 3D printed meta-sandwich structures: Failure mechanism, energy absorption and multi-hit capability. *Materials & Design*, 160: 179-193, DOI:10.1016/j.matdes.2018.08.061
- [3] Pollard, D., Ward, C., Herrmann, G., & Etches, J. (2017). The manufacture of honeycomb cores using Fused Deposition Modeling. *Advanced Manufacturing: Polymer & Composites Science*, 3(1): 21-31, DOI:10.1080/20550340.2017.1306337
- [4] de Castro, B. D., Magalhães, F. D. C., Panzera, T. H., & Campos Rubio, J. C. (2021). An assessment of fully integrated polymer sandwich structures designed by additive manufacturing. *Journal of Materials Engineering and Performance*, 30(7): 5031-5038, DOI:10.1007/s11665-021-05604-8
- [5] Qi, C., Remennikov, A., Pei, L. Z., Yang, S., Yu, Z. H., & Ngo, T. D. (2017). Impact and close-in blast response of auxetic honeycomb-cored sandwich panels: experimental tests and numerical simulations. *Composite structures*, 180: 161-178, DOI: 10.1016/j.compstruct.2017.08.020
- [6] Zaharia, S. M., Enescu, L. A., & Pop, M. A. (2020). Mechanical performances of lightweight sandwich structures produced by material extrusion-based additive manufacturing. *Polymers*, 12(8): 1740, DOI: 10.3390/polym12081740
- [7] Ingrole, A., Hao, A., & Liang, R. (2017). Design and modeling of auxetic and hybrid honeycomb structures for in-plane property enhancement. *Materials & Design*, 117: 72-83, DOI:10.1016/j.matdes.2016.12.067
- [8] Li, T., & Wang, L. (2017). Bending behavior of sandwich composite structures with tunable 3D-printed core materials. *Composite Structures*, 175: 46-57, DOI:10.1016/j.compstruct.2017.05.001
- [9] Essassi, K., Rebiere, J. L., El Mahi, A., Souf, M. A. B., Bouguecha, A., & Haddar, M. (2020). Experimental and analytical investigation of the bending behaviour of 3D-printed bio-based sandwich structures composites with auxetic core under cyclic fatigue tests. *Composites Part A: Applied Science and Manufacturing*, 131: 105775, DOI:10.1016/j.compositesa.2020.105775
- [10] Yang, S., Qi, C., Guo, D. M., & Wang, D. (2012). Energy absorption of an re-entrant honeycombs with negative Poisson's ratio. In *Applied Mechanics and Materials* (Vol. 148, pp. 992-995). Trans Tech Publications Ltd., DOI:10.4028/www.scientific.net/AMM.148-149.992
- [11] Najafi, M., Ahmadi, H., & Liaghat, G. (2022). Investigation on the flexural properties of sandwich beams with auxetic core. *Journal of the Brazilian Society of Mechanical Sciences and Engineering*, 44(2):1-11, DOI:10.1007/s40430-022-03368-3
- [12] Gohar, S., Hussain, G., Ali, A., & Ahmad, H. (2021). Mechanical performance of honeycomb sandwich structures built by FDM printing technique. *Journal of Thermoplastic Composite Materials*, 0892705721997892, DOI: 10.1177/0892705721997892
- [13] Serjouei, A., Yousefi, A., Jenaki, A., Bodaghi, M., & Mehrpouya, M. (2022). 4D printed shape memory sandwich structures: Experimental analysis and numerical modeling. *Smart Materials and Structures*, 31: 055014, DOI: 10.1088/1361-665X/ac60b5
- [14] Nath, S. D., & Nilufar, S. (2022). Performance Evaluation of Sandwich Structures Printed by Vat Photopolymerization. *Polymers*, 14(8), 1513, DOI: 10.3390/polym14081513
- [15] Kumar, R., Sharma, H., Saran, C., Tripathy, T. S., Sangwan, K. S., & Herrmann, C. (2022). A Comparative Study on the Life Cycle Assessment of a 3D Printed Product with PLA, ABS & PETG Materials. *Procedia CIRP*, 107, 15-20, DOI: 10.1016/j.procir.2022.04.003
- [16] Vikneswaran, S. K., Nagarajan, P., Dinesh, S. K., Kumar, K. S., & Megalingam, A. (2022). Investigation of the tensile behaviour of PolyLactic Acid, Acrylonitrile Butadiene Styrene, and Polyethylene Terephthalate Glycol materials. *Materials Today: Proceedings*, In press, DOI: 10.1016/j.matpr.2022.04.897
- [17] Sugiyama, K., Matsuzaki, R., Ueda, M., Todoroki, A., & Hirano, Y. (2018). 3D printing of composite sandwich structures using continuous carbon fiber and fiber tension. *Composites Part A: Applied Science and Manufacturing*, 113: 114-121, DOI: 10.1016/j.compositesa.2018.07.029

# Computer aided numerical damage analysis of the axle shaft

Hamit Adin<sup>1</sup>, Raşit Koray Ergün<sup>1\*</sup>, Mehmet Şükrü Adin<sup>1</sup>

<sup>1</sup>Batman University/ Mechanical Engineering Department, Turkey

**Orcid:** H. Adin (0000-0003-2455-967X), R.K. Ergün (0000-0002-5440-0646), M.Ş. Adin (0000-0002-2307-9669)

**Abstract:** Axle shafts are one of the most important components used in power transmission. These components, which are used in many different places, can cause great costs in case of failure or fracture. Among the main reasons for these undesirable situations are wrong axle shaft selections and inappropriate metallurgical properties. In order to prevent such unfavourable situations and to investigate the causes of damages, numerical analyses offer cost-effective solutions. In this study, the mechanical damage analysis of the axle shaft and the characteristic changes in steel materials as a result of static loading were investigated numerically. In order to observe the mechanical behaviour of the axle shaft under various loading conditions, mechanical tests should be supported by numerical analysis. Because the physical causes of damage development can be understood through numerical analysis. The aim of our study is to reach the most suitable values in the design of the axle shaft made of AISI 1035 steel. Values were obtained by performing numerical analyses of the axle shaft designed with Solidworks program. As a result of the analysis, it was observed that deformation occurred at the ends of the axle.

**Keywords:** Static load, design, numerical analysis, axle.

## 1. Introduction

Today, while transportation is constantly moving forward, costs are increasing. The aim is to obtain light structures that are suitable in terms of weight, sufficient in strength, and to save materials and energy. Axles are not only used in transport vehicles but also in buses, automobiles, and forklifts. Axles must be of a reliable structure due to their place of use. The external effects that the axles are generally exposed to are the applied loads. Damage is the inability of a structure, machine, or its parts to perform their functions [1]. Damages usually occur as a result of forcing parts by mechanical or chemical effects [2]. Damages in structural elements or machine parts occur due to mistakes made in any of the stages such as design, production, and assembly [3]. Axles are very important in vehicles. Axles are steel shafts that transmit the rotational movement from the differential to the wheels in motor vehicles. It is the part that transfers the power and torque from the engine to the wheels. It carries the entire load in vehicles, including passengers [4]. Öndürücü and Kanbir emphasized that the material used in damaged machine parts is very important in their studies. As a result, they tried to determine the cause and mode of damage by evaluating the data obtained by mechanical experiments and metallographic examinations. They found that the part was damaged due to excessive stress [5]. In this study,

Mercan focused on the causes of damage by examining the damage mechanisms of welded metal materials and aimed to create a systematic approach to use in damage analysis [6]. In this study, Dursun and Özbay performed damage analysis using a graded failure model to determine the tensile strength of bolted composite materials. The damage model was prepared with Ansys APDL software. Finite element analyses were performed using the Hashin damage criterion. Comparing the results with experimental studies, they reached similar results [7]. In this study, Turan and Kaman experimentally and numerically investigated the damage analysis of single-lap adhesive bonds obtained with adhesive in order to join composite boards. They performed the numerical work in the ANSYS program, which coordinates with the Finite Element Method. While the damage analysis, they used Hashin damage theory for composites and maximum principal stress damage theory for adhesive material. As a result, they observed that the changes in the adhesion surface areas were effective in the damage loads [8].

Yalçın et al. aimed to determine the causes of damage in 1.2367 hot work tool steel injection runner bushings, which cracked due to repeated mechanical and thermal loads, by using finite element analysis and optical research methods. They have made changes in the design of the runner bush in order to prevent crack damage. As a re-

\* Corresponding author.  
Email: raskoray.ergun@batman.edu.tr



sult, by making improvements in the design phase, they observed a reduction in the stresses formed in the injection runner bushings and achieved improvements in the face of mechanical loads [9]. In this study, Parnas et al. applied crack propagation tests to determine the mechanical properties of composite materials. A Finite Element model was created to investigate hollow composite materials. They developed a progressive damage analysis to perform a realistic simulation. They discussed the results obtained from the simulations in detail by choosing the most accurate model [10]. In this study, Şen and Pakdil experimentally investigated the damage analysis of laminated composite materials connected with a single bolt under moment loads. As a result, they observed that the lowest damage loads occurred in composite specimens without preloading torque [11].

In our study, numerical damage analysis of the axle shaft was performed. The investigated axle shaft is made of AISI 1035 steel. These shafts, which are used as machine elements in various places, are frequently preferred in load-carrying. As stated in the above-mentioned studies on various machine elements, each damage has its unique situation. The damage analysis study carried out here will bring along solutions for the prevention of damage to the axle shafts.

## 2. Material and Method

Axle shafts are one of the important parts of powertrains. In order to be able to move a vehicle, transmission organs are needed to increase the torque produced in the engine by the required amount and transmit it to the wheels and to give the vehicle traction as much as its structure allows [12]. Axle shaft damage constitutes 26% of the damages that occur in a vehicle [13]. Although the axles produced from composite materials are extremely light, the most used material in axle manufacturing is steel [14]. Tempered steels are unalloyed and alloyed machine-building steels that are suitable for hardening, especially in terms of carbon content, and show high toughness at a certain tensile strength at the end of the curing process [15].

Mechanical damage analysis has become an important engineering field with scientific methods [5].

Damage is the failure of a structure or structural element to perform its expected functions under service conditions. The causes of industrial faults that because damage are shown in Figure 1 [16].

After the damage occurs, necessary inspection activities are carried out at the location of the damaged system. The main stages to be followed in the damage analysis are shown in Figure 2 [16]. The damage analysis report is prepared as a result of the investigations. All data obtained should be recorded in the damage analysis report.

The distribution of the damages that are frequently en-

countered in the industry in terms of percentiles according to their causes is given in Figure 3 [16]. As seen in Figure 3, it has been determined that the highest factor that creates damage is “wrong material selection”. Wrong material selection is followed by manufacturing and heat treatment errors.

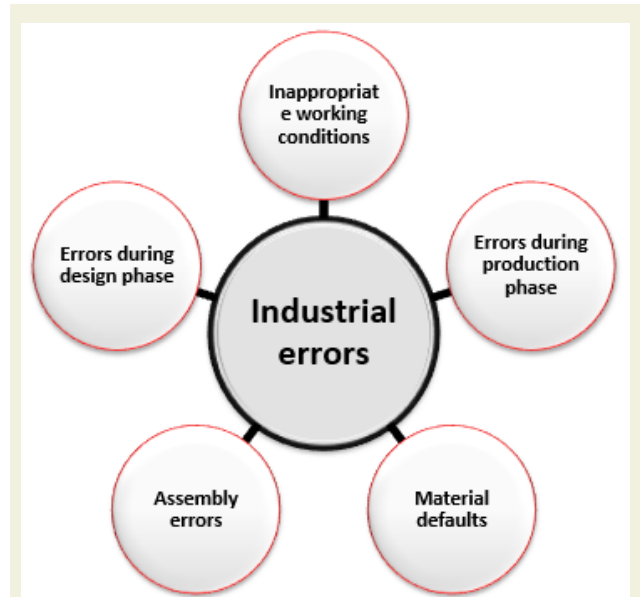


Figure 1. Industrial faults causing damage [16]

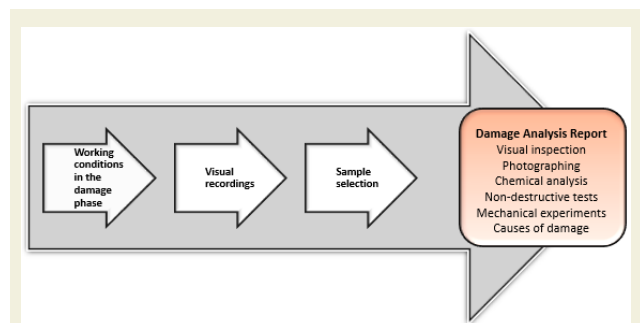


Figure 2. The main stages to be followed in the damage analysis [16]

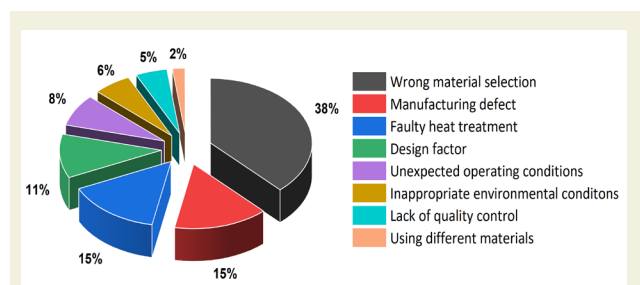


Figure 3. Causes of damage frequently encountered in industry [16].

Major damage mechanisms in axle shafts can be listed as bearing deterioration, overload, seal deformation, impact, and deterioration.

Axles are used in vehicles to transmit the movement from the differential to the wheels. Axle shafts are parts that work during vehicle movement. Axle shafts, which are

one of the powertrains of vehicles, are exposed to different loads and therefore, some damage and malfunctions may occur in the axle shafts. Axles are subjected to both torsional and bending stresses. Materials used to manufacture axle shafts must be tough to lean the pressure and loads caused by heavy weights [17]. A tough material must be produced to resist the varied stresses, resist spline wear and provide great strength to fatigue. Medium carbon alloy steel having such elements as molybdenum, chromium, and nickel is a common selection [18]. Since axles conduct the force that rotates the wheels, each vehicle requires axle shafts in order to operate properly [19]. Axles are principally responsible to transfer the rotational force and power to move the vehicle [20].

In this study, the axle shaft manufactured by utilizing AISI 1035 steel was investigated. Static analysis investigations were started after the fracture occurred in the shafts after a certain working period. The mechanical damage analysis of the axle shaft and the characteristic changes in steel materials as a result of static loading were investigated numerically. In order to observe the mechanical behaviour of the axle shaft under various loading conditions, mechanical tests were supported by numerical analysis. AISI 1035 sheets of steel are utilized in the construction of machine parts such as bolts, bearer mechanisms, axle shafts, and gear wheels. AISI 1035 sheets of steel can be hardened by induction or flame [21]. Chemical compositions, hardness values obtained from the material surface, and the hardening depth of the steel material have major importance in the selection of steel materials to be heat treated [22].

The chemical composition of AISI 1035 steel is given in Table 1.

**Table 1.** Chemical composition of AISI 1035 steel

Chemical composition of AISI 1035 steel				
Material	Elements			
AISI 1035	C	Si	Mn	Fe
Min. (wt.%)	0.32	0.15	0.50	99.03
Max. (wt.%)	0.39	0.35	0.80	89.46

In addition to its superior hardening properties, high load bearing capacity and toughness are sought in tempered steels. In order to obtain high hardening values for tempered steels, carbon is added at a higher rate than other steel types. While the machine elements perform the functions expected from them, the surfaces of the parts are exposed to higher stress and higher abrasive forces compared to their inner parts. When these stresses and forces exceed the surface strength limit of the material, cracks begin on the material surface. However, the increase in the load of the vehicle and the pressures it will be exposed to in potholes and bumps should also be considered [23]. Mechanical properties of AISI 1035 steel are given in Table 2.

**Table 2.** Mechanical properties of AISI 1035 steel

Mechanical properties of AISI 1035 steel			
AISI 1035	Diameter (mm)	Yield Strength(N/mm <sup>2</sup> )	Tensile Strength (N/mm <sup>2</sup> )
Min.	100	275	490
Max.	160	-	635

The damaged axle shaft manufactured by utilizing AISI 1035 steel is given in Figure 4. It was observed that the damages occurred at the tip of the shaft.



**Figure 4.** Damaged axle shaft

The model and applied loads of the axle shaft which are given in Figure 5 were determined by using the Solidworks program.

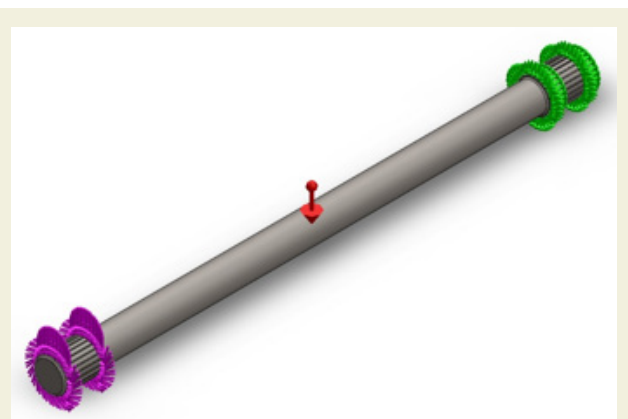


**Figure 5.** Axle shaft modelled in Solidworks

The volumetric and mass properties of the axle shaft are given in Table 3.

**Table 3.** Volumetric and mass properties of the axle shaft

Volumetric and mass properties of the axle shaft		
Mass	Volume	Density
20,0878 kg	0,00255896 m <sup>3</sup>	7.850 kg/m <sup>3</sup>

After the geometric model of the axis was created, static analyses were made using the determined mechanical properties of the material.

### 3. Results and Discussion

Static analyses are analyses to examine mechanical properties such as compression, tensile, and torque. In our study, the results of static analysis using various loads and various support points were examined. Solidworks program was used in the analysis. The head of the axle shaft is fixed and subjected to bending with a force of 250 N from its middle part. After the forces were determined, the part was meshed to be divided into finite elements.



Figure 6. Mesh structure of axle shaft

The mesh structure of the axle shaft is given in Figure 6. There are 92.767 mesh elements and 60.928 nodes in the mesh structure of the axle shaft.

The mechanical properties of the axle shaft are given in Table 4.

Table 4. Mechanical properties of the axle shaft

Mechanical properties of the axle shaft	
Material	AISI 1035
Yield Strength	2.82685e+08 N/m <sup>2</sup>
Tensile Strength	5.85e+08 N/m <sup>2</sup>
Poisson Ratio	0.29
Mass Density	7.850 kg/m <sup>3</sup>
Shear Module	8e+10 N/m <sup>2</sup>
Thermal Expansion Coefficient	1,1e-05 /Kelvin

The forces applied to the axle shaft and the reaction forces applied in the direction of the x, y, and z axes are given in Table 5.

Stress analyses of the axle shaft made of AISI 1035 steel were carried out by the Finite Element Method. Von-Mises stress criterion was used as the equivalent stress criterion in the finite element analysis of the axis. Von-Mises criterion for damage analysis is among the widely used and advanced criteria for damage analysis of steel materials. The Finite Element model of the axle shaft is a three-dimensional, tetrahedral SOLID 92 element type with 10 nodes and 30 degrees of freedom in the mesh structure.

Table 5. Axle shaft reaction forces

Axle shaft reaction forces				
	X	Y	Z	Result
Reaction Force (N)	-189,65	-1.641,96	0,678664	1.652,87
Reaction Moment (Nm)	0	0	0	0

The maximum and minimum Von-Mises values obtained at the end of the mesh process are shown in Figure 7, the maximum and minimum displacement values are shown in Figure 8, and the maximum and minimum equivalent strain values are shown in Figure 9.

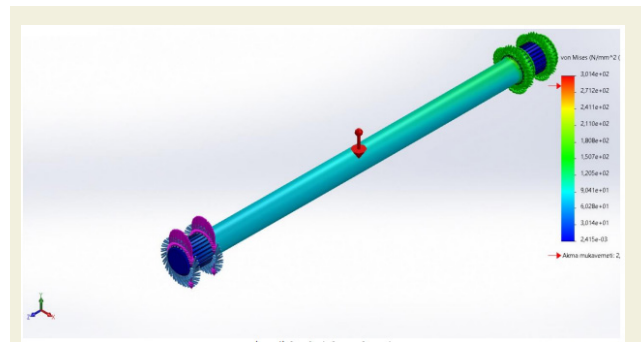


Figure 7. Maximum-minimum Von-Mises strength values

As shown in Figure 7, the maximum stress on the axle shaft was obtained as  $3.014 \times 10^2$  N/mm<sup>2</sup>. The minimum stress on the axle shaft was found to be  $2.415 \times 10^2$  N/mm<sup>2</sup>. The maximum stresses that occur as a result of the constant load applied from the middle part of the axle shaft were observed at the ends of the axle shaft. No damage is expected in the middle parts of the axle shaft and takes place in the safe zone.

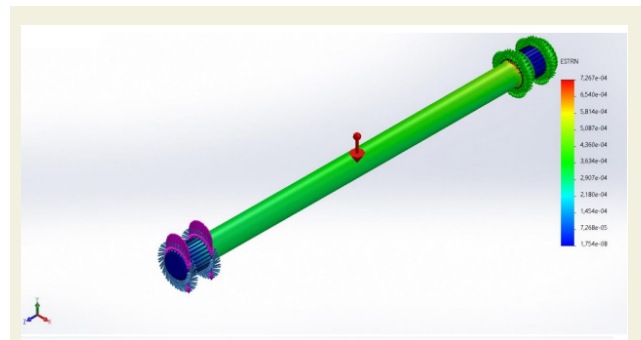


Figure 8. Maximum-minimum equivalent stresses

As shown in Figure 8, the maximum equivalent stress on the axle shaft was measured as  $7.267 \times 10^3$  N/mm<sup>2</sup>. The minimum equivalent stress on the axle shaft was measured as  $1.754 \times 10^3$  N/mm<sup>2</sup>. The maximum equivalent stress values formed as a result of the constant load applied from the middle part of the axle shaft were observed at the ends of the axle shaft. The shaft is considered to be in the safe zone since no damage has occurred in the middle parts of the axle shaft.

In this study, numerical analyses of axles used in heavy-duty vehicles were carried out in Solidworks environment under load, and the following results were obtained.

According to the analysis results, it was observed that the axles were deformed at the ends. It was determined that stress concentration occurred in the damaged parts of the axle. It has been determined that there is no deformation that may pose a danger at the midpoints of the axle shaft.

According to the numerical analysis results, the cause of the damage in the axles; is thought to be caused by the usage error of the vehicle. Sudden loads should be avoided while driving, attention should be paid to the unfavourable road conditions, and attention should be paid to the driver having adequate driving training.

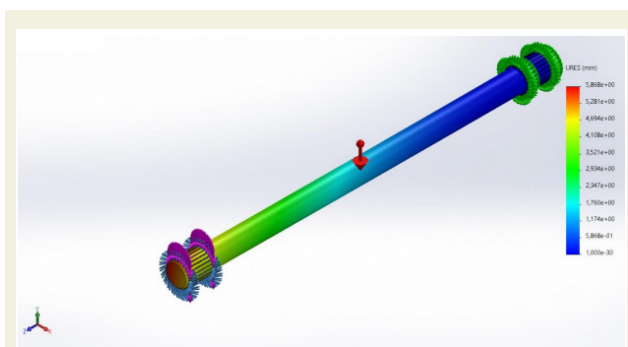


Figure 9. Maximum-minimum displacement values

As shown in Figure 9, the maximum displacement of the axle shaft was measured as 5,868 mm. The minimum displacement on the axle shaft was measured as  $1 \times 10^{-3}$  mm. It has been observed that the maximum displacements that occur as a result of the constant load applied from the middle part of the axle shaft are at the end of the axle shaft. It has been determined that the deformations that may occur in the middle parts of the axle shaft will not reach dangerous dimensions. In addition, deformations that occur in the middle parts of the axle shaft do not pose a danger, since the material does not show rigidity.

#### 4. Conclusions

In this study, numerical analyses of axles used in heavy-duty vehicles were carried out in Solidworks environment under load, and the following results were obtained.

According to the analysis results, it was observed that the axles were deformed at the ends. It was determined that stress concentration occurred in the damaged parts of the axle. It has been determined that there is no deformation that may pose a danger at the midpoints of the axle shaft.

According to the numerical analysis results, the cause of the damage in the axles; It is thought to be caused by the usage error of the vehicle. Sudden loads should be avoided while driving, attention should be paid to the unfavourable road conditions, and attention should be paid to the

driver having adequate driving training.

#### References

- [1] Eryürek, B. (1993). *Damage Analysis*. Birsen Publisher, İstanbul.
- [2] Eryürek, B., Dikicioğlu, A. (2003). The importance of damage analysis at the repair source. *Welding Technology IV. National Congress*, 67-75.
- [3] Anonim, 2002. *Failure Analysis and Prevention*. ASM International, 11, 2910s, USA.
- [4] Otopshops (2022, July 07) Axle Shafts. <https://www.otopshops.com/aks-nedir-aks-arizasi-nasil-anlasilir-haber-474>
- [5] Öndürücü, A., Kanbir, Ö. (2017). Failure analysis of gear root of a grader. *Journal of Natural and Applied Sciences*, 21(2), 599-606. doi:10.19113/sdufbed.60153.
- [6] Mercan, S. (2019). Failure analysis of weld joints. *International Journal of Innovative Engineering Applications*, 3(2), 67-75. <https://dergipark.org.tr/tr/download/article-file/902803>
- [7] Dursun, T., Özbay, M. (2020). Failure analysis of bolted laminated composite plates. *Pamukkale University Journal of Engineering Sciences*, 26(4), 613-619. doi: 10.5505/pajes.2020.99075.
- [8] Turan, K., Kaman M.O. (2010). Progressive failure analysis on the single lap bonded joints. *Pamukkale University Journal of Engineering Sciences*, 16(3), 315-323. <https://kutuphane.dogus.edu.tr/mvt/pdf.php>
- [9] Yalçın, B., Ergene, B., Nar, S. (2019). Failure analysis in injection gate brush manufactured from 1.2367 tool steel and prevention of failure with geometric design improvement. *International Journal of Technological Sciences*, 11(3), 137-146. <https://dergipark.org.tr/tr/download/article-file/918011>
- [10] Parnas, K.L. Erartsın, O., Atar, M.B., Tursun, G. (2015). Finite element analysis of perforated composite structures. *XIX. National Mechanics Congress*, 808-818.
- [11] Şen, F., Pakdil, M. (2007). Damage analysis of single bolt connected layered composite plates under moment load. *XV. National Mechanics Congress*, 703-712.
- [12] Yavuz, G. (2005). The failure analysis of the power transmission system on vehicles: shaft and axle example. *Afyon Kocatepe University Institute of Science and Technology Master Thesis*.
- [13] Heyes, A.M. (1998). *Automotive component failures*. *Engineering Failure Analysis Elsevier Science Ltd.*, 5(2), 129-141.
- [14] Temiz, V. (2022, July 07) *Machine Elements I - Shafts and Axles*. [Web.itu.edu.tr](https://web.itu.edu.tr). <https://web.itu.edu.tr/temizv/Sunular/Miller%20ve%20Akslar.pdf>
- [15] NscÇelik (2022, July 07) *Tempered Steel*. <http://www.nsc-celik.com/islahcelikleri.html>
- [16] Turan, T. (2022, July 07) *Damage Analysis*. <https://tr.linkedin.com/pulse/takim-%C3%A7eli%C4%9Fi-hasar-analizi-tuncay-turan>
- [17] Avonmachining (2022, July 07) *Axle Shafts*. <https://www.avonmachining.com/products/axle-shafts/>
- [18] Thecartech (2022, July 07) *Axle Shafts Design*. [http://thecartech.com/subjects/design/axle\\_shafts\\_design.htm](http://thecartech.com/subjects/design/axle_shafts_design.htm)

- [19] Allstate (2022, July 07) Car Axles. <https://www.allstate.com/resources/car-insurance/car-axles>
- [20] Avonmachining (2022, July 07) Axle Shafts. <https://www.avonmachining.com/what-is-an-axle-shaft/>
- [21] NetDemirÇelik (2022, July 07) Steels. <http://www.netdemircelik.com.tr/urunler/karbonlu-celikler/index.html>
- [22] Hascometal (2022, July 07) Tempered Steels. <https://www.hascometal.com/celiklerin-siniflandirilmesi/islah-celikleri-22-427>
- [23] Güven, Ş.Y., Delikanlı, K., Öncel, E. (2014). The effect to the strength of fatigue of surface hardening process by ion nitriding to the steel of AISI 4140. *SDU Journal of Technical Sciences*, 4(2), 29-39. <https://dergipark.org.tr/en/download/article-file/196141>

# Validation of A356T6 automobile wheel fatigue strength using the finite elements method

Okan Ceylan<sup>1\*</sup>, Ferhat Aydoğan<sup>1</sup>

<sup>1</sup>Döktaş R&D Center, Manisa, Turkey

**Orcid:** O. Ceylan(0000-0001-8491-312X), F. Aydoğan (0000-0002-3085-810X)

**Abstract:** In this study, A356-T6 wheel bending fatigue test limits were determined using the finite element methods and compared to experimental test results. Short and long bending fatigue tests (200.000 cycles and 1.800.000 cycles respectively) were done. Simulation models was created in Ansys by defining A356-T6 S-N curve. Simulation has been performed with test parameters. Fatigue cracks started around 210.000 and 2.000.000 cycles in accordance with simulation results. In experimental test, zinc-glycerin was applied front surfaces of wheels to obtain fatigue detects. Experimental tests were done in MAKRA BUP760 – 750 machines. The initiation cycles of fatigue cracks were recorded approximately 225.000 cycles and 2.000.000 cycles in experimental tests. According to the results, it has been revealed that the experimental, and analysis datas were parallel to each other.

**Keywords:** Bending fatigue, A356T6, Finite Element Methods, Crack, Simulation

## 1. Introduction

Wheels are very important equipment for vehicles in terms of safety, aesthetics and fuel consumption. A356-T6 material is one of the most preferred aluminum alloys in automotive wheel production due to its weight advantage and high strength properties.

Among the structural castings for automotive and aeronautical applications, A356 alloy is one of the most used cast alloys due to its good balance between casting properties and mechanical behaviour after the precipitation hardening, usually obtained by T6 heat treatment. Therefore, it represents a good candidate for fatigue critical structural applications, such as automotive wheels, engine blocks, cylinder heads, chassis, and suspension components. In particular, considering wheels, it must be pointed out that they represent an engineering component playing an important role for the safety and comfort of the vehicle.[1]

In literature, there were many studies about A356 alloys with different percentages of titanium, silisium and other alloys. However, it has been clearly seen that the fatigue strength of A356-T6 alloy were higher than other alloys.

It is known that the properties of the material change according to the variability of Casting, Heat Treatment, Machining, Painting parameters. It will be more accurate that the assumptions to be obtained as a result of using the mechanical properties of the parts obtained

with the optimized parameters in the current conditions in the simulation program to minimize these differences. For this reason, the S-N curve was obtained by performing fatigue tests at different stresses, starting from yield strength at 10 Hz and 20 Hz frequency, with samples extracted in accordance with ASTM E466 standard on wheels cast with optimized parameters at Döktaş. Obtained S-N curve data was added to Ansys software and executed on the design and verified by rotating bending fatigue tests. In this way, it is ensured that the data of the material with the same casting errors and heat treatment conditions are used.

## 2. Material and Methods

Tests were carried out on A356-T6 alloy wheels produced with LPDC method by Döktaş Dökümcülük Trade. and San. Inc. Chemical analysis tests were carried out with ARL 8820 model Optical Emission Spectrometer for the wheels to be used in this study, the chemical composition is given in Table 1. For mechanical property controls, hardness measurements were carried out in Brinell 5mm/250kg method in accordance with ISO 6506[2] standard, tensile tests were carried out in Shimadzu AGS-X 100kN device in accordance with ISO 6892[3] standard. In addition, metallographic controls were carried out with Nikon Epiphot 200 model optical metal microscope.

Mechanical properties and SDAS measurement results

\* Corresponding author.  
Email: okan.ceylan@doktas.com



are shared in Table 2.

**Table 1.** Chemical composition (wt.%) of the tested Sr-modified A356 alloy

Alloy	Si	Mg	Sr	Ti	Fe	Cu,Zn,Mn	Al
A356	6.944	0.25	0,025	0,11	0,079	<0,01	Bal.

**Table 2.** Tensile properties, SDAS, and hardness measurements of the tested alloy

Sample area of wheel	UTS, Mpa	YS, Mpa	Elongation, %	SDAS, $\mu\text{m}$	Brinell Hardness, HB
Rim	285 $\pm$ 5	220 $\pm$ 5	8 $\pm$ 2	35 $\pm$ 5	85 $\pm$ 10
Spoke	240 $\pm$ 5	200 $\pm$ 5	3 $\pm$ 1	45 $\pm$ 5	75 $\pm$ 10

## 2.1. Defining A356-T6 S-N Curve

Fatigue test specimens were extracted from A356-T6 alloy wheels casted in Döktaş. Fatigue samples were prepared in accordance with ASTM E466[4] standard as shown in Figure 1. The tests were carried out on a Shimadzu EHF-EV200k2-040-0A model fatigue test device, the image of which is shown in Figure 3.

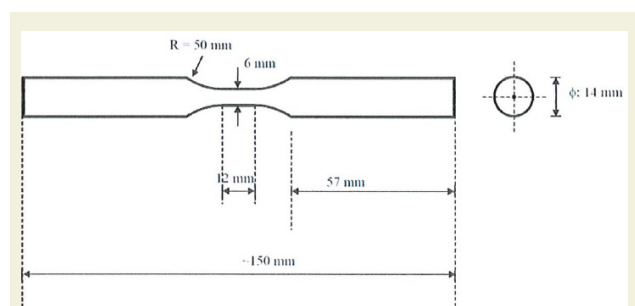


**Figure 1.** Dimensions of Döktaş Fatigue specimens acc.to ASTM E466



**Figure 2.** Fatigue specimen of Döktaş

As a result of the fatigue tests, the S-N curve in Figure 4 was obtained.

## 2.2. Rotating Bending Fatigue Test of Wheel;

Rotating bending fatigue test is done in MAKRA BUP machines. (Figure 5) In this dynamic test, wheel is fastened to adjustable test-bench within bolts from inner-rim flanges. Wheel is rigidly fixed from hub to test-bench using screws or fixing nuts according to standart manufacturer torque values. Rotating bending moment is

applied to the wheel by creating eccentric mass which is at certain distance from wheel offset.

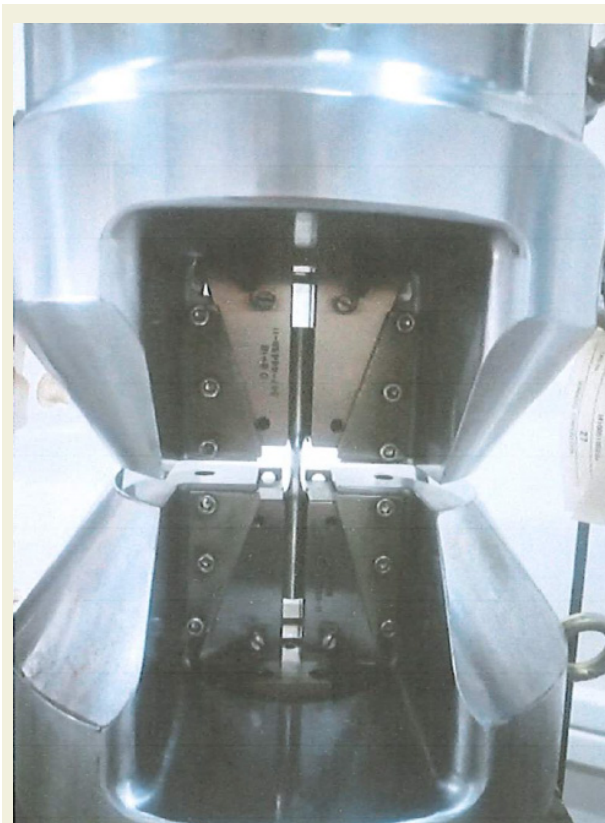


**Figure 3.** Testing configuration and fatigue specimen in testing

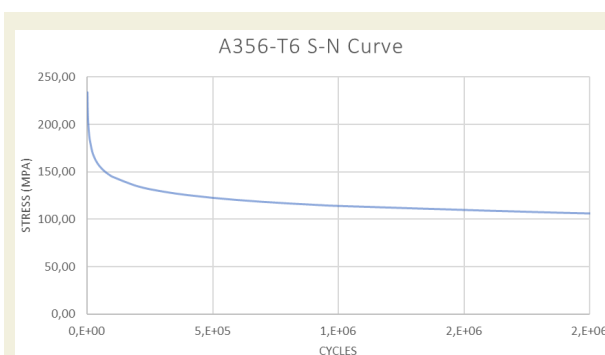


**Figure 4.** S-N curve of A356-T6 wheels



**Figure 5.** a)Scheme of the rotating bending fatigue test[5], b) testing machine

Formula for the bending moment calculation; Abbreviations appear in Figure 6.

$$M_{b_{max}} = S * [F_r (\mu * r_{dyn} + d)]$$

$M_{b_{max}}$  = Maximum reference bending moment [Nm]

$F_r$  = Maximum load capacity of wheel [N]

$r_{dyn}$  = Dynamic radius of largest tyre recommended for wheel [m]

$d$  = Inset [m]

$\mu$  = Coefficient of friction

$S$  = Factor of safety

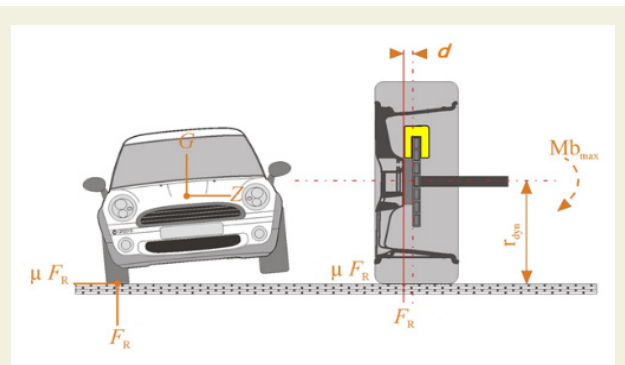


Figure 6. Bending fatigue representational image

The test is carried out with two percentage values (50 percent and 75 percent) of the max moment and on the basis of the following standards.[6] Tests performed with 75% load are considered as short tests and tests with 50% load are considered as long tests.

Short Test Cycle : 200.000

Moment of short test  $0.75 \times M_{b_{max}}$

Long Test Cycle: 1.800.000

Moment of long test  $0.5 \times M_{b_{max}}$

### 3. Simulation Design

The bending fatigue test consists of test bench and wheel. Wheel is fastened to the bench from inner-flange corners. S-N curve and mechanical properties of A356-T6 material were defined the ANSYS Workbench. 3D wheel model has created CATIA and transferred to simulation environment. Model mesh size were 5mm. Wheel dimension was 7Jx17H2 and offset was 50mm. Maximum wheel load was 700kg. Short bending test moment was 3716 N.m, long bending test moment was 2508 N.m. Maximum equivalent stresses found that 134.47 and 106.64 MPa respectively. Fully reversed model was used for fatigue life. According to fatigue life, the short and long tests were positive which means there was no any fatigue detected in test cycles. First cracks started around bolt-holes 215.000 cycles propagated to spoke regions 2.000.000 cycles in short test. In long test results, crack initiation was determined around 2.000.000 cycles and didn't propagate to

spoke or other regions.

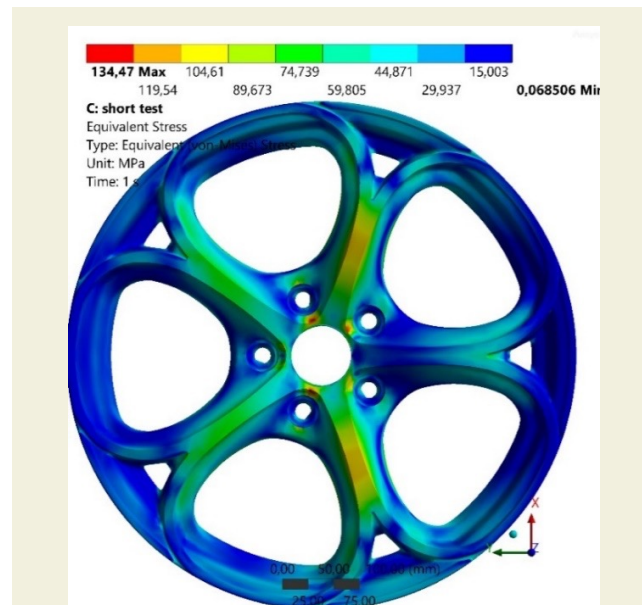


Figure 7. Maximum equivalent stress, short test

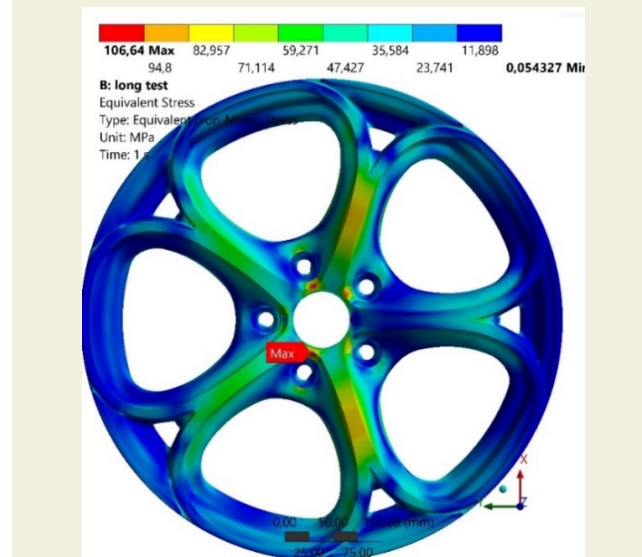


Figure 8. Maximum equivalent stress, long test

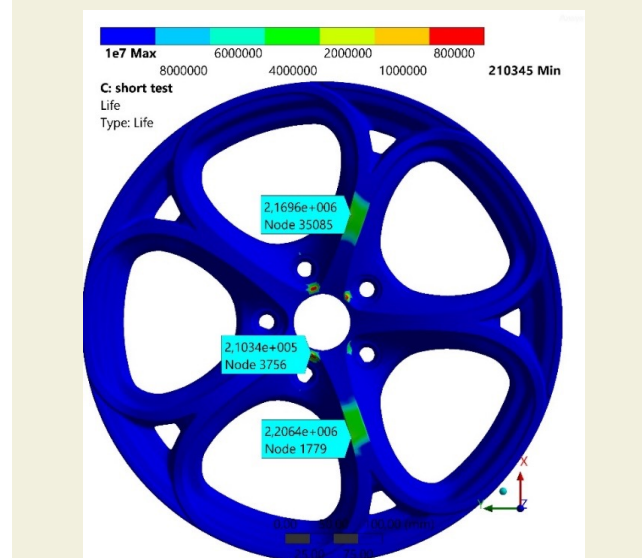


Figure 9. Fatigue life in short test

### 4. Experimental Test

A356-T6 wheel bending fatigue tests were done in MAKRA BUP 760 and BUP 750 machines in Döktaş Test Center. Zinc-gliserin was sprayed all front surfaces. Test moments and cycles were entered the test machines. In short bending fatigue test, any fatigue cracks weren't seen. Approximately 225.000 cycles cracks started around bolt-holes. After 2.100.000 cycles, cracks propagated to spoke sections. Failure occurred nearly 2.500.000 cycles. In long bending fatigue test, any crack occurred to 1.800.000 cycles. After 2.000.000 cycles, first cracks were seen around bolt-holes then spread out other bolt-holes nearly 4.000.000 and 6.000.000 cycles. Long test was performed to 10.000.000 cycles. There was no failed as occurred in short test.

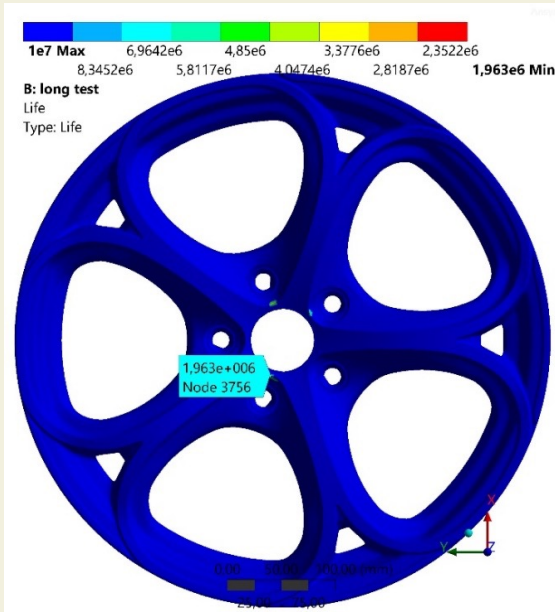


Figure 10. Fatigue life in long test

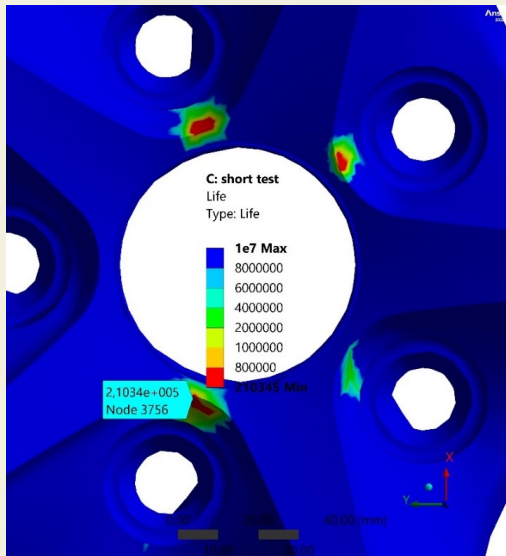


Figure 11. Fatigue life detail in short test

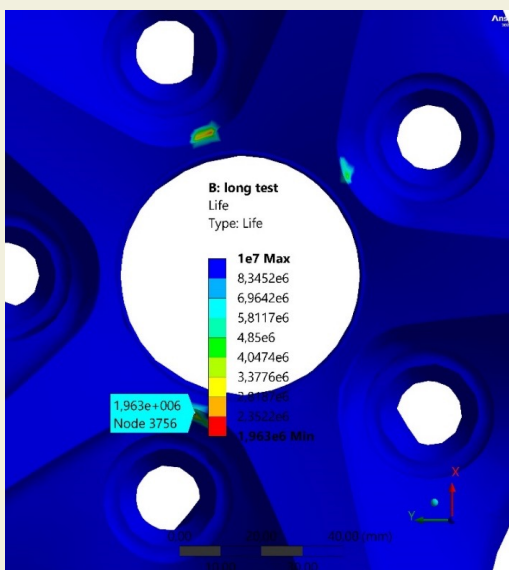


Figure 12. Fatigue life detail in long test



Figure 13. 200.000 cycles in short test



Figure 14. 225.000 cycles in short test



Figure 15. 2.100.000 cycles in short test



Figure 18. 2.00.000 cycles in long test



Figure 16. 2.500.000 cycles in short test [fail]

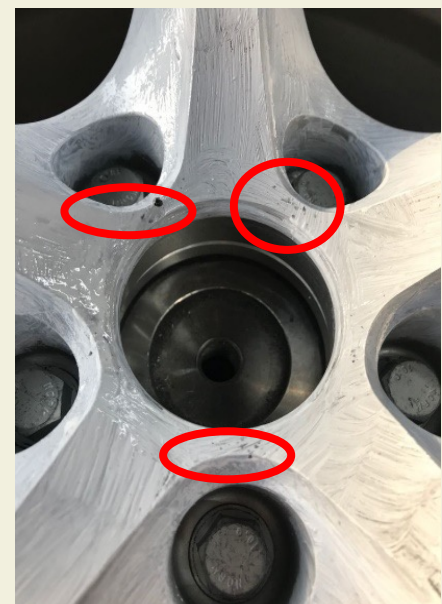


Figure 19. 4.000.000 cycles in long test



Figure 17. 1.800.000 cycles in long test



Figure 20. 6.000.000 cycles in long test



Figure 21 10.000.000 cycles in long test

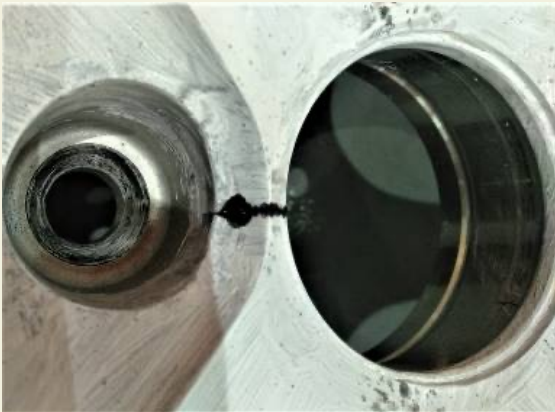


Figure 22 10.000.000 cycles in long test

- [4] ASTM., (2002). Standard Practice for Conducting Force Controlled Constant Amplitude Axial Fatigue Tests of Metallic Materials. Test.: 4–8.
- [5] TS ISO 3006., (2015). Road vehicles - Passenger car wheels for road use - Test methods (112): 18.
- [6] United Nations., (2007). Uniform Provisions Concerning The Approval Of Wheels For Passenger Cars And Their Trailers.

## 5. Conclusion

A356-T6 wheel rotating bending fatigue tests were performed in simulation environment and experimentally. S-N curve of A356-T6 was defined in accordance with standard tests. Short and long rotating bending fatigue tests were considered. Simulation and experimental crack initiation cycles were calculated and recorded. The critical crack test cycles were found that 210.000 and 225.000 cycles for short test. The crack initiation of test wheels were observed around 2.000.000 cycles in simulation and experimental tests. Therefore, fatigue strength of A356-T6 automobile wheel has been validated using the finite elements method.

## 6. References

- [1] Tebaldini, M., Petrogalli, C., Donzella, G., Gelfi, M., La Vecchia, G.M., (2018). A356-T6 wheels: Influence of casting defects on fatigue design. *Fatigue and Fracture of Engineering Materials and Structures*. 41(8): 1784–93. doi: 10.1111/ffe.12820.
- [2] TS EN ISO 6506-2., (2019). *Metallic materials - Brinell hardness test - Part 2: Verification and calibration of testing machines*.
- [3] ISO., (2019). *Metallic Materials - Tensile testing -Part 1: Method of test at room temperature (ISO 6892-1:2019)*. 2019.